POWER SYSTEM SECURITY ASSESSMENT FOR FAULTS USING DIRECT METHODS

By

Ahmad Sadeghi Yazdankhah

A DISSERTATION

Submitted to
Michigan State University
in partial fulfillment of the requirements
for the degree of

DOCTOR OF PHILOSOPHY

Department of Electrical Engineering
and Systems Science

1984

ABSTRACT

POWER SYSTEM SECURITY ASSESSMENT FOR FAULTS USING DIRECT METHODS

By

Ahmad Sadeghi Yazdankhah

Power system operators and planners have long desired to be able to simulate the transients due to electrical faults on-line and without the extensive computation and time required to solve the non-linear system differential equations. Extensive research has been devoted to developing Lyapunov methods that would eliminate the computation and thus permit (a) on-line assessment of stability by operators and (b) much more extensive evaluation of the security of the system for different faults by system planners.

The Lyapunov methods for assessing the stability of power system for a particular fault have been unable to predict whether the system will or will not be stable. Moreover, the procedures developed for eliminating the need to solve the system differential equations require either approximately the same computation as the solution of the differential equations themselves or are not accurate.

Two algorithms have recently been proposed for assessing the stability by (a) identifying a critical machine that determines whether the system will be stable and (b) determining whether the deceleration

energy of th
for the part
of this thes
accurate and
with the sy
shown to pre

The se
directly pre
for a partic
This predict
whether the
The computat
resulting o
wall and the
the differen
assessment
be quite goo
reduced towa

energy of the transmission network is sufficient to maintain stability for the particular fault and clearing time. The first contribution of this thesis is to show that these two algorithms are extremely accurate and can easily identify the critical fault clearing time at which the system just loses stability. Moreover, both methods were shown to predict identical fault clearing times.

The second contribution is to develop an accurate method of directly predicting the maximum angular deviation during the transient for a particular fault, fault clearing time, and operating condition. This prediction of peak angular deviation is required to determine whether the system is stable or unstable using the above algorithms. The computation required for this angular prediction and thus the resulting direct stability assessment method is shown to be extremely small and less than one-hundredth of that required for solution of the differential equations. The accuracy of the direct stability assessment method using the peak angle prediction method is shown to be quite good based on the extensive computational results on the Reduced Iowa System.

For my parents Homay and Rahim

and

my sisters and brothers

ACKNOWLEDGMENTS

The longer a man lives the more he realizes that his success is mostly due to the help and support received from his family and friends.

I am forever thankful to my family for their unconditional love and sacrifices, and for getting me started right.

I sincerely wish to express my thanks and appreciation to Professor R.A. Schlueter, my major advisor, for his invaluable assistance in the planning and preparation of this dissertation. I would like to extend my appreciation to the members of the guidance committee, Professors H. Khalil, R.O. Barr, W. Symes, and R.A. Schlueter, for sharing their thoughtful and constructive comments. I am also indebted to Professor J.B. Kreer, the Chairman of the Department of Electrical Engineering and Systems Science, for support of the extensive computer cost of the thesis.

Finally, my special thanks to Mrs. Carol Cole, whose fast and excellent typing of this dissertation is greatly appreciated.

LIST OF TABLES .

LIST OF FIGURES

Chapter

1. POWER SYS

1.1. Intr

2. THEORETICA
STABILITY

2.1. The

2.2. Corr
the

2.2.
2.2.
2.2.

3. INDIVIDUAL
TRANSIENT

3.1. Intr

3.2. Tran

3.3. Anal
Ener
Stab

3.3.

3.3.2

3.4. Crit

TABLE OF CONTENTS

LIST OF TABLES vii

LIST OF FIGURES ix

Chapter

1. POWER SYSTEM STABILITY 1

1.1. Introduction 1

2. THEORETICAL DEVELOPMENT ON POWER SYSTEM TRANSIENT STABILITY 10

2.1. The Dynamics of Power System During a Transient . 10

2.2. Correspondence of the Equal Area Criterion and the Transient Energy Method 12

2.2.1. Introduction 12
2.2.2. Definition of Transient Energy 16
2.2.3. The Conservative Nature of Classical Lyapunov Methods 24

3. INDIVIDUAL ENERGY FUNCTION AND ITS APPLICATION IN TRANSIENT STABILITY ASSESSMENT 30

3.1. Introduction 30

3.2. Transient Energy of Individual Machines 32

3.3. Analytical Justification of Using the Critical Energy of Individual Machines for Transient Stability Assessment 36

3.3.1. Potential Energy Boundary Surface (PEBS) Method 42

3.3.2. Local Equal Area Criterion 46

3.4. Critical Group, Generator, and Boundary 53

Chapter

4. STABILIT
ENERGY F

4.1. In

4.2. Co

4.3. Fi

4.4. Pa

5. PROPOSED

5.1. Mo

5.1

5.1

5.2. Fast

5.2.

5.3. Fast

5.3.

6. DERIVATI
MEASURE,

6.1. Int

6.2. Lin

6.3. Dis

6.3
6.3

Chapter

4. STABILITY SIMULATION STUDIES USING INDIVIDUAL ENERGY FUNCTION 60

   4.1. Introduction 60

   4.2. Cooper Case 63

   4.3. Fort Calhoun Case 76

   4.4. Raun Case 85

5. PROPOSED DIRECT STABILITY ASSESSMENT ALGORITHMS 97

   5.1. Modified Transient Energy Method 100

      5.1.1. Fault Trajectory Approximation by Cosine Series 100
      5.1.2. Trajectory Approximations by Taylor Series 102

   5.2. Fast PEBS Method 105

      5.2.1. Efficient PEBS Algorithm for Predicting Stability 110

   5.3. Fast Equal Area Method 112

      5.3.1. Efficient Equal Area Algorithm for Predicting Stability 115

6. DERIVATION, JUSTIFICATION, AND VERIFICATION OF SECURITY MEASURE, PREDICTION OF PEAK ANGLES 117

   6.1. Introduction 117

   6.2. Linearized Power System Model 117

   6.3. Disturbance Model 124

      6.3.1. Step Disturbance 125
      6.3.2. Electrical Faults 126

Chapter

6.4. L

6.

6.

6.

6.

6.5. Com
Pu

7. STABILIT
COMPUT

7.1. Int

7.2. Coo

7.3. For

7.4. Rau

8. REVIEW, C

8.1. Cha

8.2. Top

APPENDIX A . . .

A.1. Com

A.2. Com

BIBLIOGRAPHY . .

Chapter

6.4. Linear RMS Coherency Measure 128

    6.4.1. RMS Coherency Measure for Impulse Input Disturbance 132
    6.4.2. RMS Coherency Measure for Pulse Input Disturbances 137
    6.4.3. Justification of Nonlinear RMS Coherency Measure 138
    6.4.4. Theoretical Justification of Fault Security Measure for Second Order System 142

6.5. Computational Algorithm for Infinite Interval Pulse Coherency Measure 147

7. STABILITY ANALYSIS USING FAST DIRECT METHODS AND COMPUTATIONAL RESULTS 153

7.1. Introduction 153

7.2. Cooper Case 153

7.3. Fort Calhoun Case 161

7.4. Raun Case 161

8. REVIEW, CONCLUSION, AND TOPICS FOR FUTURE INQUIRY . . . 168

8.1. Chapter Review 168

8.2. Topics for Future Research 173

APPENDIX A 175

A.1. Computation of v_{k+1} 175

A.2. Computation of v_0 177

BIBLIOGRAPHY 179

Table

4.1. Reduced
conditio

4.2. Potential
of t_c for

4.3. Minimum
generator

4.4. Minimum
critical
program .

4.5. Potential
of t_c for

5.1. Comparison
fault on

7.1. Generator
RMS coher
Clearing

7.2. Generator
RMS coher
Clearing

7.3. Determinat
Cooper us

7.4. Determinat
using the

7.5a. Determinat
Fort Calho

7.5b. Determinat
Calhoun us

LIST OF TABLES

Table

4.1. Reduced Iowa System generator data and initial conditions 62

4.2. Potential energy boundary surface energy as a function of t_c for determining t_{cc} 69

4.3. Minimum of $\Delta E_2(t_B,t_c) = A_1(t_c) + A_2(t_B,t_c)$ for critical generator 2 using stability simulation program 75

4.4. Minimum of $\Delta E_{16}(t_B,t_c) = A_1(t_c) + A_2(t_B,t_c)$ for critical generator 16 using stability simulation program 82

4.5. Potential energy boundary surface energy as a function of t_c for determining t_{cc} 83

5.1. Comparison of fault trajectory angles at t = 0.4 sec. (fault on bus 15, New England system) 101

7.1. Generator peak angles $(\theta_i - \theta_{13})$ for Cooper using the RMS coherency measure and simulation programs. Clearing time = .192 seconds 155

7.2. Generator peak angles $(\theta_i - \theta_{13})$ for Cooper using the RMS coherency measure and simulation programs. Clearing time = 0.210 seconds 156

7.3. Determination of maximum potential energy (PEBS) for Cooper using the fast direct method 157

7.4. Determination of minimum energy margin (EAC) for Cooper using the fast direct method 159

7.5a. Determination of maximum potential energy (PEBS) for Fort Calhoun using the fast direct method 162

7.5b. Determination of minimum energy margin (EAC) for Fort Calhoun using the fast direct method 162

Table

1.6a. Determin
Radius

1.6b. Determin
using th

Table

7.6a. Determination of maximum potential energy (PEBS) for Raun using the fast direct method 164

7.6b. Determination of minimum energy margin (EAC) for Raun using the fast direct method 164

Figure

2.1. Power ar

2.2. Stable,
machine

3.1. Partial
(a) Su-
(b) Part

3.2. Stable,
machine s

3.3. Equal are
(a) Power
bus s
(b) Varia

3.4. 17-genera

4.1. 17-genera

4.2. Swing cu
(a) Gene
(b) Gene

4.3. Swing cu
(a) Gene
(b) Gene

4.4. Swing cu

4.5. Energy ma
Clearing
W/C = tra
N/C = tra

4.6. Energy ma
Clearing
W/C = tra
N/C = tra

LIST OF FIGURES

Figure

2.1. Power angle curves for one-machine infinite-bus system 15

2.2. Stable, unstable, and critical trajectory for a three-machine system 28

3.1. Partial energy analysis. Clearing time = .1922 seconds
(a) Sum of partial energies for generators 5 and 6
(b) Partial energy for generators 5 and 6 41

3.2. Stable, unstable, and critical trajectory for a three-machine system 44

3.3. Equal area criterion
(a) Power angle representation of one-machine infinite-bus system
(b) Variation of energy margin vs. time 48

3.4. 17-generator system (Reduced Iowa System) [13] 55

4.1. 17-generator system (Reduced Iowa System) [13] 61

4.2. Swing curves for Cooper. Clearing time = .218 seconds
(a) Generators 2, 17
(b) Generators 12, 16 64

4.3. Swing curves for Cooper. Clearing time = .220 seconds
(a) Generators 2, 17
(b) Generators 12, 16 65

4.4. Swing curves for Cooper 66

4.5. Energy margin $A_1(t_c) + A_2(t,t_c)$ for Cooper case.
Clearing time = .218 seconds. Critical generator = 2
W/C = transfer conductance included
N/C = transfer conductance excluded 72

4.6. Energy margin $A_1(t_c) + A_2(t,t_c)$ for Cooper case.
Clearing time = .220 seconds. Critical generator = 2
W/C = transfer conductance included
N/C = transfer conductance excluded 73

Figure

4.7. Swing cu
seconds
(a) Gen
(b) Gen

4.8. Swing cu
seconds
(a) Gen
(b) Gen

4.9. Energy –
Clearing
■ C = th
▼ C = th

4.10. Energy ma
Clearing
■ C = tra
▼ C = tra

4.11. Swing cur
(a) Gener
(b) Gener

4.12. Swing cur
(a) Gener
(b) Gener

4.13. Swing cur

4.14. Partial e
(a) Sum o
(b) Parti

4.15. Equal are
6-infinit
(b) Trans
respe

4.16. Equal are
Clearing
(a) [illegible]
tance
(b) Areas
exclu

Figure

4.7. Swing curves for Fort Calhoun. Clearing time = .354 seconds
(a) Generators 16, 17
(b) Generators 10, 12 77

4.8. Swing curves for Fort Calhoun. Clearing time = .356 seconds
(a) Generators 16, 17
(b) Generators 10, 12 78

4.9. Energy margin $A_1(t_c) + A_2(t,t_c)$ for Fort Calhoun case. Clearing time = .354 seconds. Critical generator = 16
W/C = transfer conductance included
N/C = transfer conductance excluded 80

4.10. Energy margin $A_1(t_c) + A_2(t,t_c)$ for Fort Calhoun case. Clearing time = .356 seconds. Critical generator = 16
W/C = transfer conductance included
N/C = transfer conductance excluded 81

4.11. Swing curves. Clearing time = .1900 seconds
(a) Generators 10, 13, 16
(b) Generators 5, 6 86

4.12. Swing curves. Clearing time = .1925 seconds
(a) Generators 2, 10, 13, 16
(b) Generators 5, 6 87

4.13. Swing curves. Clearing time = .1922 seconds 89

4.14. Partial energy analysis. Clearing time = .1922 seconds
(a) Sum of partial energies for generators 5 and 6
(b) Partial energy for generators 5 and 6 90

4.15. Equal area analysis $\Delta E(t) = A_1(t) + A_2(t)$. Raun case, 6-infinite bus. Clearing time = .18 seconds. (a), (b) Transfer conductance excluded and included, respectively 92

4.16. Equal area analysis. Raun case, 6-infinite bus. Clearing time = .1925 seconds
(a) $\Delta E(t) = A_1(t) + A_2(t)$ vs. time (transfer conductance excluded)
(b) Areas $A_1(t)$ and $A_2(t)$ (transfer conductance excluded)

Figure

4.17. Equa
Mea
(a)
(b)

4.18. Equa
Mea
(a)
(b)

5.1. Dete
era

5.2. Dete
era

Figure

4.17. Equal area analysis. Raun case, 5-infinite bus. Clearing time = .1922 seconds
(a) $\Delta E(t) = A_1(t) + A_2(t)$ vs. time (transfer conductance included)
(b) Areas $A_1(t)$ and $A_2(t)$ vs. time (transfer conductance included) 94

4.18. Equal area analysis. Raun case, 5-infinite bus. Clearing time = .1925 seconds
(a) $\Delta E(t) = A\ (t) + A\ (t)$ vs. time (transfer conductance included).
(b) Areas $A_1(t)$ and $A_2(t)$ vs. time (transfer conductance included) 95

5.1. Determination of critical boundary for critical generator using maximum potential energy $V^*_{PE}(t_c)$ method . 108

5.2. Determination of critical boundary for critical generator using minimum energy margin $\Delta E(t_B,t_c)$ method . . 114

CHAPTER 1

POWER SYSTEM STABILITY

1.1. Introduction

Since the industrial revolution, man's demand for and consumption of energy has increased steadily. A major portion of the energy needs of a modern society is supplied in the form of electrical energy.

The ever-increasing dependence of societies on electrical energy requires not only the production of a continuous electric supply but also energy within acceptable quality limits. Very complex power systems have been built to satisfy this increasing demand. The trend in electric power production is toward an interconnected network of transmission lines linking generators and loads into large integrated systems.

In the interconnected power system, the ability to provide reliable and uninterrupted srevice to the loads is the main concern for both planning and operating engineers in their decision making. In practical terms this means that both voltage and frequency must be held within close tolerances so that the consumer's equipment may operate satisfactorily. The concept of stability arises when the power system is subjected to the occurrence of a disturbance. If the disturbance does not involve any net change in power, the power

system variables,
small deviation fr
to their original s
demand is created b
conditions, a trans
The behavior of the
turbance (electrica
the transient stabi
state transition so
"swing" far enough
in the process. Usu
stability is tested
mission network. In
a fault.

When a fault oc
close to the fault lo
the other generators
tend to accelerate or
fault, from the rest
lasts long enough, e.
separates from the re
synchronism). Howeve
devices that sense t
initiate action to "
section of the netwo
Therefore, is that t

system variables, such as the rotor angles, powers, etc., undergo a small deviation from their nominal value and then return very shortly to their original state. If an unbalance between the supply and demand is created by a change in load, in generation, or in network conditions, a transition from one operating state to another results. The behavior of the system response to occurrence of a large disturbance (electrical fault, loss of a generator, etc.) is called the transient stability analysis of the power system. During this state transition some of the severely disturbed generators will "swing" far enough from their equilibrium positions to lose synchronism in the process. Usually the severe disturbance under which transient stability is tested is a short circuit in the high-voltage transmission network. In power system terminology this is referred to as a fault.

When a fault occurs, certain generators which are electrically close to the fault location are disturbed to a greater extent than the other generators which are remote from the fault. These generators tend to accelerate or decelerate, depending on the nature of the fault, from the rest of the generators in the system. If the fault lasts long enough, eventually one machine or a group of machines separates from the rest of the system, causing instability (loss of synchronism). However, the power network is equipped with automatic devices that sense the existence of the faults in the network and initiate action to "clear" the fault, i.e., isolate the faulted section of the network. A matter of great practical importance, therefore, is that the time required to clear the fault should be

less than the d
large enough to
This is the so-c
in the literatur
tem is often d
by direct metho
results obtained
methods, and
as it is subject
the critical c
of attraction of

The most
by the time sol
the observation
stability or ins
there are some

(1) Stab
tion and the ty

(2) The c
large system.

The drawba
putationally eff
date researchers
the concept of
early stages of

less than the duration of the fault that would create a disturbance large enough to cause one or more machines to lose synchronism. This is the so-called "critical clearing time (t_{cc}), commonly used in the literature on transient stability of power systems. This term is often quoted by researchers on power system transient stability by direct mechods as a figure of merit to be used (a) to compare results obtained by time simulation with those obtained by direct methods, and (b) to determine how "robust" a power network may be as it is subjected to disturbance. (The state vector, evaluated at the critical clearing time, provides a means of estimating the region of attraction of the post-fault systems.)

The most widely used transient stability analysis is obtained by the time solution of the machine's rotor angles. Then, based on the observation of the swing curves and engineering judgment, the stability or instability of the power system is decided. However, there are some disadvantages of this technique such as:

(1) Stability (or instability) depends on network configuration and the type of disturbance

(2) The computation is cumbersome and time consuming for a large system.

The drawbacks of the time solution and the need for fast, computationally efficient and approximate transient stability analysis made researchers inquire into an alternative approach. As a result, the concept of direct methods of stability was pursued. From the early stages of development, the direct methods of Lyapunov and the

energy functi
stability reg
many system o
far from imple
analysis in e
operation was
the methods
assessment.

The mis
stability in
continuous pr

(1) Th
model represe
the transfer
system is eva
of stability
saddle point,
energy integr
energy are fi
by determinin

(2) Th
tion of the co
training were

energy function analysis showed promise of assessing transient stability rapidly without the computation required to integrate the many system differential equations even though the method remained far from implementation. The use of such a method for contingency analysis in expansion planning, operation planning, and on-line operation was exciting. It is clear, however, that such approximation methods would never replace time solution for accurate stability assessment.

The historical development of the direct methods for transient stability in this area is divided into the following distinct but continuous phases.

(1) The work of Magnusson in 1947 [30] considers a classical model representation of the power system. In this representation the transfer conductance is omitted and an energy function for the system is evaluated. Then the critical energy, by which the region of stability is identified, is determined by the energy of the lowest saddle point, V_{1s}. The work of Aylett [31] is devoted to finding an energy integral. The kinetic (KE) and potential (PE) components of energy are identified and the stability of the power system is decided by determining whether KE < PE.

(2) The work in phase (1), although outstanding in the elaboration of the concept, was far from implementation. The main issues remaining were

contai

the m

excee

The w

was devote

critical e

approximat

[33] initi

which was

(3)

potential

developmen

mark the

transient

energy ev

hence a

phase wi

How

[33] show

iteratio

machine r

(a) to resolve the difficulty in obtaining all singular points,

(b) to be able to identify the correct singular point,

(c) to be able to include the transfer conductances in the model, and

(d) to identify the critical value of energy which if exceeded would result in loss of stability.

The work of El-Abiad et al. [32] and Prabhakara et al. [33] was devoted to finding the appropriate saddle points and hence the critical energy. The work of Uyemura et al. [34] was devoted to approximating the transfer conductance term, while Smith and Tavora [35] initiated the first work toward considering the critical energy which was related to the faulted trajectory.

(3) The work in references [4, 9] in the development of the Potential Energy Boundary Surface (PEBS) and [13, 14, 28] in the development of energy accounting using the transient energy function mark the latest advances of algorithms for direct assessment of transient stability. A main point of this work is that the critical energy evaluated is directly related to the fault trajectory and hence a larger region of stability is obtained. The work in this phase will be discussed in detail in Chapter 2.

However, in spite of these encouraging results, the work in [29] showed that the true region of stability is identified by consideration of local kinetic and potential energy of an individual machine rather than global kinetic and potential energies of all

generators in th
the particular
of the entire s
stability obtai
is more accurat

In this
ility of algor
using individua
investigating

(1) dev
group and the
the particular
function in th

(2) te
boundary meth
and the ease
to transient

(3) d
algorithms
Area Condit
machine ene
integration

(4)
test system
cial cases

generators in the system. This investigation attempted to identify the particular individual machine whose behavior dictates the stability of the entire system. Furthermore, it was shown that the region of stability obtained by the individual machine energy function concepts is more accurate than total system energy function concepts.

In this research, it is believed that the efficiency and reliability of algorithms for direct assessment of transient stability using individual machine energy function could be improved by further investigating the following concepts:

(1) development of a method for determining the accelerated group and the critical generator without simulating the system for the particular fault and analyzing the individual generator energy function in time frame,

(2) testing of the Local Equal Area and Local Potential Energy Boundary methods on several fault cases to show the extreme accuracy and the ease in determining the critical clearing times when applied to transient stability simulations of the faults,

(3) development of very fast and computationally efficient algorithms for implementing the algorithms based on the Local Equal Area Condition or Potential Energy Boundary Condition using individual machine energy function without simulation of the system and thus integration of the differential equations.

(4) extensive verification of the algorithms developed on a test system and extensive fault cases to determine if there are special cases for which these algorithms fail.

Th

absorb

ment st

methods

detail.

ity surf

13, 15,

On

starting

a region

This reg

energy

then pr

assump

utilize

functio

energy

This th

individ

Equal

energy

in loss

the ea

is of

To achieve the goals, the contents of Chapter 2 are devoted to describing the behavior of the power system and the concept of transient stability analysis. The historical development of the direct methods for transient stability assessment is revisited in further detail. The concepts and algorithms based on potential energy boundary surface [4, 9] and on equal area with global energy accounting [13, 15, 28] are explained.

Chapter 3 proposes and justifies two hypotheses, (a) that the stability of a group of machines and thus the system is dictated by a region of stability for one machine in that group, and (b) that this region of stability is reflected in the kinetic and potential energy of this machine. The individual machine energy function is then presented and shown to violate the conditions for it to be a Lyapunov function. A PEBS algorithm [16] is then justified that utilizes the maximum individual generator potential energy as a function of time for a fault-on trajectory ($t_c^* >> t_{cc}$) as a critical energy threshold for deciding whether the system is or is not stable. This threshold energy value is compared with the maximum of the individual generator potential energy as a function of time for some $t_c \leqq t_c^*$ to decide retention or loss of stability. The second algorithm, Equal Area Criterion (EAC), is then justified that utilizes the minimum energy margin $\Delta E^* = A_1 + A_2$ as a function of time to decide retention or loss of stability. A_1 is the accelerating energy produced during the fault period and A_2 is the decelerating energy after the fault is cleared of the individual generator with respect to the rest of

the generatio
ence should b
by clearing
generator, an

Chapte
potential ene
then presente
and hold sig
and computat

Chapte
algorithms (
the potential
other genera
requires cal
operating st
post-fault r
about the sy
jectory appr
ment these a
the first re
not sufficie

Chapte
for differen
two coherenc
point is also

the generators in the system. This minimum value of energy difference should be less than zero if stability is to be retained for any clearing time. Then the concepts of critical group, critical generator, and critical boundary are also defined.

Chapter 4 presents two algorithms based on the kinetic and potential energy conditions discussed above. Simulation results are then presented that indicate these algorithms are extremely accurate and hold significant promise for the development of both accurate and computationally efficient procedures.

Chapter 5 proposes two fast and computationally efficient algorithms (Fast PEBS and Fast EAC). Both algorithms are based on the potential energy of the individual machine with respect to the other generators in the system. Computation of this potential energy requires calculation of the initial operating states, the final operating states (peak values of generator rotor angles), and the post-fault network conditions. It is shown that this information about the system state trajectory can be obtained by one of two trajectory approximations, the Taylor series or Cosine series, to implement these algorithms without simulation. However, it is shown that the first requires extensive computation and the second is in general not sufficiently accurate.

Chapter 6 derives the Root Mean Square (RMS) coherency measure for different disturbances (step, impulse, and pulse). A nonlinear RMS coherency measure based on the critical unstable equilibrium point is also derived. The impulse RMS coherency measure is then shown to pr

second orde

last step a

efficiency

Chapt

cussed in C

results of

presented

Final

and the a

shown to predict the peak angle deviation of the generator for a second order linear single machine infinite bus system model. As a last step a computational algorithm for the finite interval pulse coherency measure is derived.

Chapter 7 applies the two fast algorithms (PEBS, EAC), discussed in Chapter 5, directly to the Reduced Iowa system. The results of these applications for different fault cases are then presented that indicate the algorithms are extremely accurate.

Finally in Chapter 8 the contribution of this investigation and the avenues for further inquiry are considered.

CHAPTER 2

THEORETICAL DEVELOPMENT ON POWER SYSTEM TRANSIENT STABILITY

2.1. The Dynamics of Power System During a Transient

When the power system is operating in normal state, all the equality and inequality constraints are satisfied, all the generators are operating at synchronous speed, and its dynamics are defined by a nonlinear vector differential equation

$$\ddot{\underline{X}} = \underline{F}(\underline{X},\underline{P}) \tag{2.1}$$

where $\underline{F}(\underline{X},\underline{P})$ is the transient stability model of the power system, and $\underline{X}$ and $\underline{P}$ are states and parameters of the system, respectively. Of special interest in the analysis of the system (2.1) is the equilibrium, which is the state of the system where the rate $\ddot{\underline{X}}$ is zero and the system is "in balance." The most significant interpretation attached to the equilibrium in a wide variety of application in engineering is stability. Stability is commonly understood as a situation where the system is in equilibrium, and if perturbed, returns in time to equilibrium. The equilibrium operating point $\underline{X}^{s1}$ (s.e.p.) of the system (2.1) is defined by

$$\ddot{\underline{X}} = \underline{F}(\underline{X},\underline{P}) = \underline{0} \tag{2.2}$$

Upon the occurrence of an electrical fault, the power system undergoes two new phases [5]:

(1) during the fault, where the dynamic behavior of the power system governed by

$$\ddot{\underline{X}} = \underline{F}_1(\underline{X},\underline{P}^f) \qquad 0 < t < t_c \tag{2.3}$$

(2) post-fault (after clearance of the fault); once the fault is cleared, the system will assume a new configuration and thus its behavior will be governed by another set of nonlinear differential equations of the form

$$\ddot{\underline{X}} = \underline{F}_2(\underline{X},\underline{P}^{pf}) \qquad t > t_c \tag{2.4}$$

where t_c is called the clearing time.

If, after the transition from the fault phase to the post-fault phase, synchronism for all the generators in the system is maintained, then transient stability results and the system trajectory will converge toward a post-fault s.e.p.

$$\underline{F}_2(\underline{X}^{s2},\underline{P}^{pf}) = \underline{0} \tag{2.5}$$

If, after this transition, synchronism of all the generators is lost, the trajectory will pass close to an unstable equilibrium point (u.e.p.) that satisfies

$$\underline{F}_2(\underline{X}^{u},\underline{P}^{pf}) = \underline{0} \tag{2.6}$$

One of the basic problems of stability analysis is to find (necessary and sufficient) conditions on the system parameters so

that the c
The most p
direct met
the explic
as (2.1).

The
tive scala
every poss
for a sin
(1).
solutions
system re

As
tion of t
and poten
has been
system.
analysis

2.2.1.

Be
ing at
ties wi
changes

that the convergence of solutions to a post fault s.e.p. takes place. The most powerful method of solving such a problem is the Lyapunov direct method [6]. The method answers questions of stability without the explicit solution of the related differential equations, such as (2.1).

The underlying idea of the Lyapunov method is to find a positive scalar function $V(\underline{X})$ with the rate of change $\dot{V}(\underline{X})$ negative for every possible state $\underline{X}$ belonging to some region of stability R except for a single equilibrium state $\underline{X}^*$ where $V(\underline{X})$ attains its minimum $V(\underline{X}^*)$. Then the function $V(\underline{X})$ will continuously decrease along the solutions of the system until it assumes its minimum $V(\underline{X}^*)$ and the system reaches the equilibrium $\underline{X}^*$.

As a candidate for Lyapunov's function $V(\underline{X})$, the energy function of the power system will be chosen. The analysis of kinetic and potential energy components at two different instants of time has been used to conclude transient stability or instability of the system. The next section is devoted to the transient stability analysis from the energy point of view.

2.2. Correspondence of the Equal Area Criterion and the Transient Energy Method

2.2.1. Introduction

Before the occurrence of the fault, the power system is operating at the nominal state (pre-fault s.e.p.) and the machine velocities with respect to a synchronous reference are zero. The fault changes the network configuration of the system and the machine

velocities
the accelera
system from
network con
during the
according t
ated genera
inertia is
system con
velocities
with respec
stability o
ducing rest
network ele

The
tial terms.
motion of
potential
elements a
system, wh
the direct
given con
system ene
certain cr
critical e
equivalen

velocities will increase, thus increasing kinetic energy. Obviously, the acceleration that increases kinetic energy also moves the system from its pre-fault s.e.p. After the fault is removed, a new network configuration results and the excess kinetic energy produced during the fault period is distributed in the post-fault network according to the network requirements. If the motion of the accelerated generators with respect to the rest of the system's center of inertia is reversed due to the kinetic energy distribution, then the system converges toward the post-fault s.e.p. where again the machine velocities are zero. If the motion of the accelerated generators with respect to the center of inertia is not reversed, a loss of stability occurs. The capability of the post-fault network for producing restoring forces is measured by the potential energy of the network elements.

The transient energy function contains both kinetic and potential terms. The system kinetic energy, associated with the relative motion of machine rotors, is independent of the network. The system potential energy, associated with the potential energy of network elements and machine rotors, is always defined for the post-fault system, whose stability is to be analyzed. The principal idea of the direct methods is that a system's transient stability can, for a given contingency, be determined directly by comparing the total system energy which is gained during the fault on period, with a certain critical potential energy. For a two-machine system this critical energy is uniquely defined and the direct analysis is equivalent to the equal area criterion.

The c

energy meth

lent single

figure the

period usi

$V(\xi^2$

is compared

equation (2

$V(\xi^4$

For A_2 = 2

A_2 = 2

For a

becomes mo

uniquely c

analysis.

energy is

mum point

saddle poi

that are v

The correspondence of the equal-area criterion and the transient energy method for a two-machine system is illustrated for the equivalent single machine infinite bus system in Figure 2.1. In this figure the kinetic energy $KE(\delta^c) = A_1$ gained during the fault-on period (using equation (2.3))

$$V(\delta^c) = KE(\delta^c) = \int_{\delta^{s1}}^{\delta^c} F_1(X,P^f)dX$$

is compared to the critical potential energy $PE(\delta^c,\delta^u) = A_2$ (using equation (2.4))

$$V(\delta^u,\delta^c) = PE(\delta^c,\delta^u) = \int_{\delta^c}^{\delta^u} F_2(X,P^{p^f})dX$$

For $A_2 = PE(\delta^u,\delta^c) \geqq KE(\delta^c) = A_1$, the system remains stable and for $A_2 = PE(\delta^u,\delta^c) < KE(\delta^c) = A_1$, the system loses stability.

For a system with three or more machines, the direct analysis becomes more difficult. In this case the critical energy is not uniquely defined and its determination becomes the key step in the analysis. According to the Lyapunov-based theorem [7], the critical energy is chosen to be the potential energy at the unstable equilibrium point. This unstable equilibrium point is called the lowest saddle point [10]. This critical energy frequently yields results that are very conservative, especially for large systems.

Figure 2

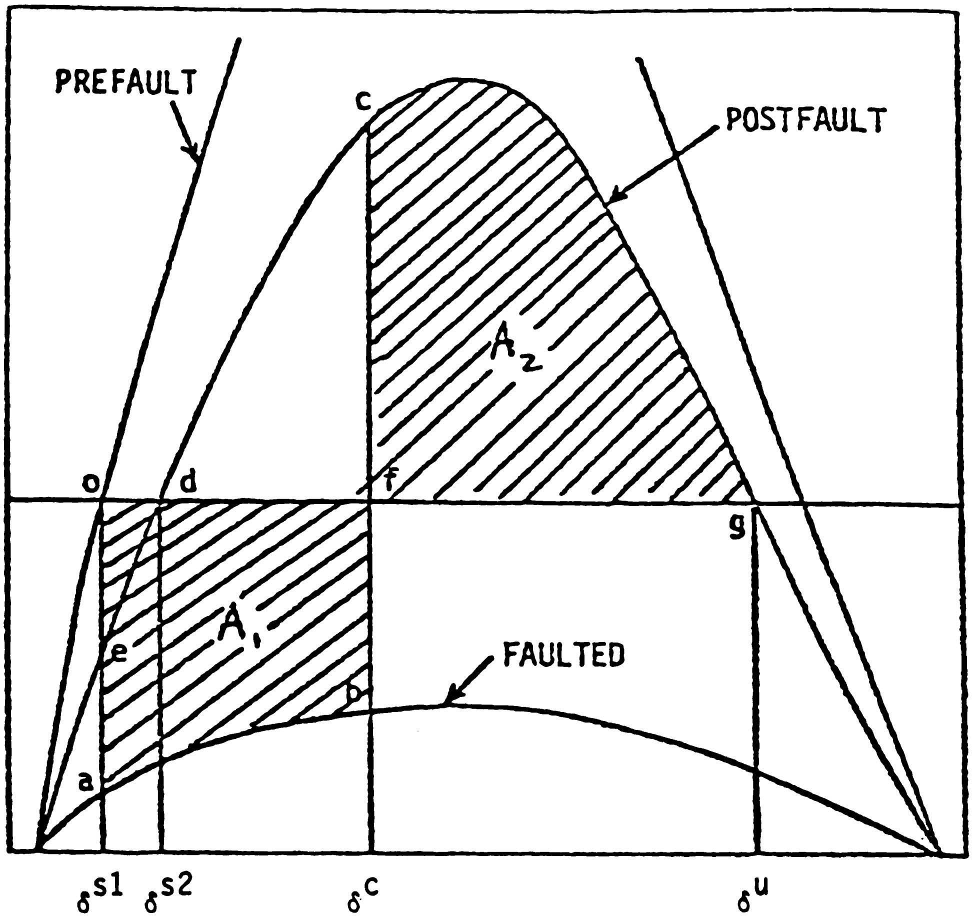

Point 0: prefault operating point; $\delta = \delta^{s1}$, $t = t_0^-$

Point a: electrical power at $t = t_0^+$, $\delta = \delta^{s1}$

Point b: electrical power at $t = t_c^-$, $\delta = \delta^{c}$

Point c: electrical power at $t = t_c^+$, $\delta = \delta^{c}$

Point d: operating point when transient subsides, $t \to \infty$, $\delta = \delta^{s2}$

Figure 2.1. Power angle curves for one-machine infinite-bus system.

2.2.2. Definition of Transient Energy

The previous section describes the sequence of functions (2.1-2.6) that characterize stability or loss of stability and the energy transfers associated with this transient stability problem. The equal area criterion, which precisely describes the energy transfers for a single machine-infinite bus (equivalent infinite machine that represents the rest of the system) model, is discussed based on Figure 2.1. Although the equal area criterion has motivated the methods used for multimachine power system, these methods have not yet been shown to achieve the desired accuracy.

This subsection will develop the multimachine classical transient stability model and present the "total" energy function for this model. Then the areas A_1 and A_2 for the equal area criterion will be defined using this energy function with the appropriate model (the fault model for A_1 and post-fault model for A_2), the appropriate terms in this expression (kinetic for A_1 and potential for A_2), and the proper limits of integration (δ^{s1} and δ^c for A_1 and δ^c and δ^u for A_2). The PEBS and UEP methods, which are both based on the definition of energy V_{cl} and V_{cr} for post-fault network and related to A_1 and A_2 respectively, are then discussed in subsection 2.2.3. The importance of the discussion of the equal area criterion is (1) its use to justify the PEBS and UEP methods for the total energy function in this chapter and the PEBS and equal area methods based on an individual machine energy function in the next chapter; and (2) the results in Chapter 4 that show the equal area criterion

based methods for the individual energy function are extremely precise and accurate for determining region of stability. These results using the individual energy function are much more accurate than the results obtained using the total energy function.

The dynamic behavior of the power system is described by two sets of differential equations. One set describes the internal structure of machine quantities and their mutual relationships, and the other set relates the terminal voltage and current of each machine to those of the other machines [2]. Because of the fact that a synchronous machine has several coupled circuits, inclusion of one or more of the coupled circuits within the machine increases the complexity of the power system model. The complexity will become more apparent if a multimachine power system is considered. For the purpose of investigation of stability for approximate and easily computed transient security assessment, a simplified classical model will be used to determine the dynamic behavior of the power system.

The classical model is characterized by [1]

(1) Mechanical input power is constant.

(2) Damping coefficient, both mechanical and electrical, is neglected.

(3) The voltage behind transient reactance of the synchronous machine is assumed to be constant.

(4) Loads are represented by constant impedances.

For the system model being considered, the equations of motion are:

where

and,

with

$$M_i\dot{\omega}_i = P_i - P_{ei}$$
$$\dot{\delta}_i = \omega_i \qquad i = 1, 2, \ldots., n \qquad (2.7)$$

where

$$P_{ei} = \sum_{\substack{j=1\\ \neq i}}^{n} [C_{ij}\sin(\delta_i - \delta_j) + D_{ij}\cos(\delta_i - \delta_j)]$$

$$P_i = P_{mi} - E_i^2 G_{ii}$$

$$C_{ij} = E_i E_j B_{ij}$$

$$D_{ij} = E_i E_j G_{ij}$$

and, for unit i,

P_{mi} = mechanical power input

G_{ii} = driving point conductance

E_i = constant voltage behind the direct axis transient reactance

ω_i, δ_i = generator rotor speed and angle deviations, respectively

M_i = moment of inertia

$B_{ij}(G_{ij})$ = transfer susceptance (conductance) in the reduced bus admittance matrix

The transformation of equations (2.7) into the center of angle coordinates provides a concise framework for the analysis of systems with transfer conductances. Define:

$$r_0 \triangleq \frac{1}{M_T}\sum_{i=1}^{n}$$

$$M_T \triangleq \sum_{i=1}^{n} M$$

then

$$M_T\ddot{r}_0 = \sum_{i=1}^{n}$$

$$\dot{r}_0 = v_0$$

By defining new

reference, $\rho_i \triangleq$

motion become

$$M_i\ddot{\rho}_i = F_i$$

$$\dot{\rho}_i = \nu_i$$

where the cente

$$\sum_{i=1}^{n} M_i\rho_i$$

The trans

by first estab

multiplying ea

$$\delta_o \triangleq \frac{1}{M_T} \sum_{i=1}^{n} M_i \delta_i$$

$$M_T \triangleq \sum_{i=1}^{n} M_i \qquad (2.8)$$

then

$$M_T \dot{\omega}_o = \sum_{i=1}^{n} (P_i - P_{ei}) = \sum_{1=1}^{n} P_i - 2 \sum_{i=1}^{n-1} \sum_{j=i+1}^{n} D_{ij} \cos \delta_{ij} \triangleq P_{COA}$$

$$\dot{\delta}_o = \omega_o \qquad (2.9)$$

By defining new anlges and speeds relative to the center of angle reference, $\theta_i \triangleq \delta_i - \delta_o$ and $\tilde{\omega}_i \triangleq \omega_i - \omega_o$, the system equations of motion become

$$M_i \dot{\tilde{\omega}}_i = P_i - P_{ei} - \frac{M_i}{M_T} P_{COA}$$

$$\dot{\theta}_i = \tilde{\omega}_i \qquad i = 1, 2, \ldots., n \qquad (2.10)$$

where the center of angle variables satisfies the constraints

$$\sum_{i=1}^{n} M_i \theta_i = \sum_{i=1}^{n} M_i \tilde{\omega}_i = 0 \qquad (2.11)$$

The transient energy function V is obtained from equation (2.7) by first establishing the n(n - 1)/2 relative acceleration equations, multiplying each of these by the corresponding relative velocity and integrat

i^3 to a

$$\sum$$

V =

The

identifia

tem is r

so it is

and the f

dissipate

use the te

integrating the sum of the resulting equations from a fixed s.e.p. (δ^s) to a variable upper limit [4]

$$\sum_{i=1}^{n-1} \sum_{j=i+1}^{n} M_i M_j (\dot{\omega}_i - \dot{\omega}_j)(\omega_i - \omega_j)$$

$$= \sum_{i=1}^{n-1} \sum_{j=i+1}^{n} (M_j P_i - M_i P_j)(\omega_i - \omega_j)$$

$$- \sum_{i=1}^{n-1} \sum_{j=i+1}^{n} (M_j P_{ei} - M_i P_{ej})(\omega_i - \omega_j) \qquad (2.12)$$

$$V = \sum_{i=1}^{n-1} \sum_{j=i+1}^{n} \Big[\frac{1}{2M_T} M_i M_j (\omega_i - \omega_j)^2 - \frac{1}{M_T} (P_i M_j - P_j M_i)(\delta_{ij} - \delta_{ij}^s)$$

$$- C_{ij}(\cos \delta_{ij} - \cos \delta_{ij}^s)$$

$$+ \int_{\delta_i^s + \delta_j^s - 2\delta_o^s}^{\delta_i + \delta_j - 2\delta_o} D_{ij} \cos \delta_{ij} d(\delta_i + \delta_j - 2\delta_o) \Big] \qquad (2.13)$$

The system transient energy components in equations (2.13) are identifiable. The first term is the kinetic energy. The second term is related directly to the rotor angle position of generators, so it is called position energy. The third term is magnetic energy and the fourth term is the dissipation energy, which is the energy dissipated in the network transfer conductances. It is common to use the term "potential energy" to indicate the last three terms.

To write t
the center of an
of angle accelera

$$V = \frac{1}{2}\sum_{i=1}^{n}$$

$$-\sum$$

$$-\int$$

where $\theta_{ij} = \theta_i -$

The physic
the transient st
fact that, for s
points are obtai
2.11 where $\overline{\ }_i =$
appropriate ini
systems because

For system
load will differ
a closed form ex
obtained. Many
tances, i.e., re
bus admittance

To write the energy function in a more convenient form using the center of angle variables, apply the above steps to the n center of angle acceleration equations (2.10)

$$V = \frac{1}{2}\sum_{i=1}^{n} M_i\tilde{\omega}_i^2 - \sum_{i=1}^{n} P_i(\theta_i - \theta_i^s)$$

$$-\sum_{i=1}^{n-1}\sum_{j=i+1}^{n}\Big[C_{ij}(\cos\theta_{ij} - \cos\theta_{ij}^s)$$

$$-\int_{\theta_i^s+\theta_j^s}^{\theta_i+\theta_2} D_{ij}\cos\theta_{ij}\,d(\theta_i + \theta_j)\Big] \qquad (2.14)$$

where $\theta_{ij} = \theta_i - \theta_j$.

The physical significance of the center of angle reference in the transient stability problem formulation is illustrated by the fact that, for systems without transfer conductances, the equilibrium points are obtained by solving n - 1 real power equations (2.10, 2.11 where $\tilde{\omega}_i = 0$, i = 1, 2, ..., n) for an n machine system, given appropriate initial angles [11]. This works satisfactorily for such systems because there is no change in load.

For systems with transfer conductances, however, the total load will differ from one operating point to another and therefore a closed form expression for the total system energy cannot be obtained. Many previous researchers have neglected transfer conductances, i.e., real part of the off-diagonal elements of the reduced bus admittance matrix, which depend not only on the transmission line resistances but

fore, these te

For trans

function as a c

energy term is

and the entire

angle space is

$$I_{ij} = \int$$

$$=$$

The tran

machine system

analogous to t

Consider

energy functio

is given by [1

$$V_{ci} = V \Bigg|$$

The fir

energy produc

area oabf of

resistances but also on loads modeled as constants impedances. Therefore, these terms can be large and in general cannot be neglected.

For transient stability assessment using the transient energy function as a direct method, an approximation to the conductance energy term is necessary since the conductance term is path dependent and the entire trajectory must be known. A linear trajectory in the angle space is assumed to express the integral term as

$$I_{ij} = \int_{\theta_i^s+\theta_j^s}^{\theta_i+\theta_j} D_{ij} \cos \theta_{ij} d(\theta_i + \theta_j)$$

$$= \frac{\theta_i + \theta_j - \theta_i^s - \theta_j^s}{\theta_i - \theta_j - \theta_i^s + \theta_j^s} \left[\sin \theta_{ij} - \sin \theta_{ij}^s\right] \cdot D_{ij} \qquad (2.15)$$

The transient energy function (2.13) or (2.14) for a two-machine system with the assumption of zero transfer conductance is analogous to the equal-area criterion.

Considering the situation at clearing time, the transient energy function, using the post-fault network and θ^{s1} as reference, is given by [13]:

$$V_{cl} = V \Big|_{\theta^{s1}}^{\theta^c} = \frac{1}{2} M(\tilde{\omega}^c)^2 - C_{12}(\cos \theta^c - \cos \theta^{s1}) - P_1(\theta^c - \theta^{s1}) \qquad (2.16)$$

The first term in the right hand side of (2.16) is the kinetic energy produced during the fault period and is proportional to the area oabf of Figure 2.1. The second and third terms add up to the

potential energy of the system during the fault which is associated with the (area cdfc - area oed). The clearing energy is thus the area

oabf + (cdfc - oed) .

The critical energy is evaluated from post-fault s.e.p. θ^{s2} to the u.e.p., θ^u. The velocity of the system at both θ^{s2} and θ^u is zero and thus the critical energy consists of only potential energy,

$$V_{cr} = V \Big|_{\theta^{s2}}^{\theta^u} \tag{2.17}$$

The right-hand side of (2.17) corresponds to the area cgf + cdf.

When V_{cr} use θ^{s2} as a reference [4], the transient energy function is not analogous to the equal area criteria. However, Fouad et al. in [13] argue that the critical energy should be evaluated. from θ^{s1} and thus a correction term of

$$V_{cor} = V \Big|_{\theta^{s1}}^{\theta^{s2}} \tag{2.18}$$

must be added to the critical energy, V_{cr}.

$$V'_{cr} = V_{cr} + V_{cor} = V \Big|_{\theta^{s2}}^{\theta^u} + V \Big|_{\theta^{s1}}^{\theta^{s2}} = V \Big|_{\theta^{s1}}^{\theta^u} \tag{2.19}$$

V'_{cr} then corresponds to the area dgcd - oed and contains the area cdfc - oed in addition to A_2. The V_{c1} in (2.16) contains area

cdfc - oed in addition to A_1. Thus, the condition $V_{cl} \leq V'_{cr}$ with the correction V_{cor} in V'_{cr} corresponds to the equal area criterion ($A_1 \leq A_2$). The critical energy can be found for multimachine power systems by computing the proper u.e.p. θ^u and knowing initial operating point θ^{s1}.

2.2.3. The Conservative Nature of Classical Lyapunov Methods

Unstable Equilibrium Point (UEP) Method. In a large interconnected network a fault followed with or without line switching will result in a mode of stability which is different for different fault locations in the system even though the post-fault configuration may be the same. For a given post-fault configuration, there are several singular points among which one is s.e.p. and others are u.e.p. or saddle points. Depending on the location of fault, severity, and type of fault, the post-fault trajectory if cleared at $t = t_{cc}$ will pass in the vicinity of one among the saddle points.

It is not possible to find a unique closed surface (boundary) in the state space separating stable and unstable regions which will give accurate results for all faults. In the past, the critical value was obtained as Min $V(\underline{X})$ evaluated at all the saddle points. Fouad [13] and Athey [14] showed that for $t = t_{cc}$, the post-fault trajectory just becomes unstable and theoretically passes through but practically approaches very close to the u.e.p. for a specific fault. The critical energy (boundary) is defined as the energy of the system when the post-fault trajectory passes very close to the u.e.p. For different fault conditions, there is a different fault trajectory and

critical energ

machine case.

A method

2^{n-1} (for n ma

without transf

equilibrium po

can be used su

solving n - 1

for an n machi

guess for the

fault stable e

$$\theta_j^u = \left\{ \begin{array}{l} \theta_j^s \\ \\ - \end{array} \right.$$

If the set of

initial guess

$$\theta_j^u = \left\{ \begin{array}{l} \\ \\ \end{array} \right.$$

This works sa

since the sta

change in loa

For syst

u.e.p. will di

trajectory and a different u.e.p., and therefore the computation of critical energy for each fault is a difficult problem in the multimachine case.

A method of selecting the proper u.e.p. from the possible 2^{n-1} (for n machine system) has been suggested in [14]. For systems without transfer conductances, the calculation of the unstable equilibrium points using a Newton-Raphson or Gauss Siedel technique can be used successfully. The recommended procedure consists of solving n - 1 real power equations (2.10) having $\dot{\omega}_i = 0$, $i = 1, \ldots, n$ for an n machine system with one reference machine. An initial guess for the u.e.p. for machine i going unstable given the postfault stable equilibrium point θ^{s2} is

$$\theta_j^u = \begin{cases} \theta_j^{s2} & j \neq i \\ \pi - \theta_j^{s2} & j \neq i \end{cases} \tag{2.20}$$

If the set of generators $\{i_k\}_{k=1}^{K}$ are assumed to go unstable, the initial guess for the unstable equilibrium point is

$$\theta_j^u = \begin{cases} \theta_j^{s2} & j \neq i_1, i_2, \ldots, i_k \\ \pi - \theta_j^{s2} & j = i_1, i_2, \ldots, i_k \end{cases} \tag{2.21}$$

This works satisfactorily for systems without transfer conductances since the starting values are close to the solution, and there is no change in load.

For systems with transfer conductances, the total load at a u.e.p. will differ from that at the s.e.p. The difference will be alloca

instal

is the

automa

not re

this (

the p

occur

based

allocated to the reference generator bus resulting in a substantial mismatch. The scalar function J, defined by

$$J \triangleq \sum_{i=1}^{n} \left(P_i - P_{ei} - \frac{M_i}{M_T} P_{COA}\right)^2 \tag{2.22}$$

is the objective function whose minimization provides an alternative approach to the calculation of the u.e.p. Even this algorithm does not readily converge based on the initial guess given above and in this case the angle from the transient stability simulation when the potential energy is maximum is used.

Having selected the proper u.e.p. and computed it, the procedure used to test for whether the system is stable or unstable is based on

$$V_{cr} = V_{PE}(\theta^u) = V_{PE}\Big|_{\theta^{s1}}^{\theta^u} = -\sum_{i=1}^{n} P_i(\theta_i^u - \theta_i^{s1})$$

$$+\sum_{i=1}^{n-1}\sum_{j=i+1}^{n}\Big[C_{ij}(\cos\theta_{ij}^{s1} - \cos\theta_{ij}^{u})$$

$$+ D_{ij}\frac{\theta_i^u + \theta_j^u - \theta_i^{s1} - \theta_j^{s1}}{\theta_i^u - \theta_j^u - \theta_i^{s1} + \theta_j^{s1}}(\sin\theta_{ij}^u - \sin\theta_{ij}^{s1})\Big] \tag{2.23}$$

when

For

stab

ener

the

mach

pote

stab

poin

cons

face

t >

trade

and c

value

$$V_{cl} = V(\theta^c) = V \Big|_{\theta^{s1}}^{\theta^c} = \frac{1}{2}\sum_{i=1}^{n} M_1 \tilde{\omega}_i^{c^2} - \sum_{i=1}^{n} P_i(\theta_i^c - \theta_i^{s1})$$

$$+ \sum_{i=1}^{n-1} \sum_{j=i+1}^{n} \Big[C_{ij}(\cos \theta_{ij}^{s1} - \cos \theta_{ij}^{c})$$

$$+ D_{ij} \frac{\theta_i^c + \theta_j^c - \theta_i^{s1} - \theta_j^{s1}}{\theta_i^c - \theta_j^c - \theta_i^{s1} + \theta_j^{s1}} (\sin \theta_{ij}^c - \sin \theta_{ij}^{s1}) \Big] \qquad (2.24)$$

where D_{ij} and C_{ij} are the parameters of the post-fault network. For $V_{cr} \geq V_{cl}$ system is stable and for $V_{cr} < V_{cl}$ system loses stability.

Potential Energy Boundary Surface (PEBS) Method. The potential energy boundary surface method [3] is an abstraction which examines the potential energy function $V_{PE}(\theta)$ in the angle space for a multi-machine power system. For a three machine system, the corresponding potential energy surface is shown in Figure 2.2 as are the actual stable and unstable system trajectories and the corresponding saddle points. The line joining the saddle points and orthogonal to the constant V_p contours is known as the potential energy boundary surface (PEBS) (dotted line). A faulted trajectory if cleared at $t > t_{cc}$ will cross the PEBS at some point on the curve. The critical trajectory (fault cleared at $t = t_{cc}$) will just touch the boundary but does not cross it. The value of V_{cr} can be taken to be the value of $V_{PE}(\underline{\theta}^B)$ (2.23) for a fault-on trajectory at the point θ^B

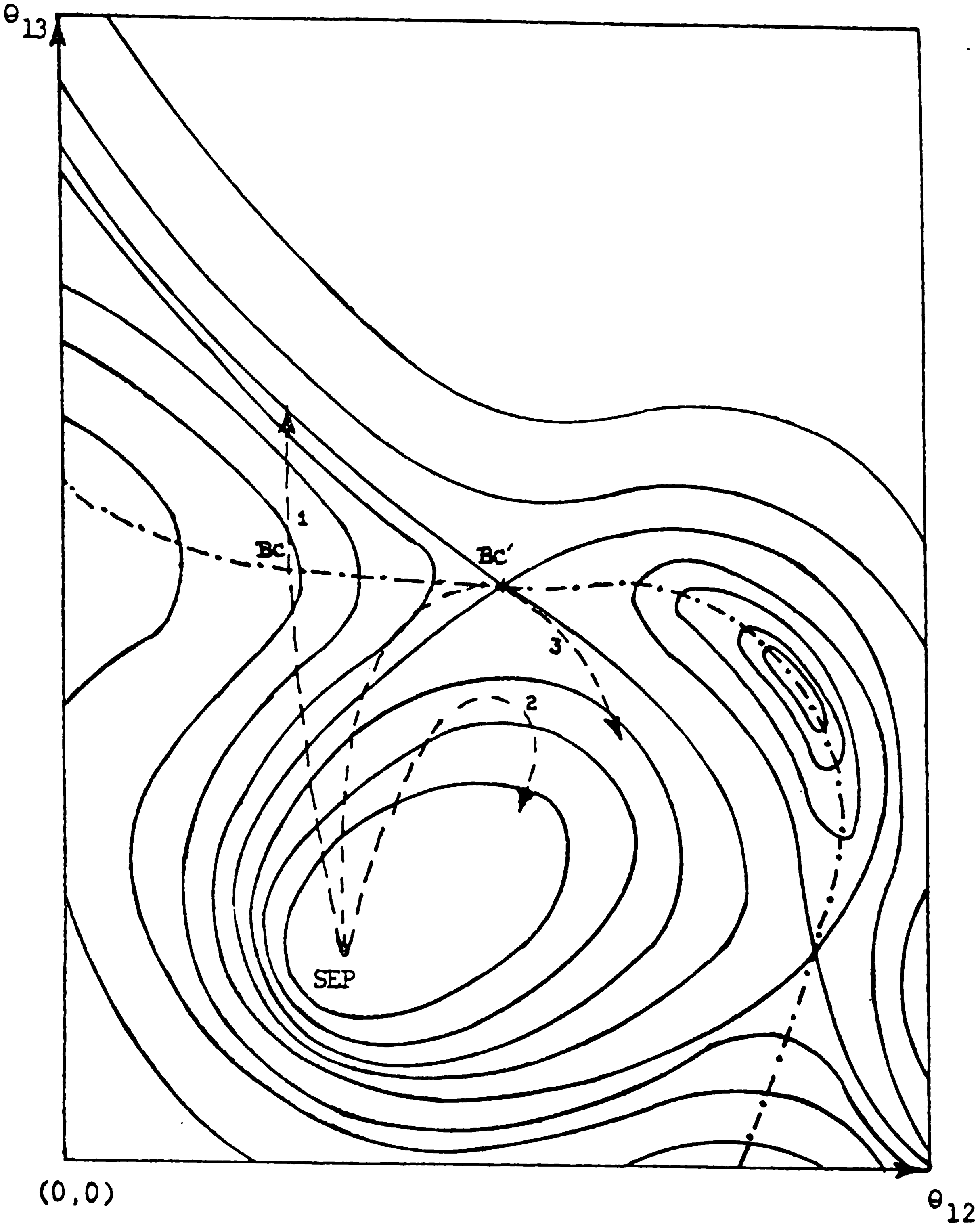
θ13
Bc
Bc′
1
2
3
SEP
(0,0)
θ12

Figure 2.2. Stable, unstable, and critical trajectory for a three-machine system.

when it crosses the PEBS. At the PEBS crossing, $V_{PE}(\theta^B)$ has a relative maximum and $V_k(\tilde{\omega})$, kinetic energy, has a relative minimum which is near zero and assumed to be zero in this method. This is the Kakimoto method [3] of detecting PEBS crossing. The stability of the system is determined by the following comparisons:

(1) If $V(\theta^c) \leq V_{cr} = V_{PE/max}$, then the system is stable.

(2) If $V(\theta^c) > V_{cr} = V_{PE/max}$, then the system is unstable.

Computational experience [8] indicates that the PEBS method of computing V_{cr} is extremely fast and results are reliable and accurate for only first swing stability cases.

In the latest effort on transient stability analysis, it is claimed that the kinetic and potential energies of the "individual" machines (and not the "total" energy) must be considered for accurately estimating the stability boundary (critical clearing time). The next chapter is denoted to derivation, discussion, and comparison of the individual energy function derived by two different methods.

In

develop

methods.

energy a

Several

ified,

(

with mi

(

(

for a

I

based

larger

clearin

gated

stabili

step, t

CHAPTER 3

INDIVIDUAL ENERGY FUNCTION AND ITS APPLICATION IN TRANSIENT STABILITY ASSESSMENT

3.1. Introduction

In Chapter 2 an attempt was made to investigate the recent development in assessment of transient stability by Lyapunov's direct methods. The concept of potential energy boundary surface [4] and energy accounting of the total system energy [13] was introduced. Several stability criteria based on "total" system energy were identified, and the boundary energy V_{cr} was calculated alternatively by

(1) computing the energy at the lowest saddle point (u.e.p. with minimum energy) θ^u;

(2) computing the energy at the u.e.p. θ^u closest to trajectory;

(3) computing the value of the potential energy of the system for a fault-on trajectory when it crosses the PEBS boundary.

It was pointed out that the region of stability evaluated based on total system energy produces conservative results. For a larger and more accurate region of stability and boundary (critical clearing time), the stability of the power system must be investigated in terms of the energy components that truly reflect loss of stability for a particular fault and post-fault network. As a first step, the separation of the total system energy into "within" and

"between" cone
potential ener
group of gener
machine or in
The "within"
energy within
the PEBS and
accurate if
energy are ac
boundary sur

The mos
determinatio
by the criti
machine is i
bility of th
vidual machi
generator de
(3) appropri
the region c
equal area c
region of st
methodology
in Chapter 4
stability fo
machine powe

"between" coherent group energies was considered. The kinetic and potential energy between the accelerated group and the stationary group of generators, which can be considered an equivalent single machine or infinite bus, was considered as the "between" group energy. The "within" group energy was defined as the kinetic and potential energy within both the stationary and accelerated groups. Although the PEBS and UEP methods described in the previous chapter are more accurate if the between group and within group kinetic and potential energy are accounted for at clearing time and at the potential energy boundary surface, the results are still conservative.

The most recent work [16,29] indicates that a much more precise determination of the region of stability and the boundary (defined by the critical clearing time) can be made if (1) an individual machine is identified as the critical generator upon which the stability of the system depends for a particular fault; (2) an individual machine energy function is defined and then developed for the generator determined as critical for the particular fault; and (3) appropriate methods are developed for defining the boundary of the region of stability. These methods are developed based on the equal area criterion which precisely determines the boundary of the region of stability for the single machine infinite bus model. The methodology based on (1)-(3) above is shown via computational results in Chapter 4 to precisely determine the boundary of the region of stability for a particular fault for several fault cases on a multimachine power system model.

The
methods fo
a particul
tively, as
that dete
fault and
Section 3
generator

For
ter 2, ar
transient
sient ene
have used
lowing tw
energy fu
(i)
matical m
the ith p
generator

M_i

Integrati
$t = t_{si}$ w

The individual machine energy function is derived and the methods for determining the boundary of the region of stability for a particular fault are developed in sections 3.2 and 3.3, respectively, assuming knowledge of how to identify the critical generator that determines stability or loss of stability for a particular fault and for which the individual machine energy function is written. Section 3.4 then develops a procedure for identifying the critical generator.

3.2. Transient Energy of Individual Machines

For the classical model described in section (2.2.2) of Chapter 2, an expression will be derived for the individual machine transient energy. Some energy functions describe the system transient energy using a synchronous frame of reference [9, 12]. Others have used a center of inertia (COI) formulation [13]-[15]. The following two subsections describe the derivation of the individual energy function with these two different reference frames:

(1) Center of Inertia (COI) Reference. Consider the mathematical model described by equations (2.10) in Chapter 2. Multiply the ith post-fault swing equation (equation of motion of critical generator by $\dot{\theta}_i$ to obtain

$$M_i \dot{\tilde{\omega}}_i \dot{\theta}_i = (P_i - P_{e_i} - \frac{M_i}{M_T} P_{COI}) \dot{\theta}_i \tag{3.1}$$

Integrating (3.1) with respect to time, using as a lower limit $t = t_{s1}$ where $\tilde{\omega}^{s1} = 0$ and $\theta(t_{s1}) = \theta^{s1}$ is the s.e.p., yields

$\frac{1}{2}$V

the equiva

V_j

This intro

the value

them in

with re

consider

be expres

V_i

Sin

tion of γ

analytical

$$\frac{1}{2} M_i\tilde{\omega}_i^2 = P_i(\theta_i - \theta^{s1}) - \sum_{\substack{j=1 \\ j\neq i}}^{n} \int_{\theta_i^{s1}}^{\theta_i} C_{ij} \sin \theta_{ij} d\theta_i$$

$$- \sum_{\substack{j=1 \\ j\neq i}}^{n} \int_{\theta_i^{s1}}^{\theta_i} D_{ij} \cos \theta_{ij} d\theta_i - \frac{M_i}{M_T} \int_{\theta_i^{s1}}^{\theta_i} P_{COA} d\theta_i \qquad (3.2)$$

or equivalently the total energy of the ith unit is,

$$V_i = \frac{1}{2} M_i\tilde{\omega}_i^2 - P_i(\theta_i - \theta_i^{s1}) + \sum_{\substack{j=1 \\ j\neq i}}^{n} \int_{\theta_i^{s1}}^{\theta_i} C_{ij} \sin \theta_{ij} d\theta_i$$

$$+ \sum_{\substack{j=1 \\ j\neq i}}^{n} \int_{\theta_i^{s1}}^{\theta_i} D_{ij} \cos \theta_{ij} d\theta_i + \frac{M_i}{M_T} \int_{\theta_i^{s1}}^{\theta_i} P_{COA} d\theta_i \qquad (3.3)$$

$$i = 1, 2, \ldots., n$$

This integral is evaluated using the values of θ_i, θ_j, $\tilde{\omega}_i$, and using the values C_{ij}, D_{ij}, and θ_i^{s1} for the post-fault network. The first term in the right-hand side of (3.3) is the kinetic energy of machine i with respect to the system inertial center. It is customary to consider the remaining terms as a potential energy. Thus (3.3) can be expressed as

$$V_i = V_{KE_i} + V_{PE_i} \qquad (3.4)$$

Since (3.3) contains path dependent integrals, the verification of V_i as being Lyapunov function cannot readily be determined analytically in closed form, and the transient stability analysis

using this energy function requires simulation of system trajectory for critical generator. The above derivation of the individual energy function can be found in [16].

(2) Synchronous Reference. Consider the mathematical model described by equations (2.7) in Chapter 2. For generator i (being known as critical generator) and an arbitrary generator j (j = 1, 2, ... i-1, i+1, ..., n) the equations of motions of these generators are written as

$$\begin{cases} M_i\dot{\omega}_i = P_i - P_{ei} \\ M_j\dot{\omega}_j = P_j - P_{ej} \end{cases} \tag{3.5}$$

Multiplying first the equation of generator i(j) by moment of inertia of the other generator $M_j(M_i)$ and then subtracting these equations from each other results in (3.6)

$$M_iM_j(\dot{\omega}_i - \dot{\omega}_j) = (M_jP_i - M_iP_j) - (M_jP_{ei} - M_iP_{ej}) \tag{3.6}$$

$$j = 1, \ldots, n \quad j \neq i$$

Equation (3.6) represents the equation of motion of the relative velocity of generator i with generator j. Multiplying (3.6) by $(\omega_i - \omega_j)$ and adding these new n - 1 equations to each other yields

$$\sum_{\substack{j=1 \\ j \neq i}}^{n} M_i M$$

$$-$$

Integrating (3

$t = t_{s1}$ where

tion of critica

$$V_i = \frac{M_i}{\Sigma M}$$

$$-$$

$$+$$

This re

in [29], conta

trajectory si

system. Howe

is the energy

separation, a 1

$$\sum_{\substack{j=1\\ j\neq i}}^{n} M_i M_j(\dot{\omega}_i - \dot{\omega}_j)(\omega_i - \omega_j) = \sum_{\substack{j=1\\ j\neq i}}^{n} (M_j P_i - M_i P_j)(\omega_i - \omega_j)$$

$$- \sum_{\substack{j=1\\ j\neq i}}^{n} (M_j P_{ei} - M_i P_{ej})(\omega_i - \omega_j) \tag{3.7}$$

Integrating (3.7) with respect to time, using as a lower limit $t = t_{s1}$ where $\omega^{s1} = 0$ and $\delta(t_{s1}) = \delta^{s1}$, results in the energy function of critical generator i

$$V_i = \frac{M_i}{2M_T} \sum_{\substack{j=1\\ j\neq i}}^{n} M_j(\omega_i - \omega_j)^2 - \frac{1}{M_T} \sum_{\substack{j=1\\ j\neq i}}^{n} (P_i M_j - P_j M_i)(\delta_{ij} - \delta_{ij}^{s1})$$

$$- \sum_{\substack{j=1\\ j\neq i}}^{n} C_{ij}(\cos \delta_{ij} - \cos \delta_{ij}^{s1})$$

$$+ \int_{\delta_i^{s1}+\delta_j^{s1}-2\delta_o^{s1}}^{\delta_i+\delta_j-2\delta_o} D_{ij} \cos \delta_{ij} d(\delta_i + \delta_j - 2\delta_o) \tag{3.8}$$

This representation of the individual energy function, derived in [29], contains only one path dependent integral and requires trajectory simulation for the transient stability analysis of the system. However, in order to obtain the critical energy V_{cr}, which is the energy at the u.e.p. corresponding to the actual boundary of separation, a linear trajectory in the angle space is assumed. This allows t

limits a

$\int$

Th

of seve

tion is

Th

potentia

could b

energy

justifie

sient s

On

is by co

saddle p

based on

discusse

sidered t

allows the term in (3.8) to be analytically evaluated between the limits δ^{s1} and δ^{u} with the expression given in (3.8a)

$$\int_{\delta_i^{s1}+\delta_j^{s1}-2\delta_o^{s1}}^{\delta_i^{u}+\delta_j^{u}-2\delta_o^{u}} D_{ij} \cos \delta_{ij} d(\delta_i + \delta_j - 2\delta_o)$$

$$= D_{ij} \frac{\delta_i^u + \delta_j^u - \delta_i^{s1} - \delta_j^{s1}}{\delta_i^u - \delta_j^u - \delta_i^{s1} + \delta_j^{s1}} (\sin \delta_{ij}^u - \sin \delta_{ij}^{s1}) \qquad (3.8a)$$

Testing the above technique of transient stability assessment on several moderately large power systems showed that the approximation is quite acceptable.

The stability criteria based on the total system kinetic and potential energy for assessing the region of stability of the system could be applied to the individual generator kinetic and potential energy function with more accurate results. The following section justifies the idea of using the individual energy function in transient stability assessment of the power system.

3.3. Analytical Justification of Using the Critical Energy of Individual Machines for Transient Stability Assessment

One way of assessing the transient stability of a power system is by comparison of the critical energy, the energy at the lowest saddle point, with the clearing energy V_{cl}. A second method is based on the concept of potential energy boundary surface (PEBS) as discussed in Chapter 2. In this method the critical energy is considered to be the potential energy at the crossing of the total system trajec

the region of

larger than t

lowest saddle

based on sim

regions of de

Theorem

region R = {Y

V(Y) be the de

f(0) = 0. If

in R, then

(1) the

and

(2) eve

the origin as

To obtai

use of the the

hypotheses of

shown that the

group of machine

proceeding to t

priate to show

satisfied for t

of the total sys

proven when the

system trajectory and the PEBS. It was pointed out previously that the region of stability obtained by the application of the PEBS is larger than the one resulting by consideration of the energy at the lowest saddle point. Theoretically, these different approaches are based on similar Lyapunov stability theorems but with different regions of definiteness. This is clarified by the following theorem.

Theorem--Let $V(\underline{X})$ be a scalar function. Suppose that the region $R = \{\underline{X} | V(\underline{X}) < k\}$ which contains the origin is bounded. Let $\dot{V}(\underline{X})$ be the derivative of $V(\underline{X})$ along the solutions of $\dot{\underline{X}} = f(\underline{X})$; $f(\underline{0}) = 0$. IF $V(\underline{X})$ is positive definite and $\dot{V}(\underline{X})$ negative definite in R, then

(1) the origin is an asymptotically stable equilibrium state, and

(2) every solution of $\dot{\underline{X}} = f(\underline{X})$ starting in R converges to the origin as $t \to \infty$.

To obtain the best estimate for the domain of attraction by the use of the theorem, one chooses the largest value $k = \hat{k}$ for which the hypotheses of this theorem are satisfied. In the following, it is shown that the individual machine energy function of the critical group of machines does satisfy the hypotheses of the theorem. But before proceeding to the proof for the critical group of machines, it is appropriate to show how the conditions of the theorem can be shown to be satisfied for the total system energy function. The sign definiteness of the total system energy function V and its derivative $\dot{V}$ cannot be proven when the transfer conductance term is included in V [14, 18].

However, the total system energy function restricted to a suitably small region of interest can be shown to be positive. The derivative of this total system energy function without mechanical damping is zero for $t \geqq t_c$ based on simulation results for all system trajectories. This observation is then coupled with a proof that the effect of the mechanical damping is negative definite to suggest that $\dot{V}(\underline{X}) \leqq 0$. This same "proof" has been attempted for the individual energy function. This proof is now outlined and then shown to be incorrect. This suggests that the individual energy may not be a Lyapunov function and thus that one may not be able to apply normal Lyapunov theory to establish a region of convergence. The excellent computational results obtained using the individual energy function and the physical understanding of how loss of stability occurs in relation to the individual energy function are the basis for using it at this point in its development.

Consider the mathematical model including the mechanical damping

$$M_i \dot{\omega}_i = P_i - P_{ei} - D_i \omega_i$$

where D_i presents the mechanical damping for i = 1, 2, ..., n.

Writing the equation of motion in terms of center of angle results in (3.9)

$$M_i \dot{\tilde{\omega}}_i = (P_i - P_{ei} - D_i \omega_i) - \frac{M_i}{M_T} P_{COA} + \frac{M_i}{M_T} \sum_{j=1}^{n} D_j \omega_j$$

$$= (P_i - P_{ei} - \frac{M_i}{M_T} P_{COA}) - (D_i \omega_i - \frac{M_i}{M_T} \sum_{j=1}^{n} D_j \omega_j) \qquad (3.9)$$

From (3

time derivati

$$-\sum_{i=1}^{n} [$$

$$=$$

The right-han

$$-\sigma < -$$

Conditi

derivative of

is zero resu

indeed negat

to estimate a

taken in this

the negative

(1) to

small subregi

(2) to

in simulation

function is z

(3) to

conditions is

of the energy

From (3.9) the contribution of the mechanical damping to the time derivative of the energy function is

$$-\sum_{i=1}^{n}\left[D_i\omega_i - \frac{M_i}{M_T}\sum_{j=1}^{n} D_j\omega_j\right]\tilde{\omega}_i$$

$$= -\left[\sum_{i=1}^{n} D_i\omega_i\tilde{\omega}_i - 0\right] = -\left[\sum_{i=1}^{n} D_i\omega_i^2 - \sum_{i=1}^{n} D_i\omega_i\omega_o\right] \quad (3.10)$$

The right-hand side of (3.10) is negative, if

$$\omega_o < \omega_i \qquad i = 1, 2, \ldots., n \qquad (3.11)$$

Condition (3.11) and the fact that (from simulation) the time derivative of energy function of a model without mechanical damping is zero results in $\dot{V} < 0$. If V is indeed positive definite and $\dot{V}$ is indeed negative definite, one is able to apply an invariance theory to estimate a larger region of stability. In summary, the steps taken in this analysis [16] of the positive definiteness of V and the negative definiteness of $\dot{V}$ are

(1) to show that the energy function is positive in a suitable small subregion;

(2) to suggest that the constant energy of the undamped system in simulation results indicates the time derivative of the energy function is zero; and

(3) to suggest that the contribution of damping under certain conditions is negative and thus results in a negative time derivative of the energy function.

able
deri
to th
does
There
Figur
betwe
of th
the p
the s
betwe
natur
and 3
deri
not a
invar
algor
made

stabi
justif
3.3.1
the ve
ing th

Despite the above argument outlined from [16], one is not able to make any judgment on the sign definiteness of the time derivative of the individual machine energy function. In contrast to the case of the total system energy, the individual machine energy does not maintain a constant value after the fault clearing time. There is always a transfer of energy back and forth between machines. Figure 3.1a illustrates the sum of the potential energy produced between generators 5 and 6 (critical group) and all of the generators of the stationary group. Figure 3.1b depicts two plots: one for the potential energy produced between generator 5 and the rest of the system, and a similar one for the partial potential energy between generator 6 and the rest of the system. The oscillatory nature of the potential energy of the critical group in Figures 3.1a and 3.1b clearly displays the nondefinite behavior of the time derivative of the energy. Thus, the individual energy function is not a Lyapunov function for weakly damped systems and thus the invariant theorem cannot be used as the theoretical basis of the algorithm developed in later sections even though the argument was made in [16].

These algorithms need not be justified based on Lyapunov stability theory because there are sound physical arguments for justifying these algorithms, which are presented in the subsections 3.3.1 and 3.3.2 for the PEBS and equal area methods. Furthermore, the very high accuracy of the algorithm in predicting critical clearing times based on application to several fault cases on different

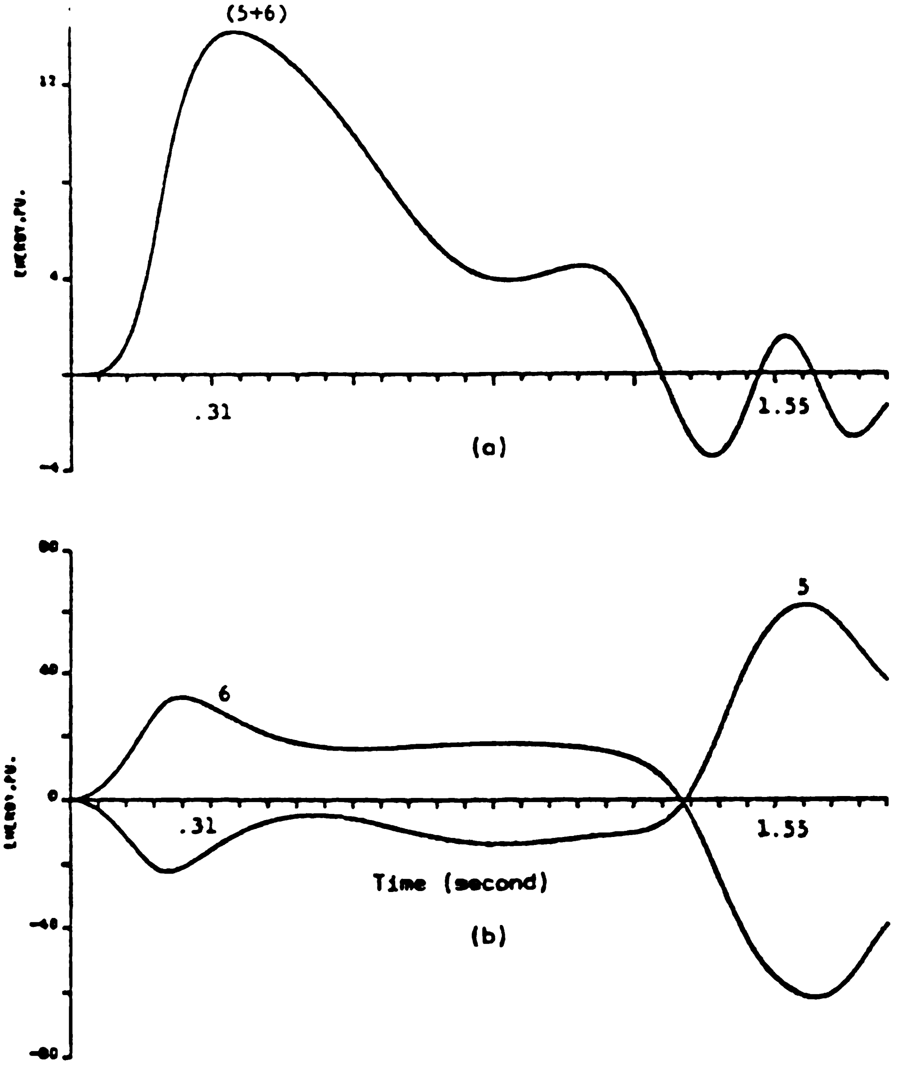

Figure 3.1. Partial energy analysis. Clearing time = .1922 seconds.
(a) Sum of partial energies for generators 5 and 6.
(b) Partial energy for generators 5 and 6.

power s
criteri

3.3.1.

By
of the
orthogo
saddle p
ary surf
PEBS, th
boundary
is approx
PEBS. If
surface,
maximum a
the point
The magni
when the
clearing t
the PEBS,
larger tha
PEBS.

The a
for the tot
function de
fault [16,

power system data bases further justifies the algorithm and stability criteria based on the individual generator energy function.

3.3.1. Potential Energy Boundary Surface (PEBS) Method

By making use of total system energy functions, the boundary of the region of stability is determined by hypersurfaces which are orthogonal to the equipotential surfaces and which pass through the saddle points. These hypersurfaces form the principal energy boundary surface (PEBS) as shown in Figure 2.2 in Chapter 2. At the PEBS, the potential energy for the system is maximum, and on the boundary of the region of stability, the total energy of the system is approximately equal in magnitude to the potential energy at the PEBS. If the system trajectory never crosses the potential energy surface, since it is stable, the potential energy should reach a maximum and the kinetic energy should reach a minimum at or near the point where the trajectory most closely approaches the PEBS. The magnitude of this maximum potential energy for the trajectory, when the fault is cleared at a clearing time t_c less than the critical clearing time t_{cc}, should then be less than the potential energy at the PEBS, since the potential energy for points along the PEBS are larger than points in the region of stability near but not at the PEBS.

The above properties of the potential energy boundary surface for the total energy function are also true for the individual energy function defined for the critical generator for the particular fault [16, 18]. Moreover, it was suggested in [16] that the

individual machine potential energy for the critical generator will be nearly constant for all points on the PEBS.

The results in Chapter 4 suggest that the potential energy at the point on the PEBS when the fault clearing time t_c equals t_{cc} is significantly larger than the points on the PEBS crossed by the system trajectory when $t_c > t_{cc}$. A method for determining stability requires the determination of the maximum potential energy along the trajectory for a particular fault as a function of clearing time. The clearing time at which this function is maximum is the critical clearing time t_{cc} and the system is stable if $t_c \leqq t_{cc}$. A second method, which is not as accurate, uses the potential energy at the PEBS for a fault on trajectory as the critical energy V_{cr} based on the incorrect assumption that the energy along the PEBS is constant. This method may not be accurate in determining t_{cc} or determining whether the system is stable or not if the peak potential energy along the trajectory is greater than this value of V_{cr}. However, the method will determine whether the system is stable if the peak potential energy along the trajectory is less than V_{cr} since at this value the trajectory never reaches the potential energy boundary surface. Figure 3.2 indicates selecting V_{cr} as the value of the potential energy at the PEBS for a fault on trajectory results in an interval around t_{cc} where stability or loss of stability cannot be determined. However, for development of fast on-line stability assessment by operators, this interval of uncertainty appears to be

Figure 3.2. Stable
machin

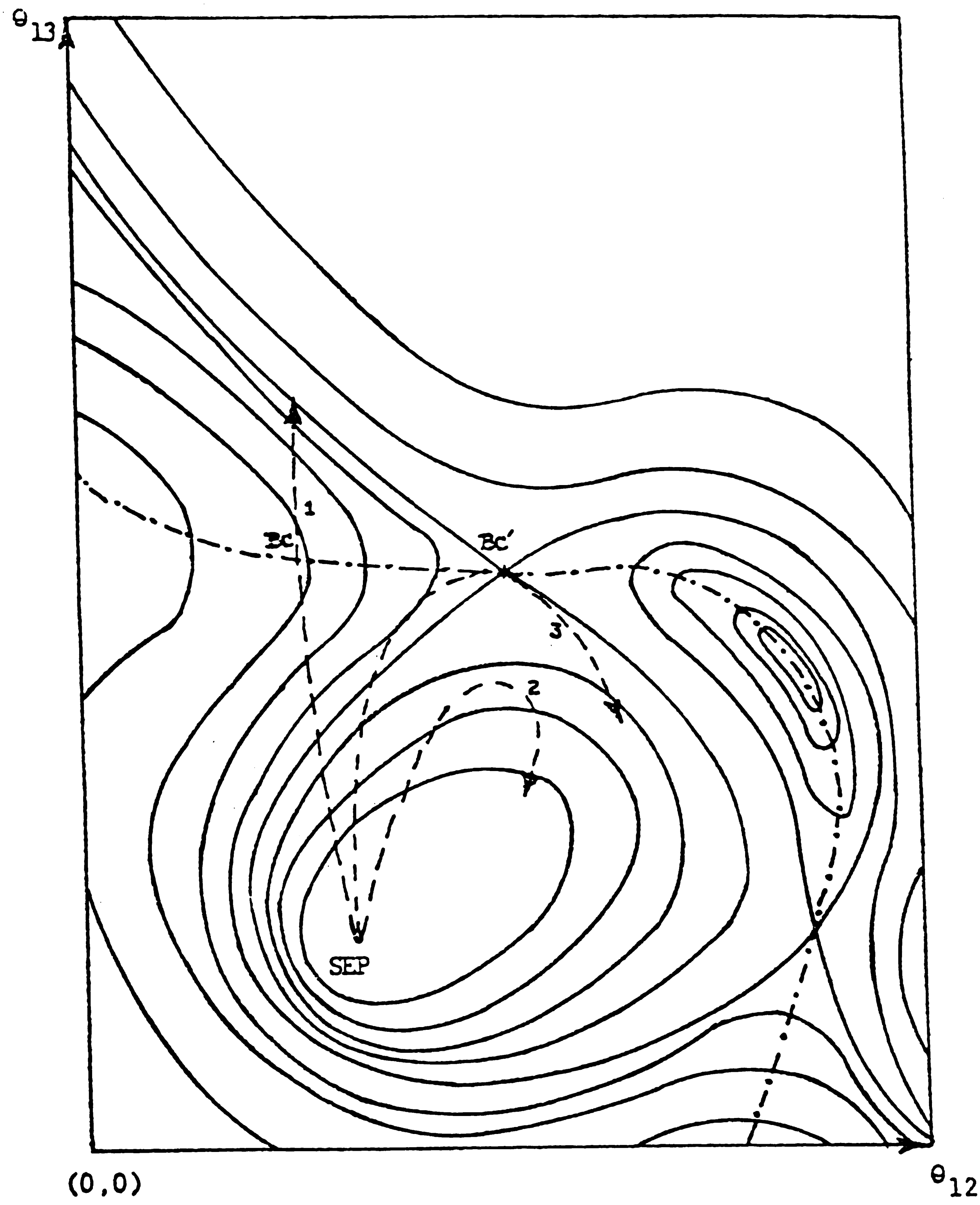
θ_{13}
1
Bc
Bc′
3
2
SEP
(0,0)
θ_{12}

Figure 3.2. Stable, unstable, and critical trajectory for a three-machine system.

accept

more l

transi

outlin

t^{si}, t

all i,

$t_c > t$

values

acceptable in terms of the accuracy required in determining t_{cc} or more likely the stability for a particular fault.

The procedure for transient stability assessment using the transient energy of individual machines (or groups of machines) is outlined below:

(1) For the post-fault network, the stable equilibrium point δ^{s1}, the admittance matrix Y_{BUS}, and the parameters C_{ij} and D_{ij} for all i, j = 1, ..., n are determined.

(2) For the particular fault and a fault on trajectory where $t_c > t_{cc}$, using the special computer program compute the energy values

$$V_i = \frac{M_i}{2M_T}\sum_{\substack{j=1\\ j\neq i}}^{n} M_j(\omega_i - \omega_j)^2 - \frac{1}{M_T}\sum_{\substack{j=1\\ j\neq i}}^{n} (P_iM_j - P_jM_i)(\delta_{ij} - \delta_{ij}^{s1})$$

$$-\sum_{\substack{j=1\\ j\neq i}}^{n} C_{ij}(\cos\delta_{ij} - \cos\delta_{ij}^{s1}) + D_{ij}\,\frac{\delta_i + \delta_j - \delta_i^{s1} - \delta_j^{s1}}{\delta_i - \delta_j - \delta_i^{s1} + \delta_j^{s1}}$$

$$\cdot\,(\sin\delta_{ij} - \sin\delta_{ij}^{s1}) \qquad (3.12)$$

for i = 1, 2, ..., n along the faulted trajectory at every time interval Δt.

(3) By examining the value of $V_i = V_{PE_i} + V_{KE_i}$ and its components at each time step, determine the value of V_i where V_{PE_i} has maximum value and the value of V_{KE_i} is near zero (this particular value of energy V_i is called the critical energy and defined as $V_{i/critical} = V_{PE_{i/max}}$) and store for each fault location.

(4) Repeat step (3) for the same fault for the particular clearing time $t_c < t_{cc}$ to be investigated and determine the maximum potential energy along this trajectory and let this value of maximum potential energy be denoted as $V_{i/t=t_c}$.

(5) Check for the stability of the machine i. If $V_{i/t=t_c} \leq V_{i/critical}$, machine i is stable, and if $V_{i/t=t_c} > V_{i/critical}$ machine i would be unstable.

3.3.2. Local Equal Area Criterion

The second method for determining the region of stability boundary of stability for a multimachine power system is based on the well-known "equal-area criterion" of one machine infinite bus systems. The local equal-area method is an extension of equal-area criterion in the sense that a particular machine of the critical group is considered against the rest of the generators in the power system. Then by comparison of the energy transfers between this particular generator and the rest of the system during and after the fault period, a decision on the stability of the entire power system is made for a fault at or near this generator. The discussion conc

next

crite

crite

where

Consi

ing t

durin

P_2 si

syste

fault

tivel

match

elect

inert

power

with

the e

mechan

The cr

concerning determination of the critical generator is left to the next section. In order to clarify the concept of this equal-area criterion applied to a multimachine power system, the equal-area criterion applied to a single machine infinite bus is reviewed.

For the one-machine infinite bus model,

$$M\dot{\omega} = P_m - P_e \tag{3.13}$$

where

$$P_e = \frac{E_1E_2}{X_{12}} \sin \delta = C \sin \delta \tag{3.14}$$

Consider the power angle representation P_e of Figure 3.3 illustrating the behavior of the single machine against the infinite bus during the transition from one state to another where $P_0 \sin \delta$, $P_2 \sin \delta$, and $P_1 \sin \delta$ represent the electrical real power of the system before the occurrence of the fault (pre-fault), during the fault period and after the fault is cleared (post-fault), respectively. The area A_1 in Figure 3.3a which is obtained from the mismatch of power existing between the mechanical input and the faulted electrical output, represents the kinetic energy of the generator's inertia that resulted from the fault that reduced the electrical power P_e below mechanical input power P_m. The area A_1 is compared with a critical energy A_2, which is shown in Figure 2.1 and represents the energy capacity of the transmission network for a particular mechanical power P_m, network configuration and fault clearing time. The critical energy A_3 shown in Figure 3.3a is the amount of

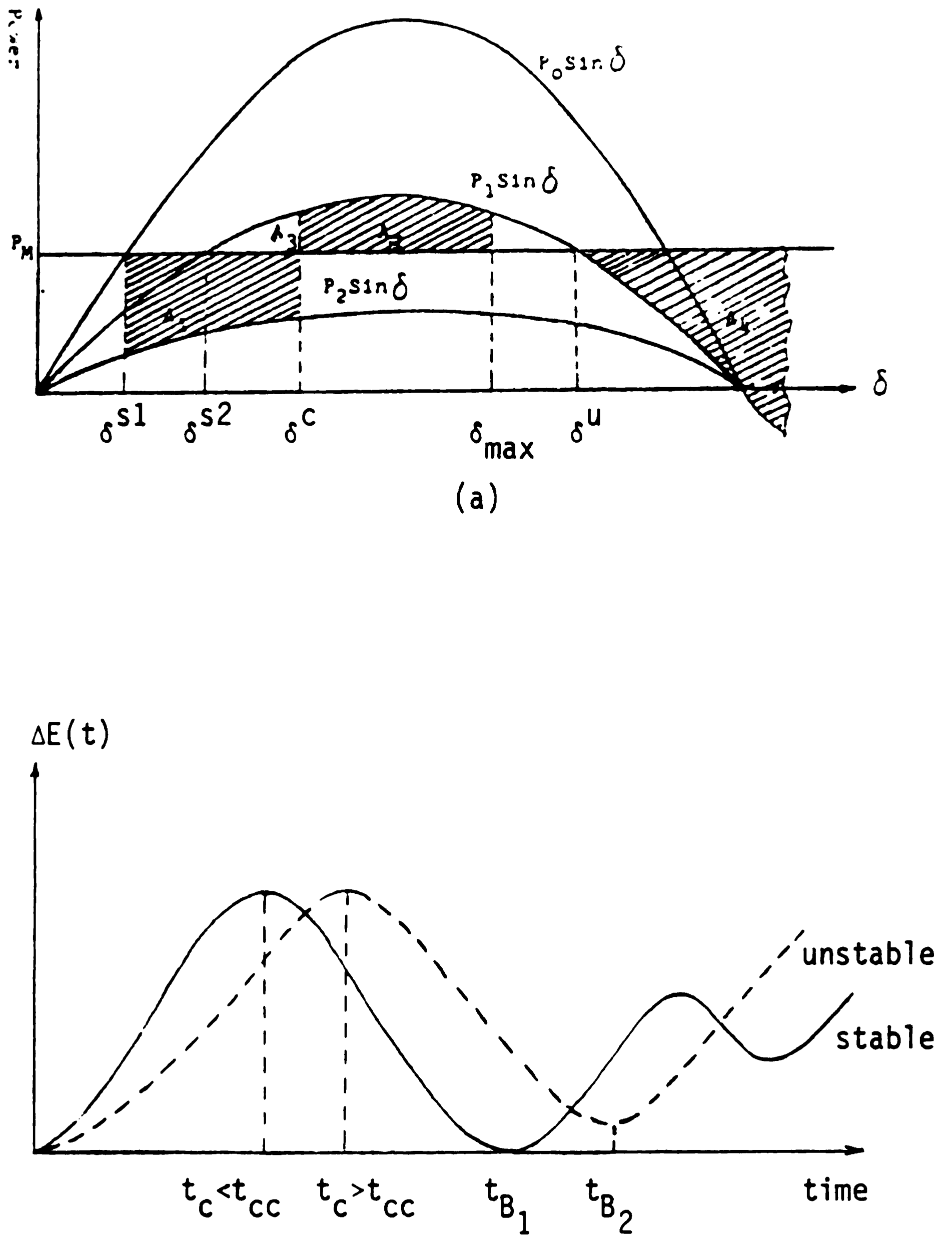

Figure 3.3. Equal area criterion
(a) Power angle representation of one-machine infinite-bus system.
(b) Variation of energy margin vs. time.

decelerating en

for the accelera

rotor angle pos

decrease and os

rotor angle als

angle. If the

machine and ca

then the gener

defining A_1 a

$\Delta E(t) =$

angle positio

$A_1(t_c)$

$A_3(t) = \{$

Figure 3.

of time. In th

value at the cle

assume the post-decelerating energy produced by the post-fault network to compensate for the acceleration energy A_1. Note that for any $t_c < t_{cc}$ the rotor angle position $\delta(t)$ peaks when $|A_1| = |A_3|$ and starts to decrease and oscillate afterwards. If the system is damped then the rotor angle also damps out and assumes the post-fault steady-state angle. If the post-fault transmission network cannot decelerate the machine and cause a reversal of direction of motion at some time t_B, then the generator will lose stability. This can be understood by defining A_1 and A_3 and $\Delta E(t)$.

$\Delta E(t) = A_1(t_c) + A_3(t)$ is defined to be a function of rotor angle position which in turn is a function of time as follows:

$$A_1(t_c) = \begin{cases} \displaystyle\int_{\delta^{s1}}^{\delta(t_c)=\delta^c} (P_M - P_2 \sin \delta) d\delta & \delta(t) < \delta^c \\ 0 & \delta(t) \geqq \delta^c \end{cases}$$

$$A_3(t) = \begin{cases} 0 & \delta(t) < \delta^c \\ \displaystyle\int_{\delta(t_c)=\delta^c}^{\delta(t)} (P_M - P_1 \sin \delta) d\delta & \delta(t) \geqq \delta_c \end{cases} \qquad (3.15)$$

Figure 3.3b depicts the quantity $\Delta E(t) = A_3 + A_1$ as a function of time. In the fault period $\Delta E(t) > 0$, and reaches its maximum value at the clearing time t_c. At t_c, the network is switched to assume the post-fault network and hence for $t_c \leqq t_{cc}$, $\Delta E(t)$ decreases until it becomes zero at t_B (decelerating energy $A_3(t_B) < 0$, provided by the post fault network is capable of capturing the accelerating (kinetic) energy $A_1(t_c)$ produced by the fault). For $t_c = t_{cc}$ the minimum of $\Delta E(t)$ takes a longer time to become zero. Note that t_{B_1} is also the time at which the rotor angle position is maximum ($\delta(t_{B_1}) = \delta_{max}$). For $t_c > t_{cc}$, the quantity $\Delta E(t) = A_1(t)$ increases with time for $t < t_c$ and then decreases ($\Delta E(t) = A_1(t_c) + A_3(t)$) for $t > t_c$. However, in this case $\Delta E(t_B) = \text{Min } (\Delta E(t)) > 0$ and occurs where $\delta(t) = \delta^u$ at $t = t_{B_2}$. Thus, the decelerating energy capability of the post-fault network $A_3(t_{B_2})$ is less than the acceleration energy $A_1(t_c)$. Since $\Delta E(t_{B_2}) = A_1(t_c) + A_3(t_{B_2}) > 0$ is a measure of the net decelerating energy and the kinetic energy remaining in the machine's inertia and since $\Delta E(t)$ remains positive and never reaches zero for all $t > 0$, the machine angle $\delta(t)$ never changes its direction of motion and continues to increase for $t > t_{B_2}$ as shown in Figure 3.2. Thus $\Delta E(t) = A_1(t_c) + A_3(t_{B_2}) + A_4(t)$ for $t > t_{B_2}$ where

$$A_4(t) = \begin{cases} 0 & \delta(t) < \delta^u \\ \displaystyle\int_{\delta(t_{B_2}) = \delta^u}^{\delta(t)} (P_M - P_1 \sin \delta) d\delta & \delta(t) > \delta^u \end{cases} \qquad (3.16)$$

where $A_4(t) > 0$

It should be noted that increasing t_c for $t_c < t_{cc}$, t_{B_1} where $\Delta E(t_{B_1}) = 0$, increases since more accelerating energy $A_1(t_c)$ is put in

For

ex

fa

di

wh

sys

whe

by

ass

gen

pot

into the system and thus a longer time for $\Delta E(t_{B_1}) = A_1(t_c) + A_3(t_B) = 0$. For $t_c > t_{cc}$, t_{B_2} decreases for increasing t_c since there is a larger excess accelerating and thus kinetic energy $\Delta E(t_{B_2}) = A_1(t_c) + A_3(t_{B_2}) > 0$, which permits the trajectory to reach the PEBS faster. Thus the maximum t_{B_1} and t_{B_2} occurs when $t_{B_1} = t_{B_2}$ for $t_c = t_{cc}$. Therefore, the boundary of stability (t_{cc}) can be predicted by the following two different ways:

(2) the maximum value of t_c for which the minimum value of $\Delta E(t)$ over t is zero; or

(2) the maximum time t_{B_1} for $t_c \leqq t_{cc}$ or t_{B_2} for $t_c \geqq t_{cc}$ at which $\Delta E(t)$ reaches its minimum value which satisfies $t_{B_1} = t_{B_2}$ and $\Delta E(t_{B_1}) = \Delta E(t_{B_2})$ for $t_c = t_{cc}$.

This equal area criterion is now extended to multimachine systems represented as

$$M_i \dot{\tilde{\omega}}_i = P_i - P_{ei} - \frac{M_i}{M_T} P_{COA}$$

$$\dot{\theta}_i = \tilde{\omega}_i \qquad\qquad i = 1, \ldots., n \qquad\qquad (3.17)$$

where

$$P_{ei} = \sum_{\substack{j=1 \\ j \neq i}}^{n} [C_{ij} \sin \theta_{ij} + D_{ij} \cos \theta_{ij}]$$

by attempting to apply a similar equal area analysis to the energy associated with accelerating and decelerating torques between critical generator i and the rest of the generators $j \neq i$ in the system. The potential energy measure is in part contributed by the torques on machine i

necting g

observati

equal are

multimach

case. Be

limitatio

(1)

less syst

(2)

occur whe

with resp

i reverse

machines

accelerat

ual energ

i reverse

positive.

(3)

as an inf

decelerat

$A_1(t_c)$ an

It

ated by a

negative

machine i and all $j \neq i$ from the equivalent transmission lines connecting generator i to the rest of the generators in the system. By observation of the behavior of $\Delta E(t) = A_1 + A_3$, in Chapter 4, the equal area criterion based on either (1) or (2) above apply to the multimachine model (3.17) just as in the single-machine infinite bus case. Before going to the next chapter, the following remarks and limitations are in order.

(1) The concept of equal area is justified only for the lossless systems.

(2) The loss of stability in a multimachine system will not occur when the generator i (critical generator) reverses direction with respect to a synchronous reference but rather when the generator i reverses direction with respect to the inertial center of the other machines in the power system model. Since these generators also accelerate with respect to a synchronous reference the minimum residual energy $\Delta E_i(t_B)$ of generator i at the boundary, where generator i reverses direction with respect to the inertial center, may be positive.

(3) The generators in a multimachine power system do not act as an infinite bus or even as a single equivalent machine. The deceleration energy $A_3(t_B)$ may exceed the acceleration kinetic energy $A_1(t_c)$ and thus $\Delta E(t_B)$ could be negative.

It will be shown in Chapter 4 that if one generator is accelerated by a fault the minimum residual energy value $\Delta E(t_B)$ will be negative for any clearing time $t_c < t_{cc}$ for that fault, since the other generators do not act as a single machine and the network has more deceleration energy than acceleration energy due to that fault. If, however, a fault accelerates a large number of generators the minimum residual energy $\Delta E(t_B)$ for this fault will be positive since generator i reverses direction with respect to the other generators when it still has some kinetic energy with respect to a synchronous reference.

The last and possibly most important point of interest in direct stability analysis of the power system based on the individual energy function is to determine which of the accelerated generators will dictate the stability of the group and in general the stability of the system. The following section proposes a procedure for identifying this individual generator (critical generator) that dictates stability of the system.

3.4. Critical Group, Generator, and Boundary

It was argued previously that once the individual machine energies are related to the entire system rotor angle position and angular velocity, it could be used to estimate the boundary of the region of stability of the entire system. Knowing that it is possible to predict the critical clearing time by an individual machine raises the argument that one has to identify a particular individual machine whose behavior dictates most accurate the stability of the entire power system.

In response to occurrence of a fault, the group of generators which are most affected and disturbed by the fault energy (those generators which are electrically closer to the fault location) is called the accelerated group. The longer the fault remains on the system, the larger will be the number of generators in this group. For example, in the Cooper case where the fault is applied to the high side of the transformer connected to generator 2 and the fault is cleared at $t_c = .220$ seconds, only generator 2 is contained in the accelerated group. On the other hand, if the fault is kept on for a longer time and cleared at $t_c = .24$ seconds, then generator 17 also joins to the accelerated group. Note that from Figure 3.4 generator 17 (Neb. CT, bus 774) is close to fault location and thus would logically enter the accelerated group as the fault clearing time increases. The rest of the generators in the system constitute the stationary group (generators which are least affected by the fault energy and remain relatively close to their pre-fault conditions). Based on the fact that the behavior of the generators of the accelerated group is very different from that of their pre-fault condition, it is believed that the specific generator dictating the transient stability of the entire system is contained in the accelerated group. It is worth noting that the generators initially forming the accelerated group do not necessarily remain in this group, and some of them may decelerate and join the less accelerated or "stationary" group at a later time. The stationary group plays the role of the infinite bus in the classical equal area criterion for the single machine infinite bus model.

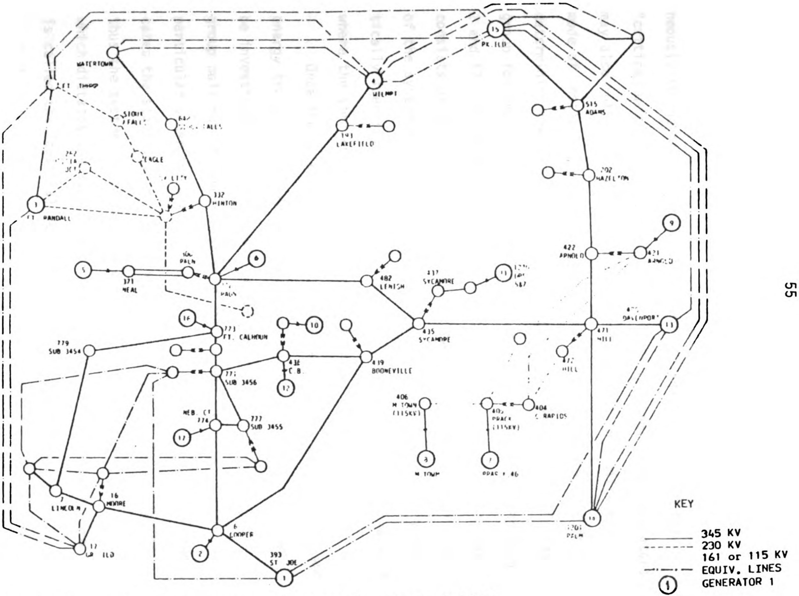
WATERTOWN
FT. THOMP
SIOUX FALLS
EAGLE
FT. RANDALL
332 HINTON
371 NEAL
PALN
4 HELMPT
141 LAKEFIELD
15 PK. ILD
515 ADAMS
202 HAZELTON
422 ARNOLD
421 ARNOLD
482 LENISH
437 SYCAMORE
435 SYCAMORE
471 HILL
472 HILL
DAVENPORT
773 FT. CALHOUN
779 SUB 3454
771 SUB 3456
438 C.B.
419 BOONEVILLE
406 M.TOWN (115KV)
405 PRAIR (115KV)
404 C.RAPIDS
M.TOWN
NEB. CT 774
777 SUB 3455
7 LINCOLN
16 MOORE
17 LR. ILD
6 COOPER
393 ST. JOE
PALM
KEY
345 KV
230 KV
161 or 115 KV
EQUIV. LINES
GENERATOR 1

Figure 3.4. 17-generator system (Reduced Iowa System) [13].

Fo
generato
neously
"critica
may also
mode of
determin
group fo
2 and 17.
consists
of the s
tically i
where the

Onc
energy tr
be invest
group pul
particula
cates the
thus the
which di
is called
encircli
The criti
ary whose

For a given small clearing time a generator or a group of generators which accelerates and pulls out of the system simultaneously is the one which causes instability and it is called the "critical group." For a longer fault clearing time, other generators may also pull out from the system and thus result in a different mode of instability, but these generators do not play any role in determining the stability of the system. For example, the critical group for the Cooper case consists of generator 2 and not generators 2 and 17. As another example, the critical group for the Raun case consists of both generators 5 and 6. These two generators pull out of the system simultaneously. A more detailed discussion for practically identifying the critical group will be presented in Chapter 4 where the simulation results are considered.

Once the critical group is identified, the dynamic behavior and energy transfers between the individual machines in this group must be investigated. Although all of the generators of the critical group pull out of synchronism with the system, there is only one particular generator whose stability or instability accurately indicates the stability or loss of stability of the critical group and thus the system. This particular generator in the critical group, which dictates the stability or instability of the critical group, is called the "critical generator." The appropriate boundary encircling the critical generator is called the "critical boundary." The critical boundary determines a potential or kinetic energy boundary whose violation results in instability. The kinetic energy boundary is evidenced by a minimum of energy Min $(A_1 + A_3)$ in equal-area criterion. The crossing of a potential energy boundary for the critical generator is evidenced by a maximum in potential energy of the critical generator after the fault is cleared (PEBS).

Generators of the critical group will each cross their own potential or kinetic energy boundary with respect to the generators of the stationary group one at a time and the critical generator is the last one in the critical group which crosses a potential or kinetic energy boundary. If the critical generator crosses its potential or kinetic energy boundary, then the entire critical group loses synchronism with the stationary group. If this critical generator never crosses its potential or kinetic energy boundary, the critical group will remain stable. To clarify the loss of synchronism between the critical generator and the generators of the stationary group, a very simplified example is in order.

Consider the real power transmitted between two generators i and j connected by a lossless line with reactance X_{ij},

$$P_{ij} = \frac{|E_i||E_j|}{X_{ij}} \sin \delta_{ij} \tag{3.18}$$

where $\delta_{ij} = \delta_i - \delta_j$ and E_i, E_j are the magnitude of voltage at buses i and j. If E_i and E_j are kept constant, then

$$P_{ij} = P_{max} \sin \delta_{ij} \tag{3.19}$$

where $P_{max} = \dfrac{|E_i||E_j|}{X_{ij}}$.

The real power transmitted from bus i to bus j through line ij clearly depends on the phase angle difference between buses i and j. When the phase angle difference (due to load increase or a change in generation due to a fault) is forced to attain a value near 90°, the power transmitted will reach P_{max}, the maximum value, and any additional phase angle difference (beyond 90°) will decrease the transmitted power. At the point where $\delta = 90°$ (the static stability limit), the system "pulls apart electrically" and the synchronism between bus i and j is lost [20] if buses i and j are only connected through this one path. If buses i and j are operating in such a way that the phase angle difference is small, then these two generators are said to be operating in synchronism or *strongly coupled*. In contrast, if the angle difference exceeds 90°, buses i and j are *weakly coupled*. If there are several paths connecting two sets of buses I and J, then all buses $i_k \varepsilon I$ and $j_\ell \varepsilon J$ must be weakly coupled for I and J to lose synchronism. One can now argue that once the potential energy of the line connecting bus i_k to bus j_ℓ achieves its maximum capacity, then generators i_k and j_ℓ become weakly coupled. In a dynamic sense, if all of the generators i_k belonging to the critical group and all generators j belonging to the stationary group exceed the potential energy capacity of the equivalent line connecting them, the two groups lose synchronism and thus the critical group goes unstable. The last generator in the critical group which approaches its potential energy boundary of the lines connecting it to the stationary group decides the stability of the critical group and henc

are inves

estimates

discusse

and hence the entire system. In Chapter 5, two boundary conditions are investigated and the accuracy of the critical clearing time estimates which are based on these stability boundaries will be discussed.

CHAPTER 4

STABILITY SIMULATION STUDIES USING INDIVIDUAL ENERGY FUNCTION

4.1. Introduction

The power network used in the validation studies of this research is an equivalent of the real Iowa system (referred to here as the Reduced Iowa System) [28]. This network consists of 17 generators and 163 buses. Figure 4.1 shows a one-line diagram of the Reduced Iowa System.

The study done at Iowa State University confirms that this reduction preserves the dynamic behavior of the system for "first swing" stability. The generator data, together with the initial conditions including the generator internal voltages, are given in Table 4.1.

The Reduced Iowa System model was tested by running stability studies for three different fault cases: the Cooper case (BUS 6), the Fort Calhoun case (BUS 773), and the Raun case (Bus 372).

The objectives of this chapter are:

(1) To establish the critical generator concept on several fault cases as well as on the Raun case where the critical group consists of more than one generator. The critical generator must be identified

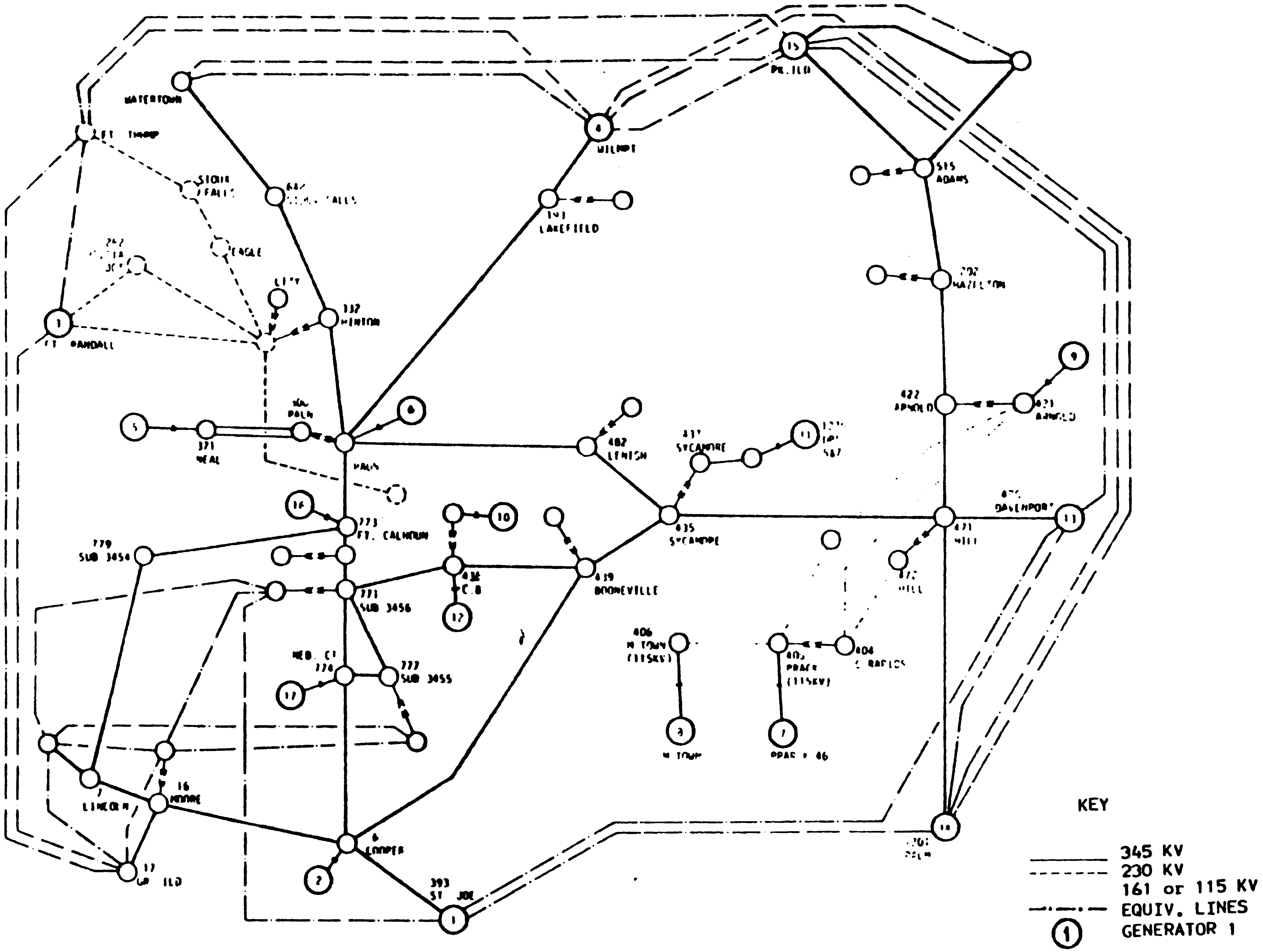
WATERTOWN
15
PR. ILD
4
WILMOT
515
ADAMS
642
FALLS
141
LAKEFIELD
292
HAZLETON
SIOUX
FALLS
EAGLE
132
HINTON
CITY
1
FT. RANDALL
422
ARNOLD
421
9
5
371
NEAL
PALM
8
482
LEHIGH
SYCAMORE
567
11
635
SYCAMORE
471
HILL
DAVENPORT
11
16
773
FT. CALHOUN
10
779
SUB 3454
438
C.B
12
771
SUB 3456
639
BOONEVILLE
472
HILL
406
N TOWN
(115KV)
404
RAPIDS
PRAIR
(115KV)
NEB. CI
774
777
SUB 3455
17
3
N TOWN
7
PRAI 46
7
LINCOLN
16
MOORE
14
17
ILD
6
COOPER
2
393
ST JOE
1
KEY
345 KV
230 KV
161 or 115 KV
EQUIV. LINES
GENERATOR 1

Figure 4.1. 17-generator system (Reduced Iowa System) [13].

Table 4.1. Reduced Iowa System generator data and initial conditions.

	Generator Parameters[a]		Initial Conditions		
				Internal Voltage	
Generator Number	H (MW/MVA)	x'_d (p.u.)	P_{mo}[a] (p.u.)	E (p.u.)	(degrees)
1	100.00	0.004	20.000	1.0032	-27.92
2	34.56	0.043	7.940	1.1333	- 1.37
3	80.00	0.0100	15.000	1.0301	-16.28
4	80.00	0.0050	15.000	1.0008	-26.09
5	16.79	0.0507	4.470	1.0678	- 6.24
6	32.49	0.0206	10.550	1.0505	- 4.56
7	6.65	0.1131	1.309	1.0163	-23.02
8	2.66	0.3115	0.820	1.1235	-26.95
9	29.60	0.0535	5.517	1.1195	-12.41
10	5.00	0.1770	1.310	1.0652	-11.12
11	11.31	0.1049	1.730	1.0777	-24.30
12	19.79	0.0297	6.200	1.0609	-10.10
13	200.00	0.0020	25.709	1.0103	- 8.10
14	200.00	0.0020	23.875	1.0206	-26.76
15	100.00	0.0040	24.670	1.0182	-21.09
16	28.60	0.0559	4.550	1.1243	- 6.70
17	20.66	0.0544	5.750	1.116	- 4.35

[a] on 100-MVA base

properly to
function mu

(2) T
bility using
in extremel
compared to

(3) T
methods in t

(4) T
of the PEBS
or excluded

The fo
the results
ter 7, these
testing the
described i

A thr
removed by

The s
ing times a
and 16 are
their beha
energy sepa
most accele
of the gene

properly to determine the machine for which the individual energy function must be constructed.

(2) To show that the PEBS method for assessing transient stability using the transient energy of the critical generator results in extremely accurate determination of the critical clearing times compared to similar total transient energy methods.

(3) To compare the accuracy of PEBS and Local equal area methods in terms of determining critical clearing time.

(4) To determine the effect of conductances on the accuracy of the PEBS method by comparing the results when they are included or excluded in individual transient energy function.

The following sections discuss these objectives by showing the results of simulation runs for each fault case. Later in Chapter 7, these results will be compared to the results obtained by testing the proposed fast stability algorithms (which will be described in Chapter 5) on each fault case.

4.2. Cooper Case

A three-phase fault is applied to generator 2 (Cooper) and is removed by clearing line 6-439.

The system trajectory was simulated for different fault clearing times and it was observed that although the generators 1, 17, 12, and 16 are electrically close to the fault location (see Figure 4.1), their behavior is different than that of generator 2. The fault energy separated the system into two groups; one consisting of the most accelerated (critical) generator 2, and the second of the rest of the generators in the system. Figures 4.2, 4.3, and 4.4 depict

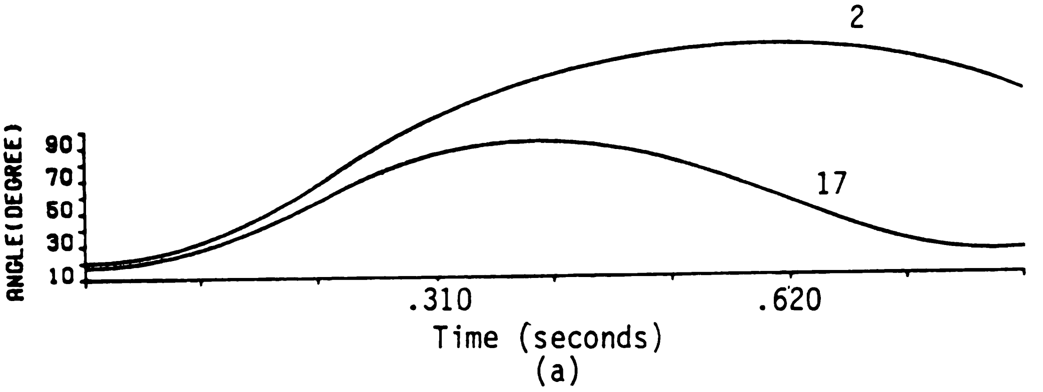

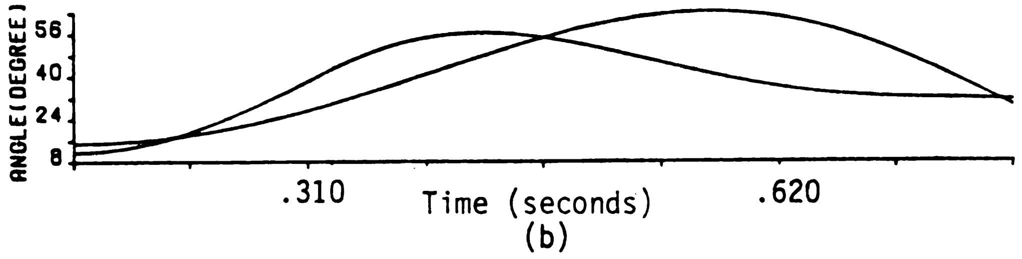

Figure 4.2. Swing curves for Cooper. Clearing time = .218 seconds.
(a) Generators 2, 17
(b) Generators 12, 16

Figure 4.

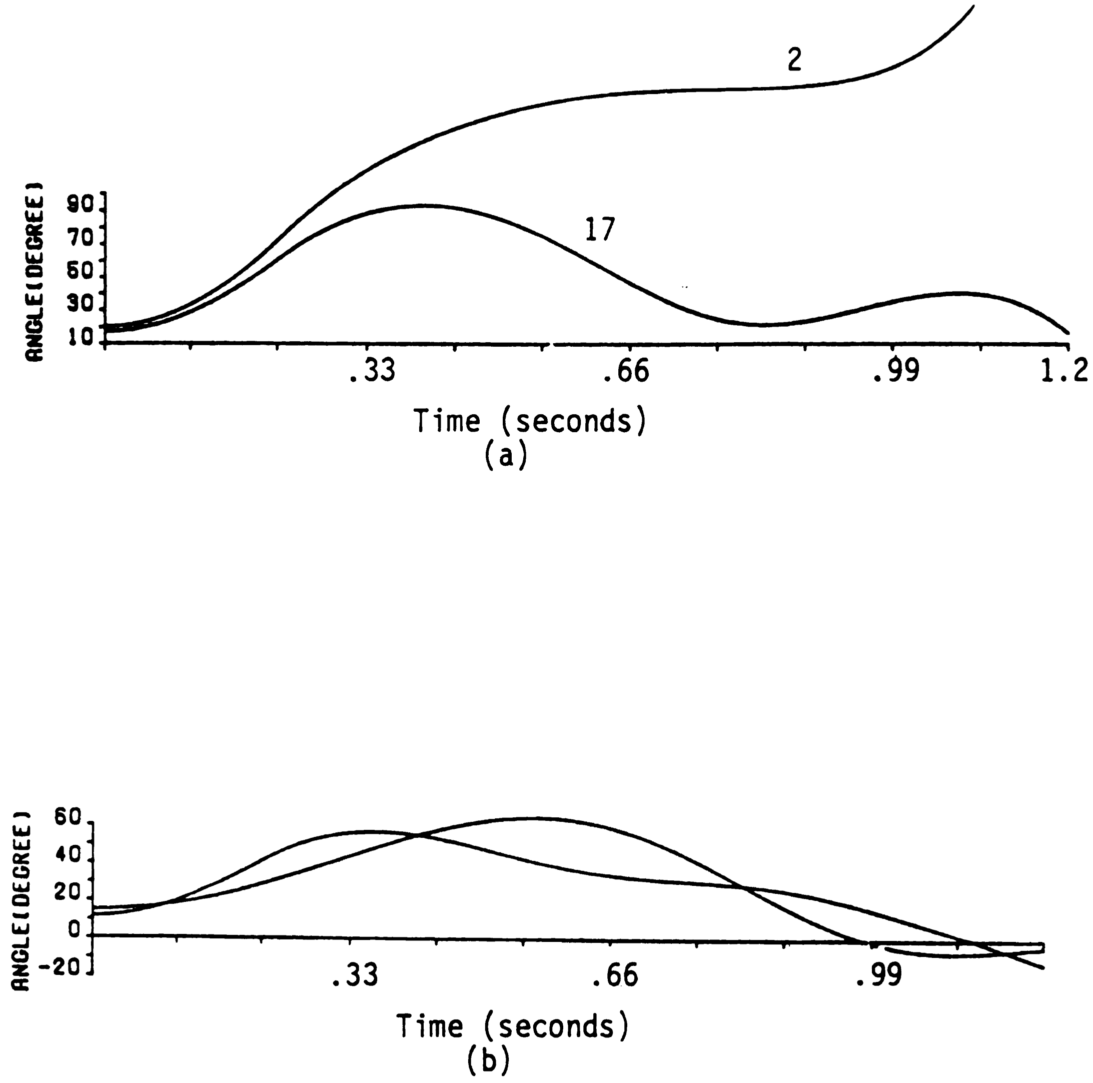

Figure 4.3. Swing curves for Cooper. Clearing time = .220 seconds.
(a) Generators 2, 17
(b) Generators 12, 16

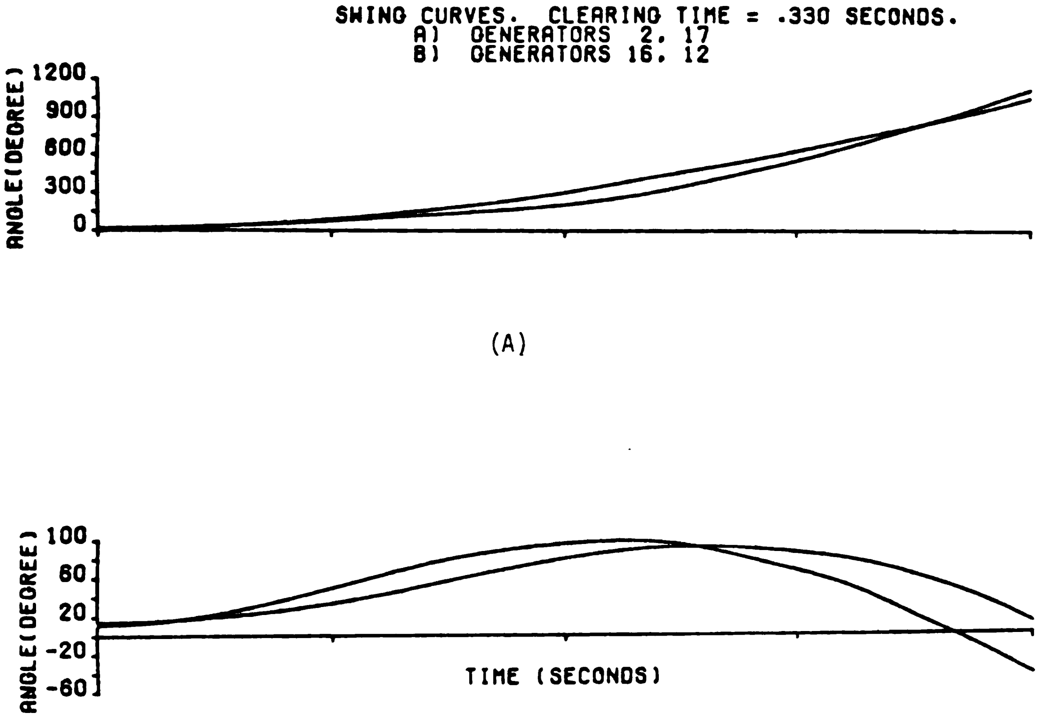

(A)

(B)

Figure 4.4. Swing curves for Cooper.

the swing curves for generators 2, 17, 16, and 12 for fault clearing times of t_c = .218, .220, and .330 seconds, respectively. When the fault is cleared at t_c = .218 all the generators stay stable, and although the peak of the swing curves of generator 2 reaches approximately 150° ($\theta_2 > 90°$), it ultimately decelerates and remains stable with the rest of the system. Figure 4.3, however, illustrates that for a longer clearing time (t_c = .220 seconds) generator 2 accelerates and pulls away from the rest of the system and hence by definition is the critical generator and the critical group. As a further step, Figure 4.4 illustrates that for t_c = .330 seconds both generators 2 and 17 lose synchronism with respect to the rest of the system, but the group consisting of these two generators, which did not lose synchronism simultaneously, is not considered as the critical group. Once the critical generator or group is determined, it is appropriate to calculate the critical energy of the individual energy function for this critical generator using the transient stability simulation program.

The critical boundary or the PEBS for Cooper is based on the maximum of potential energy as a function of time for $t > t_c$

$$V_{PE_2}(t) = \frac{1}{M_T} \sum_{\substack{j=1 \\ j\neq 2}}^{n} (P_2M_j - P_jM_2)(\theta_{2j}(t) - \theta_{2j}^{s1}) + \sum_{\substack{j=1 \\ j\neq 2}}^{n} C_{2j}(\cos\theta_{2j}(t) - \cos\theta_{2j}^{s1}) - D_{2j}\,\frac{\theta_2(t) + \theta_j(t) - \theta_2^{s1} - \theta_j^{s1}}{\theta_2(t) - \theta_j(t) - \theta_2^{s1} + \theta_j^{s1}}\,[\sin\theta_{2j}(t) - \sin\theta_{2j}^{s1}] \tag{4.1}$$

This critical generator maximum potential energy is calculated for different clearing times t_c and the results are summarized in Table 4.2. The maximum potential energy (4.1) as a function of time is determined for each clearing time t_c. The time $t_B(t_c)$ occurs at the point in time when the trajectory most closely approaches the potential energy boundary surface for the individual energy function of the critical generator for the case where the clearing time t_c is less than the critical clearing time t_{cc}. For clearing times t_c greater than the critical clearing time, the maximum potential energy occurs at the point in time $t_B(t_c)$ when the trajectory crosses the potential energy boundary surface. The peak potential energy $V_{PE_2}(t_B(t_c))$ should clearly increase for increasing clearing time t_c when the clearing time t_c is less than the critical clearing time t_{cc}. The peak potential energy function $V_{PE_2}(t_B(t_c))$ has been claimed to be nearly constant for all t_c greater than the critical clearing time in the previous literature [16]. It is clear from Table 4.2 that $V_{PE_2}(t_B(t_c))$ decreases slowly for t_c greater than critical clearing time since $V_{PE_2}(t_B(t_c))$ decreases for $t_c > 0.220$ seconds, where it is clear that the system is unstable for $t_c = .220$ seconds from Figure 4.3. There is a very significant peak in $V_{PE_2}(t_B(t_c))$ when t_c is close to t_{cc}, making it easy to accurately identify t_{cc}. The decrease in the peak potential energy for increasing t_c beyond the critical clearing time is due to the fact that the generator 17 and ultimately 16 and 12 will lose stability with generator 2 and thus the angle differences between generator 2 and these generators

Table 4.2. Potential energy boundary surface energy as a function of t_c for determining t_{cc}.

	with conductance		without conductance	
t_c	$V^*_{PE}(t_B)$	t_B	$V^*_{PE}(t_B)$	t_B
.192	6.546	.368	4.961	.368
.208	8.105	.448	6.586	.448
.210	8.362	.480	6.879	.480
.217	10.173	.644	8.876	.637
.218	10.843	.687	9.549	.687
.219	12.897	.814	11.042	.821
.220	15.133	.935	13.924	.946
.222	13.672	.848	11.388	.848
.224	12.021	.672	11.241	.672
.240	9.403	.432	8.180	.464

t_B - time at which the maximum of potential energy occurs

t_c - clearing time

at $t_B(t_c)$ will be smaller making $V_{PE_2}(t_B(t_c))$ decrease with clearing time $t_c > t_{cc}$. From the above discussion the critical clearing time should occur precisely at the time that $V_{PE_2}(t_B(t_c))$ is maximum. For the Cooper case it is estimated that the actual critical clearing time is $t_c \varepsilon$ (.219-.220) seconds based on the above criteria for selecting t_{cc}. This predicted critical clearing time is very accurate compared to the results in [16] and very well comparable to simulation results that indicate the critical clearing time lies in (.219-.220).

The local equal-area critierion for Cooper is based on the minimum overtime of the energy margin

$$\Delta E_2(t;t_c) = A_1(t_c) + A_2(t,t_c) \qquad (4.2)$$

where

$$A_1(t_c) = V_{PE_2} \Bigg|_{\theta^{s1}}^{\theta(t_c)}$$

is evaluated using the local potential energy function $V_{PE_2}(t)$ with the faulted network admittance matrix and

$$A_2(t;t_c) = V_{PE_2} \Bigg|_{\theta(t_c)}^{\theta(t)} \qquad (4.3)$$

is the local potential energy function with the post-fault network admittance matrix. The local EAC (t_c) is thus

$$\text{EAC}\ (t_c) = \min_{t > t_c} \Delta E_2(t;t_c) = \Delta E_2(t_B;t_c) \tag{4.4}$$

Figures 4.5 and 4.6 show the simulation of $\Delta E_2(t;t_c)$ performed with small integration step for two different clearing times, .218 and .220 seconds. In both figures $\Delta E_2(t;t_c)$ starts from zero value at time $t = 0$ and increases with time until it peaks at clearing time $t_c = .218$ and .220 seconds. This increase of energy margin is due to the excess kinetic energy (accelerating energy) A_1 of generator 2 during the fault period where A_1 is positive energy and $A_2 = 0$.

After the fault is cleared $t > t_c$, the post-fault network starts to absorb the kinetic energy at clearing time and the minimum $\Delta E_2(t_B;t_c)$ is reached at some time t_B after the clearing time. For $t_c = .218$ seconds, the minimum of $\Delta E_2(t_B;t_c)$ occurs at $t_B = .676$ and $t_B = .687$ with and without conductance term included, respectively, in equation (4.1). The value of EAC(t_c) being negative for $t_c < t_{cc}$ indicates that the post-fault network is completely capable of absorbing the faulted energy and decelerates the critical generator to a point where its direction of motion is changed and the system remains stable. However, for large clearing time $t_c > t_{cc}$, more kinetic energy is produced during the fault-on period which causes the post-fault network to absorb more kinetic energy but no longer all of it. As a result, the minimum of $\Delta E_2(t_B,t_c)$ for $t_c > t_{cc}$ never reaches zero and remains positive $|A_1| > |A_2|$, indicating the fact that the critical generator does not change its direction of

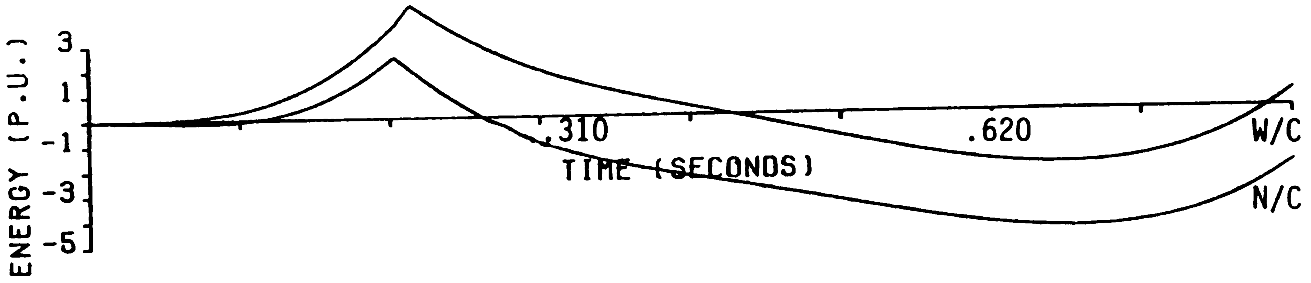

Figure 4.5. Energy margin $A_1(t_c) + A_2(t,t_c)$ for Cooper case. Clearing time = .218 seconds. Critical generator = 2.
W/C = transfer conductance included.
N/C = transfer conductance excluded.

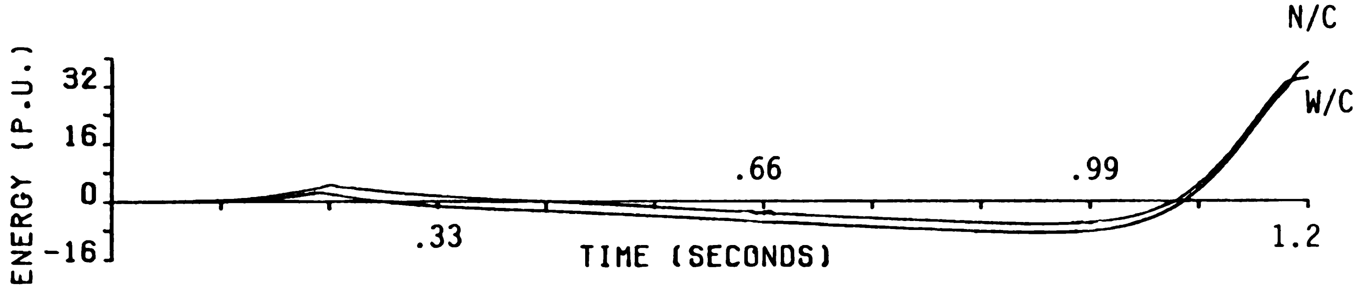

Figure 4.6. Energy margin $A_1(t_c) + A_2(t,t_c)$ for Cooper case. Clearing time = .220 seconds.
Critical generator = 2.
W/C = transfer conductance included.
N/C = transfer conductance excluded.

motion and the system loses stability. In contrast to the case of the equal-area criterion of one-machine infinite bus, the minimum $\Delta E_2(t_B;t_{cc})$ in a multimachine power system is negative and not zero when the system is stable. As was discussed earlier, this phenomenon was expected because of the fact that the non-critical machines do not behave as an infinite bus and thus require more deceleration energy A_2 to reverse the direction of motion of the critical generator than if they acted in unison as a single bus.

The stability simulation program was run for different clearing times to predict the critical boundary using Minimum Energy Equal-Area Criteria and the results are summarized in Table 4.3. The minimum of $\Delta E_2(t_B;t_c)$ occurs at $t_B = .946$ for both cases where the transfer conductances are and are not included. This observation certainly shows that for the qualitative analysis the concept of the equal-area criterion can be extended for a multimachine case.

From Table 4.3 it is clear that the estimated critical clearing time is $t_c \in (.219-.220)$ seconds which is comparable to simulation results $t_c \in (.219-.220)$. Note that the very sharp narrow minimum for $\Delta E_2(t_B,t_c)$ for t_c near t_{cc} makes accurate identification of t_{cc} quite easy.

The results of both algorithms PEBS and EAC in Tables 4.2 and 4.3 show that increasing t_c for $t_c < t_{cc}$ causes $t_B(t_c)$ to increase since the angle deviation of the accelerated generators from their nominal (initial operating) state becomes larger and it takes more time for generators to reverse their directions and return to the

Table 4.3. Minimum of $\Delta E_2(t_B,t_c) = A_1(t_c) + A_2(t_B,t_c)$ for critical generator 2 using stability simulation program.

	with conductance		without conductance	
t_c	$\Delta E_2(t_B,t_c)$	t_B	$\Delta E_2(t_B,t_c)$	t_B
.192	.423	.368	-2.199	.368
.208	.011	.464	-2.578	.480
.210	- .036	.495	-2.695	.495
.217	-1.522	.637	-4.067	.637
.218	-2.111	.676	-4.647	.687
.219	-3.873	.821	-5.910	.821
.220	-6.358	.946	-8.826	.946
.222	-5.422	.848	-7.266	.848
.224	-4.032	.688	-5.909	.672
.240	1.399	.496	-1.041	.464

t_B - time at which the minimum of $\Delta E_2(t,t_c)$ occurs

t_c - clearing time

previous stable position. The maximum $t_B(t_c)$ occurs when $t_c = t_{cc}$. Thus there are two indicators of t_{cc} by observing the minimum value of $\Delta E_2(t_B)$:

(1) the maximum value of t_c for which the minimum value of $\Delta E_2(t,t_c)$ over time is the smaller than some value ε

(2) the maximum time $t_B(t_c)$ at which the minimum of $\Delta E_2(t,t_c)$ is less than ε.

4.3. Fort Calhoun Case

A three-phase fault is applied to generator 16 (Ft. Calhoun) in Figure 4.1 and is removed by clearing line 773-779.

From Figure 4.1 the generators electrically close to the fault location are generators 17, 12, 10, 5, and 6. For different fault clearing times the system trajectory was simulated and generator 16 was found to be the first generator which was accelerated and separated from the rest of the generators. Therefore, generator 16 constitutes the critical group and the critical generator. Based on simulation, it is observed that for clearing time of t_c = .354 seconds the system is stable but that for t_c = .356 seconds the system becomes critically unstable. Figures 4.7 and 4.8 illustrate the swing curves of some of the generators of the stationary group and the critical generator for clearing times of .354 and .356 seconds, respectively. Note that the peak of the swing curves of the stationary group is somewhere around 80°-100° while that of the critical generator is about 170°-180° for the stable case, confirming the fact that the critical generator is initially pulling away from the stationary group but at

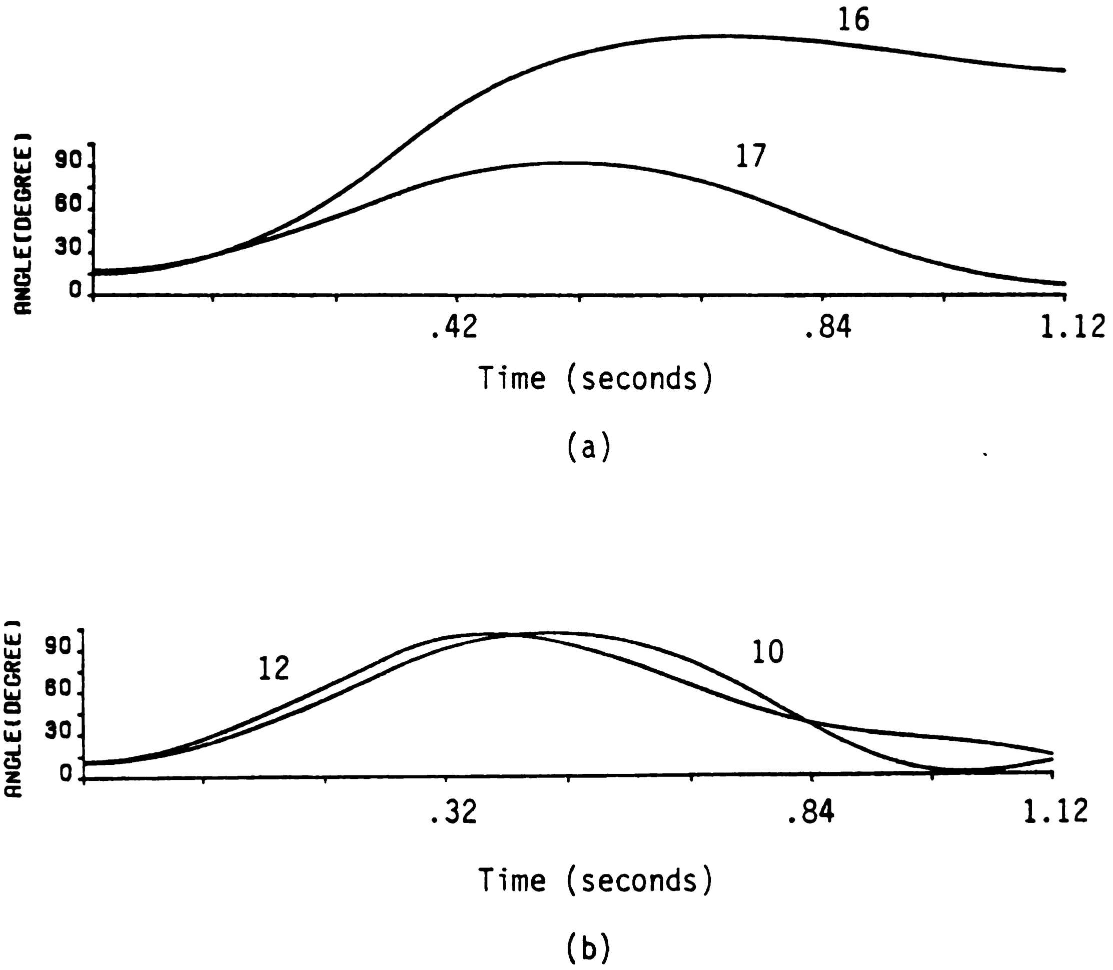

Figure 4.7. Swing curves for Fort Calhoun. Clearing time = .354 seconds.
(a) Generators 16, 17.
(b) Generators 10, 12.

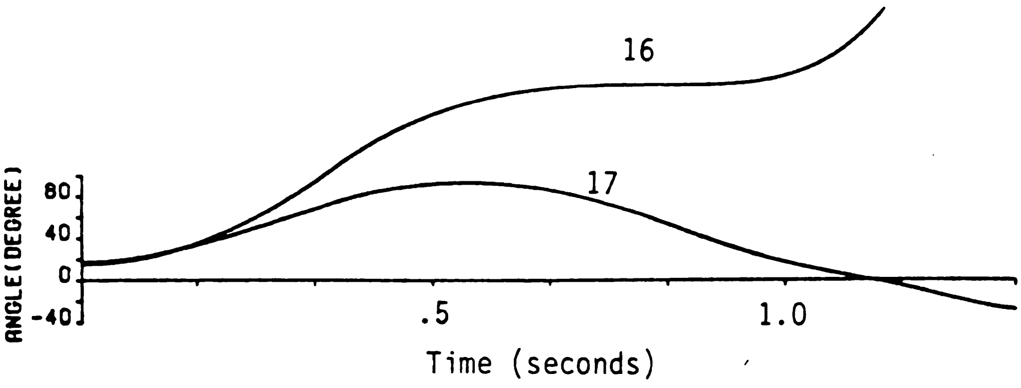

(a)

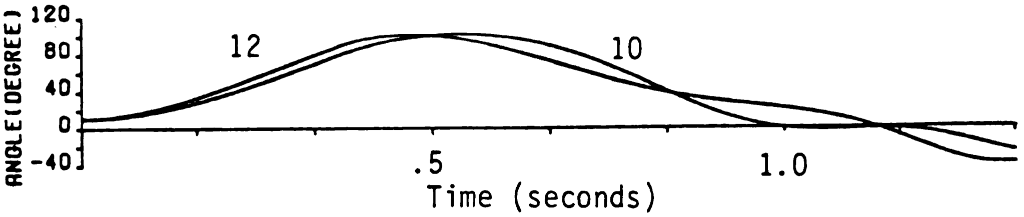

(b)

Figure 4.8. Swing curves for Fort Calhoun. Clearing time = .356 seconds.
(a) Generators 16, 17.
(b) Generators 10, 12.

a later time all of the generators decay and resume a relatively small angle indicating stability.

For clearing times $t_c = .354$ and $t_c = .356$ seconds, Figures 4.9 and 4.10 illustrate the energy margin $\Delta E_{16}(t,t_c) = A_1(t_c) + A_2(t,t_c)$ produced between critical generator 16 and all of the generators of the stationary group. From Figure 4.9, it is clearly seen that the minimum of $\Delta E_{16}(t,t_c)$ occurs at $t_B = 1.2$ seconds and it has negative value, i.e., $|A_1| < |A_2|$, indicating that the post-fault network captures the total kinetic (accelerating) energy produced during the fault period and hence changes the direction of motion of the critical generator; therefore the system is stable. For the larger clearing time $t_c = .356$ seconds, Figure 4.10 shows that the minimum of $\Delta E(t,.356) = EAC(.356)$ occurs at earlier time $t_B = .997$ seconds (because the post-fault network does not have the capability of absorbing the faulted energy completely and it takes less time to reach the minimum of $(A_1 + A_2)$. Table 4.4 shows the minimum of $\Delta E_{16}(t,t_c)$ for different clearing times. From the entries of this table it is clear that the lowest possible value occurs close to $t_c = .354$ seconds, indicating critical clearing time. Note that $\Delta E_{16}(t_B,t_c)$ has a sharp narrow minimum, making the accurate identification of t_{cc} easy.

Similar analysis was done for different clearing times to calculate the boundary energy (Maximum Potential Energy) of the critical generator using the PEBS method. The stability simulation program was run and the maximum of potential energy was calculated at each clearing

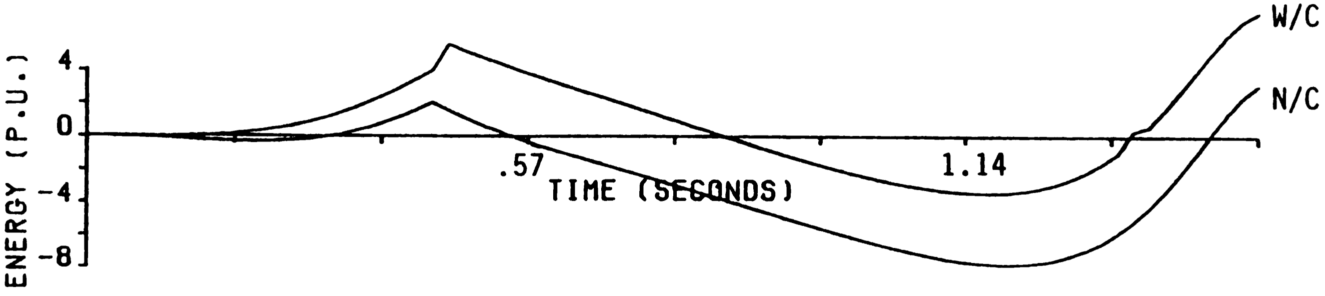

Figure 4.9. Energy margin $A_1(t_c) + A_2(t,t_c)$ for Fort Calhoun case. Clearing time = .354 seconds. Critical generator = 16.
W/C = transfer conductance included.
N/C = transfer conductance excluded.

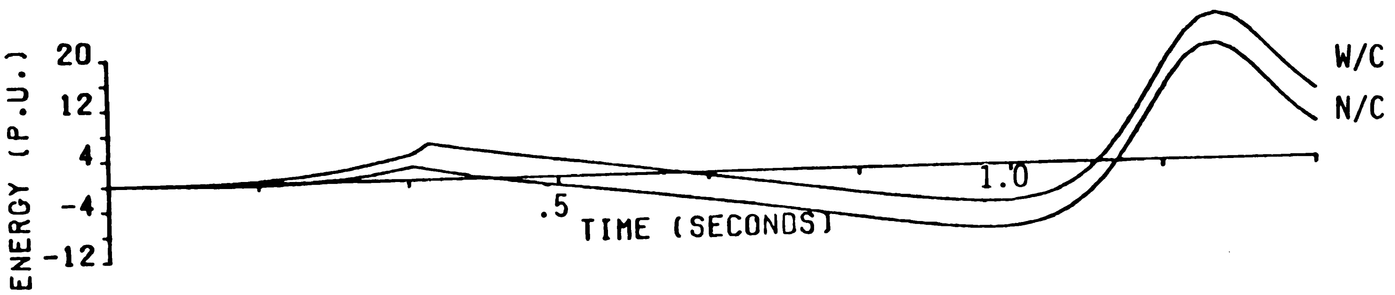

Figure 4.10. Energy margin $A_1(t_c) + A_2(t,t_c)$ for Fort Calhoun case. Clearing time = .356 seconds. Critical generator = 16.
W/C = transfer conductance included.
N/C = transfer conductance excluded.

Table 4.4. Minimum of $\Delta E_{16}(t_B,t_c) = A_1(t_c) + A_2(t_B,t_c)$ for critical generator 16 using stability simulation program.

	with conductance		without conductance	
t_c	$\Delta E_{16}(t_B,t_c)$	t_B	$\Delta E_{16}(t_B,t_c)$	t_B
.320	.486	.624	- 3.287	.624
.345	- .064	.885	- 4.107	.885
.352	-3.440	.928	- 7.836	.944
.354	-6.220	1.200	-11.149	1.200
.356	-5.880	.997	- 9.982	.997
.357	-5.442	.959	- 9.400	.959
.360	-4.315	.900	- 8.011	.900
.368	-2.005	.816	- 5.428	.816

t_B - time at which the minimum of $\Delta E_{16}(t,t_c)$ occurs

t_c - clearing time

Table 4.5. Potential energy boundary surface energy as a function of t_c for determining t_{cc}.

	with conductance		without conductance	
t_c	$V^*_{PE_{16}}(t_B)$	t_B	$V^*_{PE_{16}}(t_B)$	t_B
.320	7.681	.624	5.672	.624
.345	12.561	.885	9.825	.885
.352	14.402	.960	11.888	.944
.354	18.267	1.200	15.315	1.200
.356	16.382	.997	14.265	.997
.357	15.708	.959	13.741	.959
.360	14.230	.888	12.528	.900
.368	11.848	.800	10.428	.816

t_B - time at which the maximum of potential energy occurs

t_c - clearing time

time for two different cases, one with transfer conductances included and the other with transfer conductances not included. The results of this analysis are summarized in Table 4.5.

The entries in columns 2 and 4 of Table 4.5 indicate that for clearing time $t_c = .354$ seconds the maximum potential energy of the critical generator has its largest value. This potential energy value represents the boundary energy and the corresponding clearing time (close to .354 seconds in this case) is called the critical clearing time t_{cc}. The accurate identification of t_{cc} is again possibly due to the sharp narrow peak of $V_{PE_{16}}(t_B)$. It should also be noted that the critical generator trajectory for this particular clearing time achieves the potential energy maximum at a time $t_B(t_{cc})$ which is larger than all the trajectories for which the fault was cleared at $t_c \neq t_{cc}$. This phenomenon happens because of the fact that for $t_c = t_{cc}$ the angle deviation of the accelerated generators from their initial operating state has the largest value and it takes the longest time for generators to reverse their directions and return to their previous stable position.

The results obtained for the Fort Calhoun case indicate that the concepts of the selection of the critical generator and both EAC and PEBS are valid for multimachine power systems and both predict the critical clearing time very accurately $t_c \in (.354, .356)$.

This investigation of the accuracy of assessing critical clearing time by (a) identifying a critical generator, and (b) using the PEBS or equal area method with the critical generator's individual machine energy function is extremely accurate and indicates these methods truly capture the energy conditions that cause loss of stability. This attempt to determine the accuracy of the PEBS and equal area criterion methods using the critical generator's individual energy function has shown that there are very large changes in $V_{PE}(t_B;t_c)$ for PEBS and $\Delta E(t_B;t_c)$ for equal area when t_c is near t_{cc}. This makes very accurate assessment of t_{cc} quite easy.

The previous research using the PEBS method on an individual energy function [16] did not attempt to determine how accurate the method was and only indicated the critical clearing time belonged to intervals of .011 and .008 seconds rather than .002 and .001 for the Fort Calhoun and Cooper cases, respectively, as in this research.

4.4. Raun Case

A three-phase fault is applied to the high side of the transformer connected to generator 6 (Raun) and is removed by clearing line 372-193.

Stability run for Raun case was done earlier in Reference [29]. To complete the thesis, the analysis and the results obtained are summarized here. For different fault clearing times the system trajectory was simulated and it was observed that generator 5 was electrically closest to the fault location and thus possesses similar behavior to that of generator 6. The fault energy separated the system into two groups, one consisting of the accelerated generators (5 and 6) and the other by the rest of the system. Figures 4.11 and 4.12 show the swing curves of the generators for fault clearing

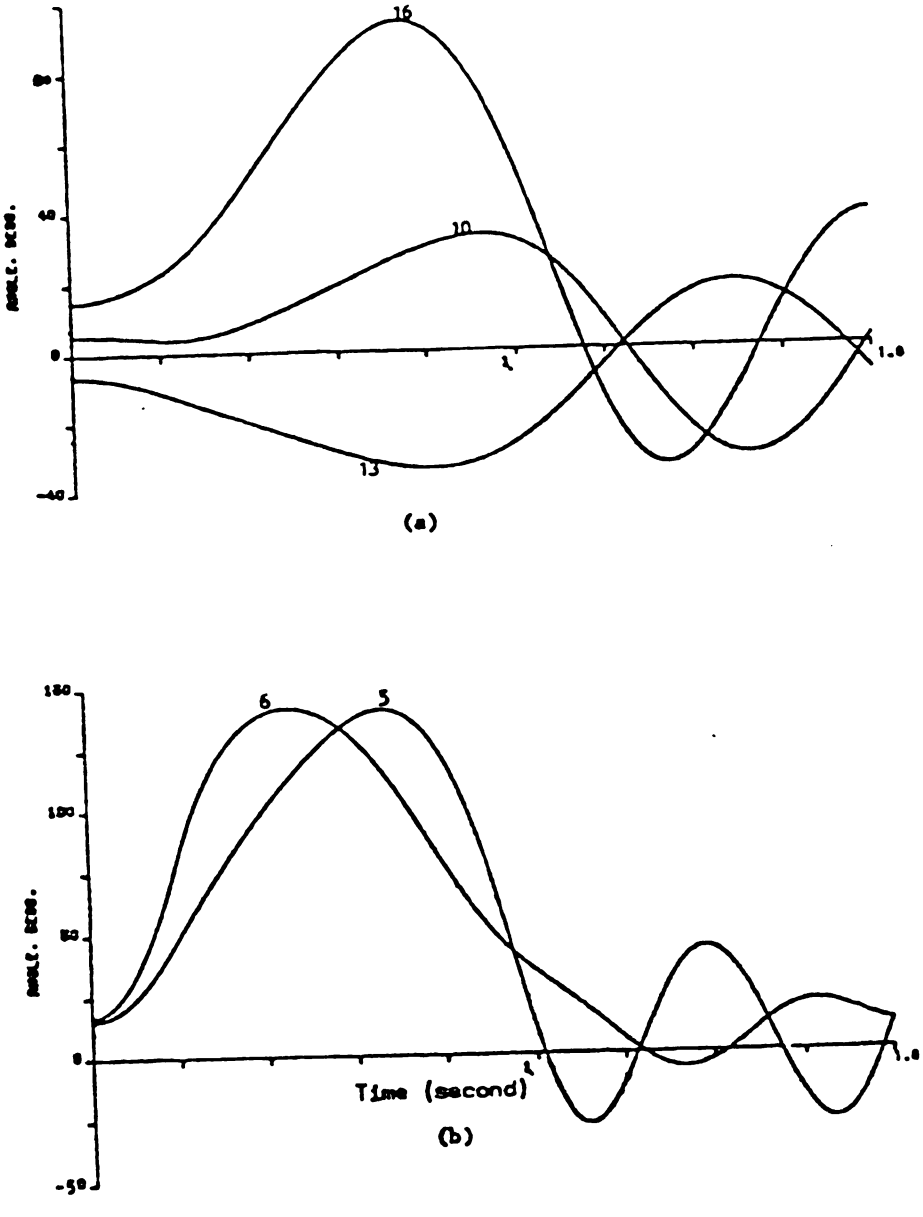

Figure 4.11. Swing curves. Clearing time = .1900 seconds.
(a) Generators 10, 13, 16.
(b) Generators 5, 6.

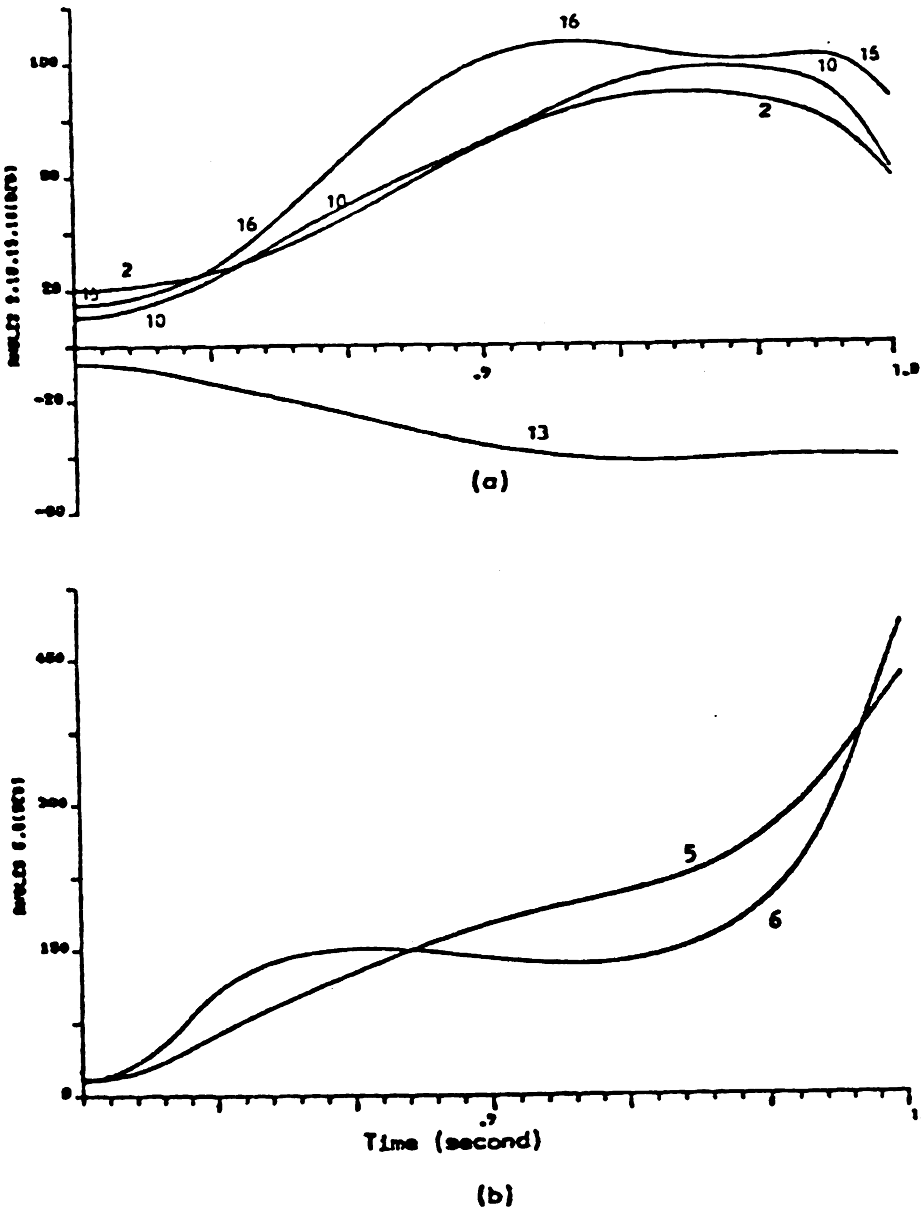

Figure 4.12. Swing curves. Clearing time = .1925 seconds.
(a) Generators 2, 10, 13, 16.
(b) Generators 5, 6.

times t_c of 0.19 and 0.1925 seconds, respectively. For $t_c = 0.19$ seconds all the rotor positions do not exceed the stability limit and do not accelerate indefinitely. However, it is clear that the behavior of generators 5 and 6 is different from that of the other generators. Figure 4.12, where the fault was cleared at $t_c = 0.1925$ (sec.), also indicates the similarity in behavior of generators 5 and 6, but here they are both accelerated and thus pull out of step from the rest of the system, causing instability. Based on simulation, it was observed that for clearing time of $t_c = 0.1922$ seconds the system was critically stable as shown in Figures 4.13a and 4.13b. Note that the peak of the swing curves of the stationary group is somewhere around 90°-100°, while that of the critical group is about 160°-170°, confirming the fact that the critical group is initially pulling away from the stationary group but at a later time all of the generators resume a relatively small angle indicating stability. For the same clearing time, i.e., $t_c = .1922$ seconds, Figure 4.14a illustrates the sum of the potential energy produced between generators 5 and 6 and all of the generators of the stationary group. Figure 4.14b shows the plot for the potential energy produced between generator 5 and the stationary group and a similar one for the partial potential energy between generator 6 and the stationary group. The peak of the partial potential energy of generator 6 indicates the maximum energy capacity of the transmission network connecting generator 6 to the stationary group. Before reaching the peak of potential energy, there is a strong coupling between generator 6 and the

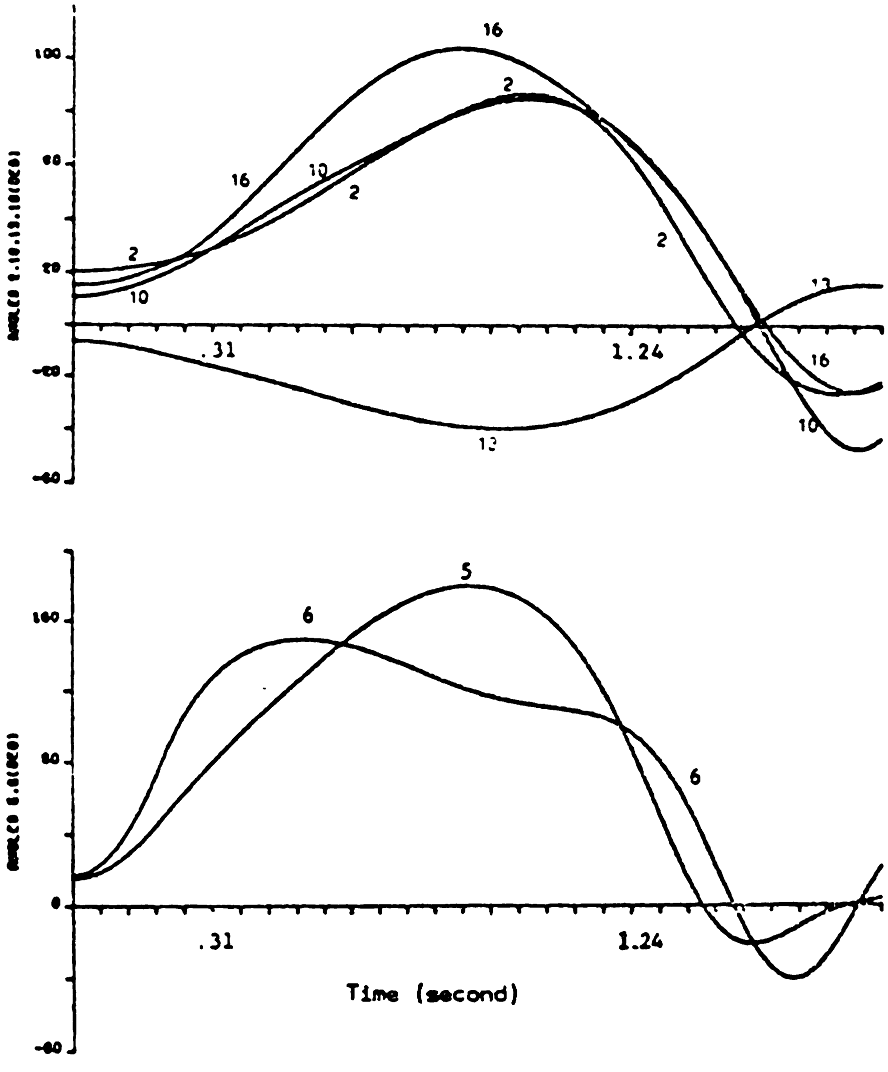

Figure 4.13. Swing curves. Clearing time = .1922 seconds.

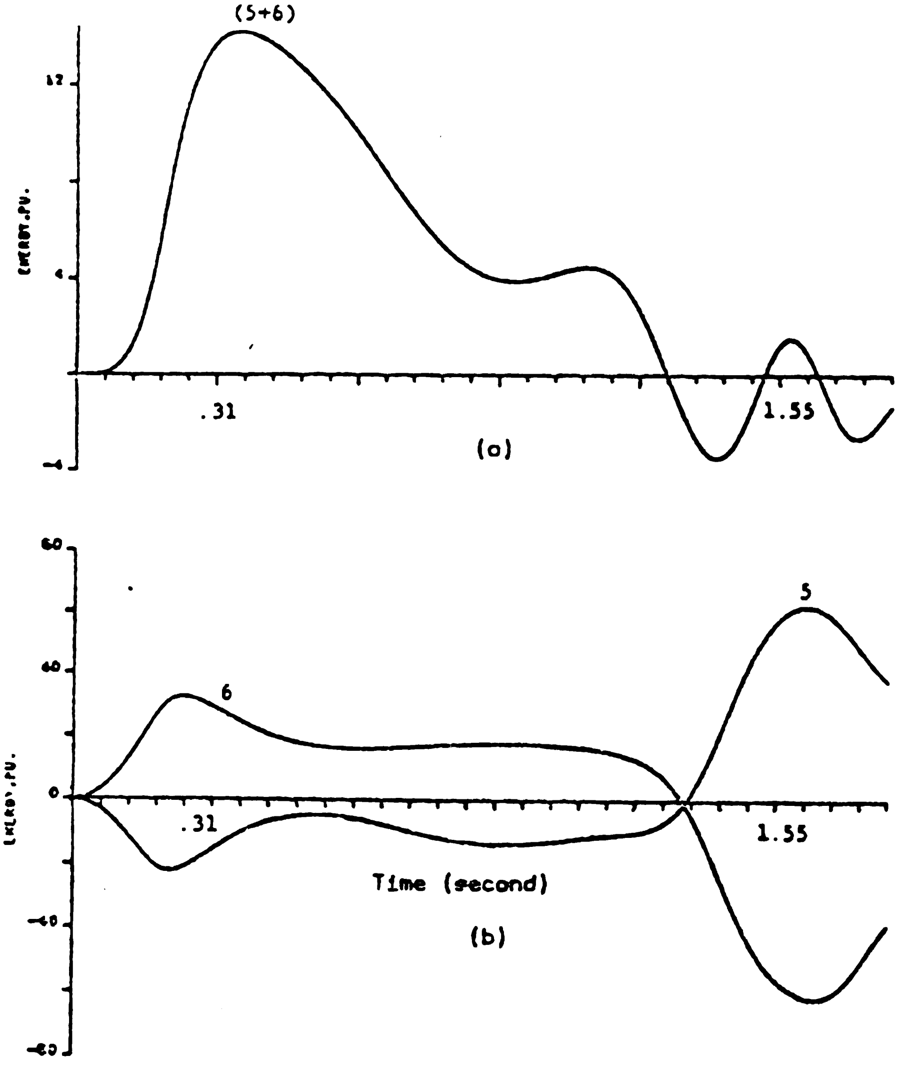

Figure 4.14. Partial energy analysis. Clearing time = .1922 seconds.
(a) Sum of partial energies for generators 5 and 6.
(b) Partial energy for generators 5 and 6.

stationary group, and after the energy exceeds the maximum potential energy capacity of all lines connecting 6 and the stationary group, the magnetic coupling between generator 6 and the stationary group becomes weakly coupled. If generator 6 was the only machine in the critical group, one could conclude that generator 6 would pull away from the system and thus lose synchronism. However, for this case, where generator 5 is also in the critical group, one cannot yet make any decision on the loss of stability. Now consideration of the energy behavior of generator 5 reveals that the peak of the partial potential energy of generator 5 is reached at a later time, indicating the fact that although generator 6 is trying to pull away from the system, generator 5 maintains a strong coupling to the stationary group. Thus, among the generators of the critical group (5 and 6), generator 5 is the last generator to exceed its potential energy boundary capacity and therefore is by definition the critical generator.

Now that the critical generator is identified, it still remains to identify a boundary of stability. For both the inclusion and exclusion of the transfer conductances, several simulation runs for different clearing times were performed by Rastgoufard [29]. Figures 4.15-4.18 illustrate some of these results. Figure 4.15 depicts the partial potential energy across the boundary of generator 6, cleared at $t_c = .18$ seconds. It is clearly seen that for this case the minimum of $\Delta E_6(t,t_c)$ is negative (for both cases with and without transfer conductances), confirming the stability of the system. However, in contrast to the case of equal area criterion of one

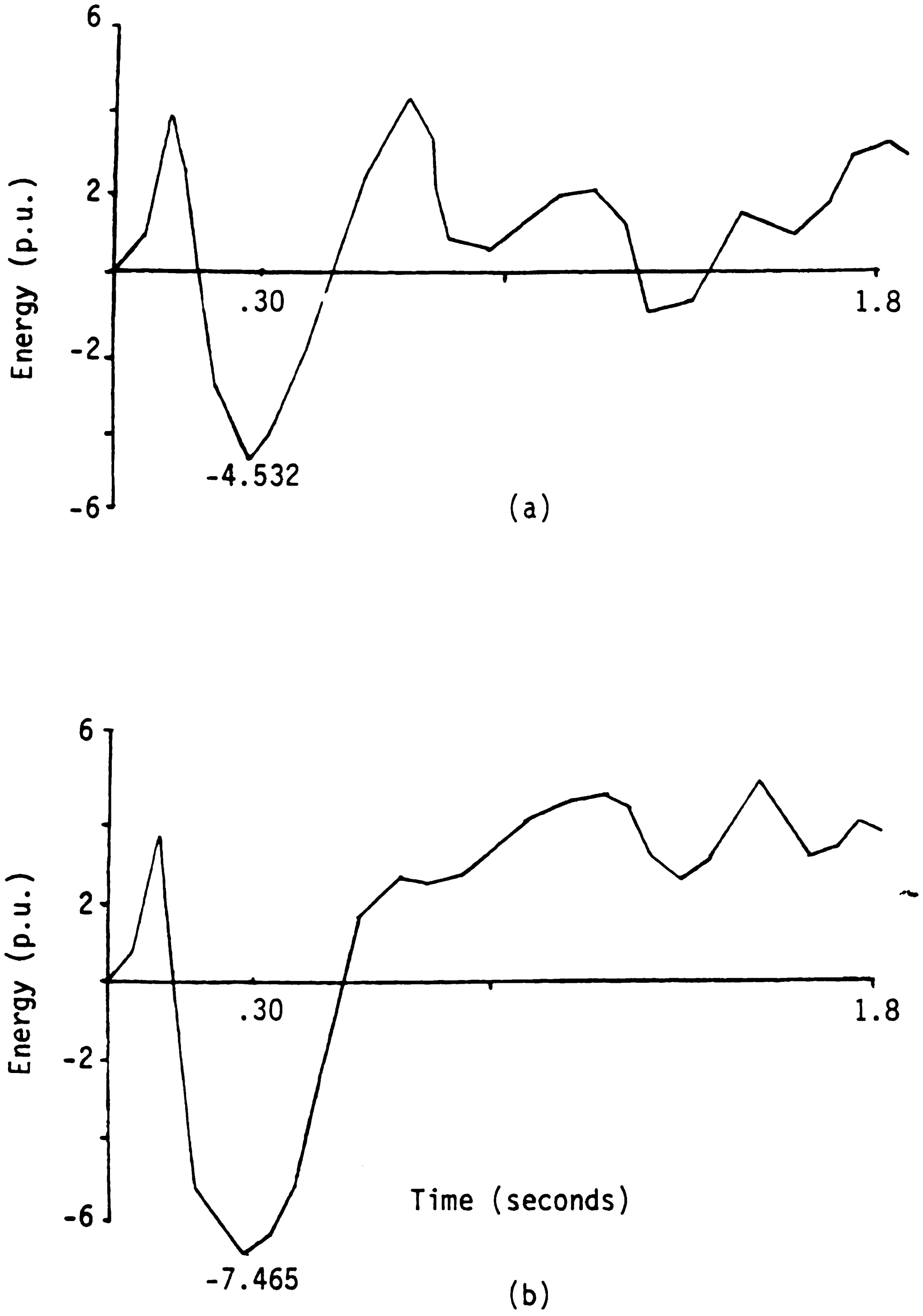

Figure 4.15. Equal area analysis $\Delta E(t) = A_1(t) + A_2(t)$. Raun case, 6-infinite bus. Clearing time = .18 seconds. (a), (b) Transfer conductance excluded and included, respectively.

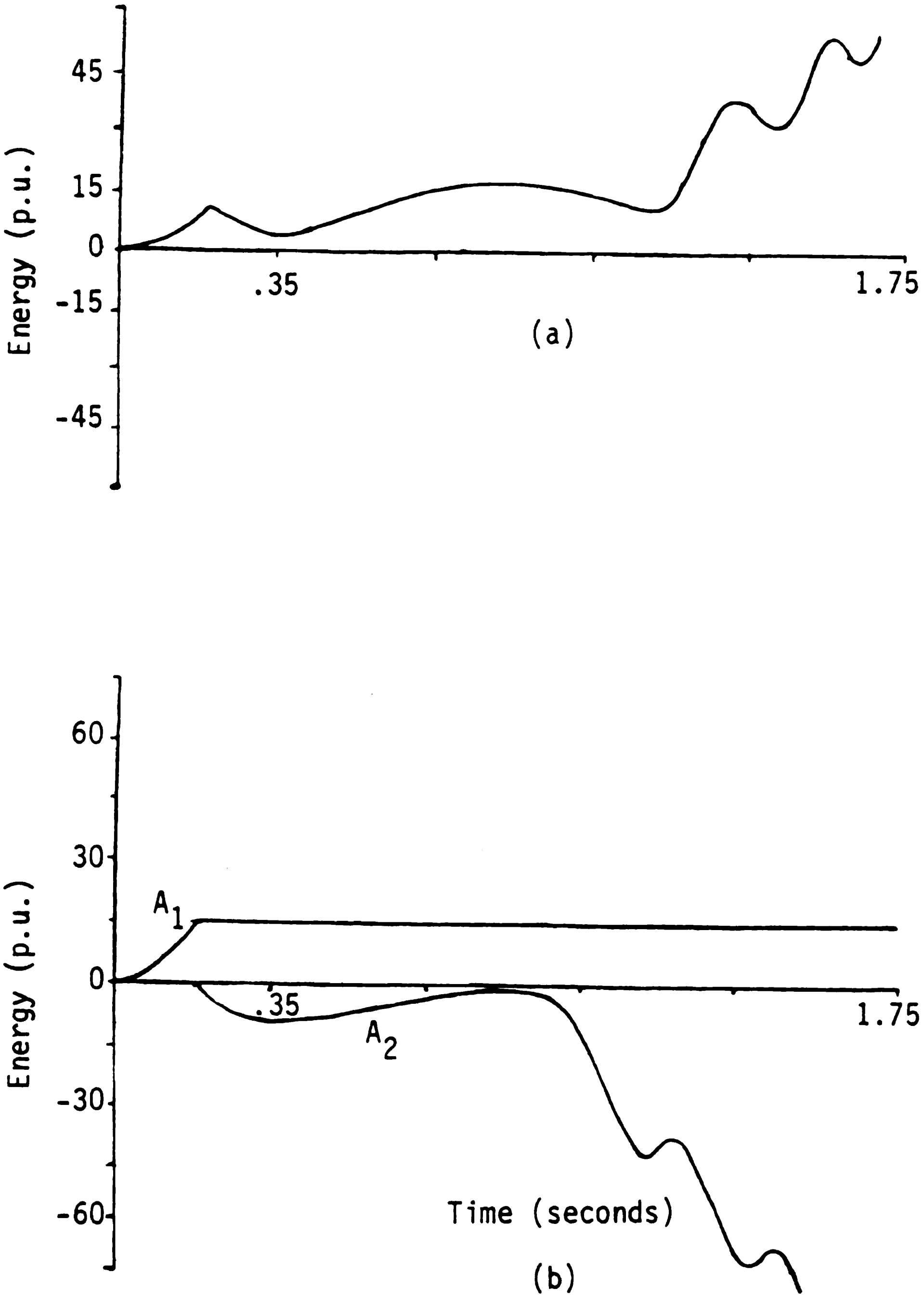

Figure 4.16. Equal area analysis. Raun case, 6-infinite bus. Clearing time = .1925 seconds.
(a) $\Delta E(t) = A_1(t) + A_2(t)$ vs. time (transfer conductance excluded).
(b) Areas $A_1(t)$ and $A_2(t)$ (transfer conductance excluded).

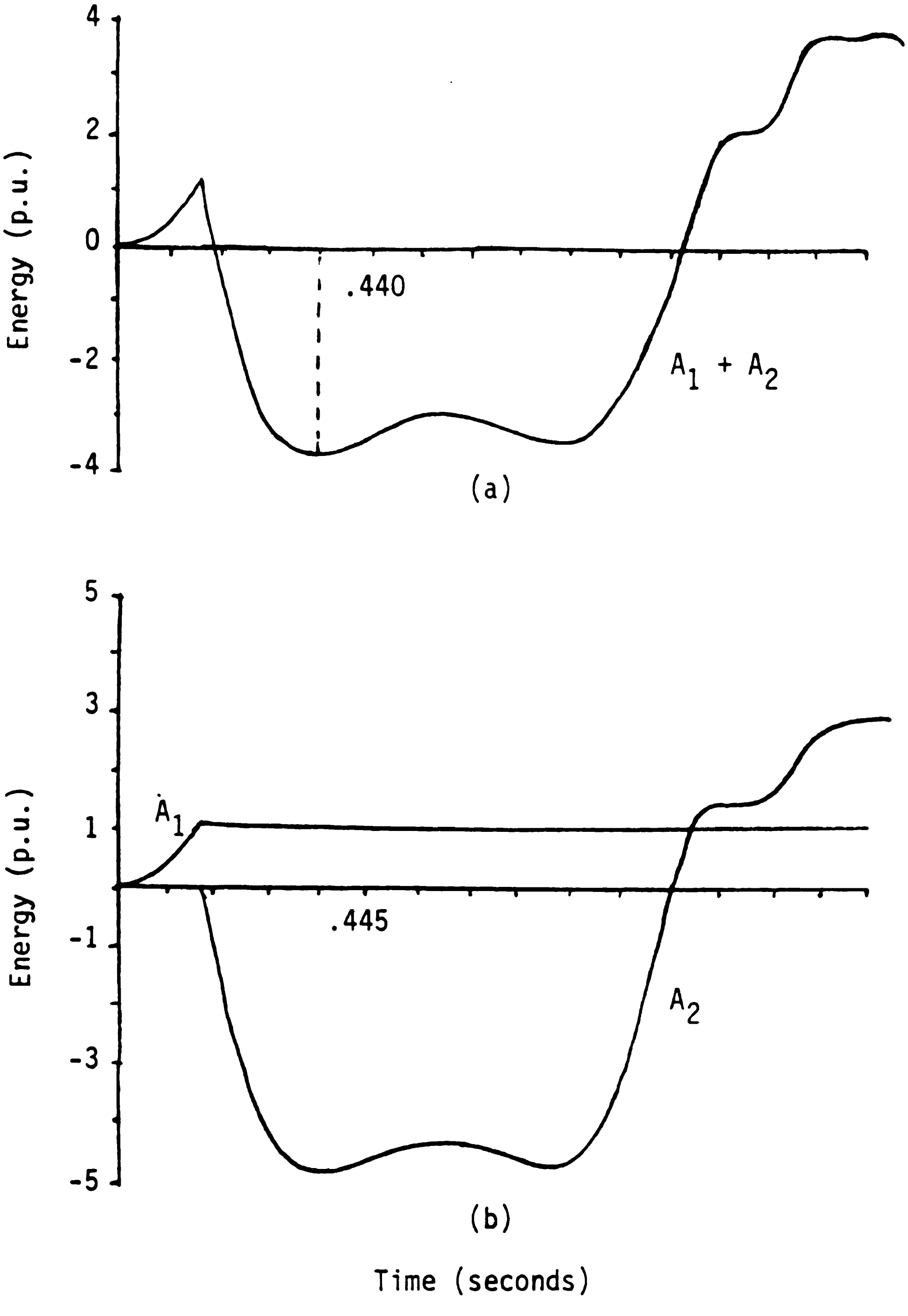

Figure 4.17. Equal area analysis. Raun case, 5-infinite bus. Clearing time = .1922 seconds.
(a) $\Delta E(t) = A_2(t) + A_1(t)$ vs. time (transfer conductance included).
(b) Areas $A_1(t)$ and $A_2(t)$ vs. time (transfer conductance included).

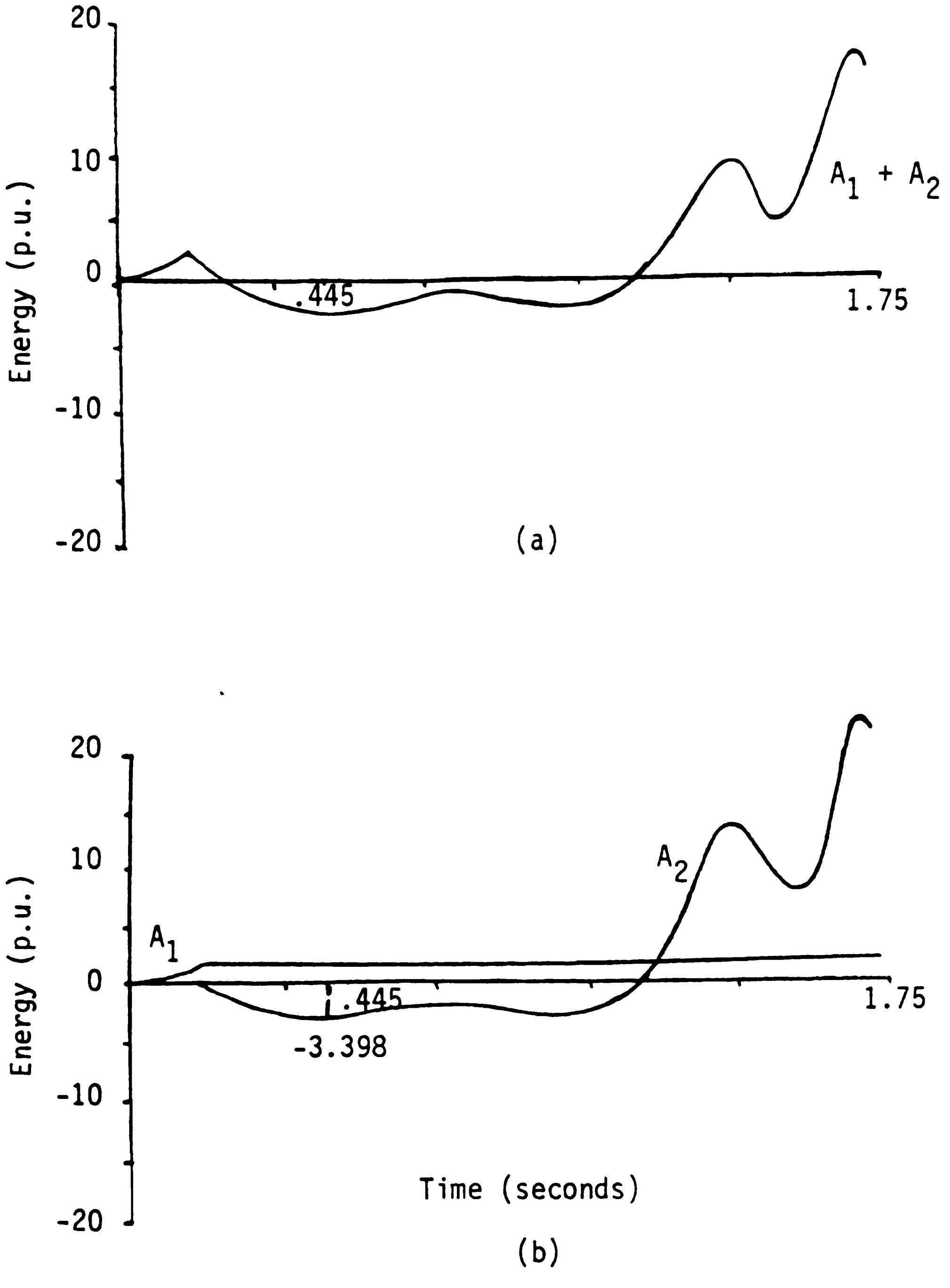

Figure 4.18. Equal area analysis. Raun case, 5-infinite bus. Clearing time = .1925 seconds.
(a) $\Delta E(t) = A_1(t) + A_2(t)$ vs. time (transfer conductance included).
(b) Areas $A_1(t)$ and $A_2(t)$ vs. time (transfer conductance included).

machine infinite bus, the minimum of $\Delta E_6(t,.18)$ is not zero. As was discussed earlier, this phenomenon was expected. In Figure 4.16, where the fault is cleared at $t_c = 0.1925$, the minimum of energy margin $\Delta E_6(t,t_c)$ has positive value ($|A_1| > |A_2|$), indicating loss of stability.

Figures 4.17 and 4.18 depict the generator 5 potential energy boundary for $t_c = .1922$ and $.1925$ seconds, respectively. In comparing the behavior of generator 5 with that of generator 6, it is seen that the minimum of $\Delta E(t,t_c)$ for generator 5 takes place at a later time than that of generator 6. Although the energy boundary of both generators predicts $t_{cc} \in (.1922, .1925)$, the fact that the minimum of $\Delta E(t,t_c)$ for generator 5 occurs at a later time confirms that generator 5 is the critical generator.

Both the PEBS and EAC methods using the individual energy function accurately determined the critical clearing time for the cases studied. However, these results were based on step-by-step integration of system differential equations to evaluate the individual potential energy required at each integration step. The major point of interest here is to test the proposed direct methods (to be described in Chapter 5) on the same Reduced Iowa System and compare the results of predicting the boundary of stability with that of simulation results.

CHAPTER 5

PROPOSED DIRECT STABILITY ASSESSMENT ALGORITHMS

The purpose of this chapter is to develop a fast PEBS method and a fast equal area method using the individual machine energy functions. The results of the previous chapter indicated that both the PEBS method and equal area method using the individual machine energy function are extremely accurate in determining the critical clearing time for a particular fault, which is a measure of its ability to test whether a system is stable for that fault and the clearing time and the margin of stability. However, these results were based on simulation of the system differential equations to evaluate the individual potential energy:

$$\begin{aligned} V_{PE_i}(t) = {} & \frac{1}{M_T}\sum_{\substack{j=1\\ j\neq i}}^{n} (P_iM_j - P_jM_i)(\theta_{ij}(t) - \theta_{ij}^{s1}) \\ & + \sum_{\substack{j=1\\ j\neq i}}^{n} C_{ij}(\cos\theta_{ij}(t) - \cos\theta_{ij}^{s1}) \\ & - D_{ij}\,\frac{\theta_i(t) + \theta_j(t) - \theta_i^{s1} - \theta_j^{s1}}{\theta_i(t) - \theta_j(t) - \theta_i^{s1} + \theta_j^{s1}}\,[\sin\theta_{ij}(t) - \sin\theta_{ij}^{s1}] \end{aligned} \tag{5.1}$$

required for the PEBS and equal area methods at each integration step. Thus the results of Chapter 4 suggest that the equal area and PEBS methods are extremely accurate in confirming the conclusion concerning whether the system is stable or unstable, which can also be determined by observing the simulated system trajectory. Thus the PEBS and equal area methods are totally dependent on the transient stability simulation and only provide a quantitative measure in terms of energy of the relative margin of stability or instability.

The objective in developing the PEBS and equal area methods was to develop fast stand alone algorithms that could determine whether a system is stable or unstable; the margin of stability for a particular fault, clearing time, and operating condition; and the sensitivity of the stability to such operating conditions as network configuration, load level, generation dispatch, etc. These stand alone algorithms obviously should not require time step integration of the transient stability model but should provide the same results and conclusions concerning the stability of the system; the margin of stability for the fault, clearing time, and operating conditions; and sensitivity to operating conditions.

The fast PEBS and fast equal area methods require methods for:

(1) Obtaining the total energy which the system gains during the fault-on period. This has previously been accomplished by performing a step-by-step integration of the faulted system equations and simultaneously calculating the appropriate energy;

(2) Determining the critical generator and thus the generator for which the individual energy function is evaluated;

(3) Determining the actual critical energy by calculating the peak potential energy using the PEBS method;

(4) Computing the energy at the proper unstable equilibrium point (u.e.p.) using the UEP method.

Two algorithms have been proposed for producing system trajectory approximations that could provide the above information required by fast PEBS and fast equal area methods. These Taylor series and cosine series approximations algorithms are discussed in this chapter and shown to either be inaccurate or require computational requirements comparable to simulating the system trajectory.

A fast PEBS and a fast equal area method are then proposed based on using an RMS coherency measure to accurately predict the state when the system trajectory either most closely approaches or crosses the PEBS. These fast PEBS and equal area methods do not require approximating the faulted system trajectory over time but rather only require predicting the trajectory when it comes closest to or crosses the PEBS for a specific fault and fault clearing time.

The cosine and Taylor series approximations of the system trajectory are discussed first before the fast PEBS and equal area methods based on the RMS coherency measure [21]. The RMS coherency measure is then developed in Chapter 6.

5.1. Modified Transient Energy Method

5.1.1. Fault Trajectory Approximation by Cosine Series

From the concepts of the previous section it is understood that a knowledge of the faulted system trajectory is necessary or very useful.

A simple approximation of the system fault trajectory developed by Athay et al. has been proven to be sufficiently accurate in some cases for the four purposes mentioned above. Representing the center of angle referenced accelerating powers of the faulted system by f_i (i.e., f_i = the right hand side of equation (2.10)), the form of the approximation is

$$f_i = a_i + b_i \cos \omega t \qquad i = 1, 2, \ldots., n \qquad (5.2)$$

The The method for determining the unknown constants a_i, b_i, $i = 1, 2, \ldots., n$ and the frequency ω are quickly summarized; basically, two power flow solutions are utilized [17]. The first, at the instant of fault application, determines the parameters a_i, b_i, $i = 1, 2, \ldots., n$ for a given frequency ω. The second, along an approximate trajectory shortly after the fault, is used to compute ω. Angles obtained from this fault trajectory approximation are given in Table 5.1 for a particular case on the ten machine New England System. The comparison of the actual angles and those obtained by this approximation indicates that the approach can be quite accurate in some cases. The approach will not be accurate at all for long faults where the post-fault network determines the

Table 5.1. Comparison of fault trajectory angles at t = 0.4 sec. (fault on bus 15, New England system).

unit	actual	cosine approximations
1	- 38.0	- 38.1
2	55.7	55.4
3	63.2	63.2
4	98.5	98.8
5	91.2	91.0
6	95.0	95.7
7	100.7	101.2
8	43.9	42.4
9	71.7	71.5
10	8.2	9.4

critical generator that loses stability and not the initial acceleration during the fault. Thus, the cosine approximation can only be used in cases where the fault clearing time is small and stability is assured.

5.1.2. Trajectory Approximations by Taylor Series

The Taylor series method proposed in Ref. [19] is conceptually attractive. The absolute rotor angles $\delta_i(t)$, i = 1, 2, ..., n are approximated by Taylor series expansion and the coefficients of the series are computed from the prefault operating point δ^{s1} using the faulted admittance matrix. Because of the fact that all $\dot{\delta}_i$'s are zero, the computation of the Taylor series coefficients would be simplified because all the odd coefficients are zero.

A more accurate form of this method would be to update the Taylor series coefficients at successively smaller time intervals until the desire accuracy is achieved. This procedure is in contrast with the alternative of increasing the order of the Taylor series until the desired accuracy is achieved. This updating procedure involves more terms since the $\dot{\delta}_i$'s are no longer zero at each update. The form for updating at $t = t_o$ for the fourth order series is

$$\delta_i(t) = \delta_i^{(o)}(t_o) + \delta_i^{(1)}(t_o)(t - t_o) + \frac{\delta_i^{(2)}(t_o)(t - t_o)}{2!} + \frac{\delta_i^{(3)}(t_o)(t - t_o)^3}{3!} + \frac{\delta_i^{(4)}(t_o)(t - t_o)^4}{4!} \tag{5.3}$$

where

$$\delta_i^{(1)}(t) = \omega_i(t) = \delta_i^{(1)}(t_0) + \delta_i^{(2)}(t_0)(t - t_0)$$

$$+ \frac{\delta_i^{(3)}(t_0)(t - t_0)^2}{2!} + \frac{\delta_i^{(4)}(t_0)(t - t_0)^3}{3!} \tag{5.4}$$

where t_0 is the time of last update

$$\delta_i^{(2)}(t) = \frac{1}{M_i}\Big[P_i - \sum_{\substack{j=1\\ j\neq i}}^{n} (C_{ij} \sin \delta_{ij}(t) + D_{ij} \cos \delta_{ij}(t))\Big] ,$$

$$\delta_i^{(3)}(t) = \frac{1}{M_i}\sum_{\substack{j=1\\ j\neq i}}^{n} \Big\{\big[D_{ij} \sin \delta_{ij}(t)$$

$$- C_{ij} \cos \delta_{ij}(t)\big]\big[\delta_i^{(1)}(t) - \delta_j^{(1)}(t)\big]\Big\} ,$$

$$\delta_i^{(4)}(t) = \frac{1}{M_i}\sum_{\substack{i=1\\ i\neq i}}^{n} \Big\{ \big[D_{ij} \sin \delta_{ij}(t)$$

$$- C_{ij} \cos \delta_{ij}(t)\big]\big[\delta_i^{(1)}(t) - \delta_j^{(1)}(t)\big]^2$$

$$+ \big[D_{ij} \sin \delta_{ij}(t) - C_{ij} \cos \delta_{ij}(t)\big]\big[\delta_i^{(2)}(t) - \delta_j^{(2)}(t)\big]\Big\} \tag{5.5}$$

To implement this Taylor series updated given $t_0 = 0$ and $\{\delta_i(0)\}_{i=1}^n$ and $\{\omega_i(0)\}_{i=1}^n = 0$:

(1) Set $m = 0$.

(2) Compute the new $\{\delta_i^{(k)}(t_0)\}_{i=1}^n$ for $k = 0, 1, 2, 3, 4$ at $t_0 = m \cdot \Delta$.

(3) Set the new $t = (m + 1) \cdot \Delta$ (time of update).

(4) Utilizing $\delta_i^{(k)}(t_0)$, t_0, and t, compute $\{\delta_i(t)\}_{i=1}^n$ and $\{\omega_i(t)\}_{i=1}^n$ using (5.3) and (5.4).

(5) If $(m + 1) \cdot \Delta \geqq t_f$, stop; otherwise return to step (2) with $m = m + 1$.

These approximated trajectories produce very nearly the same energy functions as the exact trajectories. From numerical results of the fault on cases studied, a single update at $t = 0.2$ was enough to give the same results as the exact trajectory.

Although it is found that the Taylor series method of Ribbens Pavella [19] avoids integration of the differential equations and gives acceptable accuracy, updating this Taylor series which calculates the rotor angles $\{\delta_i(t)\}_{i=1}^n$ and their successive derivatives $\delta_i^{(k)}(t_0)$ for $k = 0, 1, 2, 3, 4$ at each updating time using equations (5.4) and (5.5) requires a large number of algebraic operations (additions, multiplications, and divisions) which is comparable to the number of operations needed to solve load flow equations using a Gauss Seidel method at each integration step for a transient stability simulation.

Thus the computation for each update of the Taylor series algorithm at time step $m \cdot \Delta$ is comparable to that for solving the network equations using a Gauss Seidel algorithm at each integration step. Since the time step for the Taylor series update and the integration step sizes are comparable, the Taylor series algorithm does not appear to significantly reduce computation compared to a conventional transient stability simulation even though the Taylor sieres can be quite accurate.

Having presented the two methods that have been proposed for fast transient stability simulation, the PEBS and equal area methods using the individual machine energy function are now reviewed in terms of the information required to produce a fast transient stability assessment procedure. The results of this review of these methods is that one could produce an extremely fast method for transient stability assessment if a direct method for predicting the state of the system when the system trajectory most closely approaches the boundary energy (stable case) or crosses it (unstable case) for a particular fault and clearing time could be developed. A method for direct prediction of this state using the RMS coherency measure is then proposed in the next chapter.

5.2. Fast PEBS Method

Using the individual machine energy function, the boundary of the region of the stability is determined by the potential energy boundary surface (PEBS) as discussed in Chapters 2 and 3. At the PEBS which is defined for the post-fault network, the potential energy of the critical generator with respect to the rest of the generators in the system is maximum, and on the boundary of the region of stability the total energy of the critical generator with respect to the rest of the system is equal in magnitude to the potential energy at PEBS. Since at the PEBS the potential energy is maximum, stability is maintained if the system kinetic energy is totally converted to potential energy (single machine infinite bus system) or if the system kinetic energy is minimum (multiple machine system) before reaching the PEBS. This maximum of potential energy as a function of time (5.1) varies with clearing time $t_c < t_{cc}$ since the maximum $\theta_i(t)$ depends on t_c. Thus, one can write Max $V_{PE}(t,t_c) = V_{PE}(t_B,t_c) = V^*_{PE}(t_c)$ where $t_B(t_c)$ is the time where $V_{PE}(t,t_c)$ is maximum for clearing time t_c. Increasing t_c for $t_c < t_{cc}$ will increase this maximum value of the potential energy of the critical generator $V^*_{PE}(t_c)$ and it reaches its highest value for $t_c = t_{cc}$. This particular maximum value of potential energy for $t_c = t_{cc}$ is called the critical energy of generator i with respect to the rest of the system generators and it is denoted by V_{cr}. For large clearing times $t_c > t_{cc}$, some of the generators in the stationary group may start accelerating and also become separated from the rest of the generators in the stationary group. As a result of this phenomenon, the system kinetic energy is not totally converted to potential energy (i.e., the power system does not behave as a single machine and infinite bus system) and even for large system the system kinetic energy is not minimum at the PEBS based on the individual machine energy function. Therefore as t_c keeps increasing for $t_c > t_{cc}$, the maximum of potential energy $V_{PE}(t_c)$ at PEBS decreases. In order to determine the precise value of the critical energy as well as the critical clearing time, one has to compute the maximum of potential energy for different clearing times and search for the highest value among these maximum potential energies.

Based on the fact that the rate of change of the maximum of potential energy for $t_c > t_{cc}$ may be small, one could use the maximum potential energy $V^*_{PE}(t_c)$ of the critical generator or group for some arbitrary large clearing time $t_{c_1} > t_{cc}$, and compare it with the potential energy of the critical generator or group at clearing time $t_c < t_{cc} < t_{c_1}$ where the stability is desired to be tested. If $V^*_{PE}(t_{cc})$ is much greater than $V^*_{PE}(t_{c_1})$, as shown in Figure 5.1., one could use $V^*_{PE}(t_{c_1})$ as V_{cr} if $V^*_{PE}(t_c)$ rises very rapidly for values of t_c slightly less than t_{cc}. Utilizing $V^*_{PE}(t_{c_1})$ for $t_{c_1} = .240$ would indicate the system is stable for $t_c < .217$ rather than for $t_c \leq t_{cc} = .220$ in the Cooper case from Table 4.2. Utilizing $V^*_{PE}(t_{c_1})$ for $t_{c_1} = .368$ would indicate the system is stable for $t_c < .345$ rather than $t_{cc} \cong .354$ in the Fort Calhoun case from Table 4.5. As t_{c_1} were to increase the error in being able to determine t_{cc} or judging values of t_c for which the system is stable would increase. The error does not appear unacceptable for the applications of a fast transient stability assessment method such as a screening tool for assessing fault contingencies in operation or expansion planning or for use by operators in control centers.

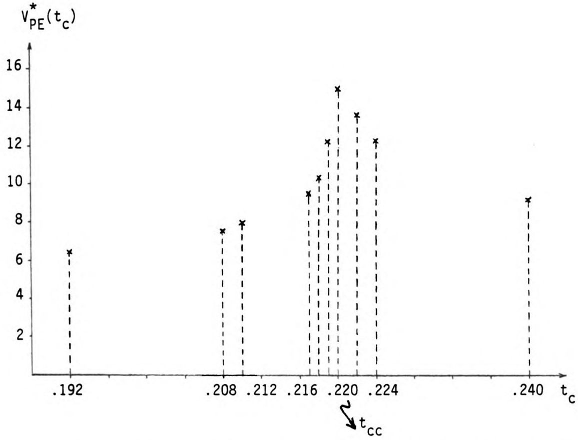

Figure 5.1. Determination of critical boundary for critical generator using maximum potential energy $V^*_{PE}(t_c)$ method.

Determination of the critical generator or group as well as the states (rotor angles of the generators) of the system at time t_B is the critical requirement for calculating the critical energy

$$V_{PE}(t_c) = V_{PE}\Big|_{\theta^{s1}}^{\theta(t_B,t_c)}$$

for either t_{c_1} or t_c using equation (5.1). Transient stability simulation study shows that the rotor angles of the generators of the system at time t_B are at their peak values. The previous algorithms discussed earlier in determining the generator angles at any specific time dealt with the simulation of the trajectories and thus required a significant amount of computations.

The RMS coherency measure (linear/nonlinear) technique developed by Schlueter in 1978 [21] seems to be appropriate to use as a direct method of predicting the peak angles $\theta(t_B,t_c) = \theta^{max}$ and also the critical generator or group of the system. If one used the RMS coherency measure to predict the state $\underline{\theta}(t_B;t_c)$ at which the trajectory most closely approaches or crosses the potential energy boundary surface for any clearing time in order to evaluate $V^*_{PE}(t_c)$, the error in determining t_{cc} by maximizing the function $V^*_{PE}(t_c)$ is only the error in predicting $\theta(t_B;t_c)$ for each t_c. However, if one evaluates $V^*_{PE}(t_{c_1})$ for some $t_{c_1} > t_{cc}$ using the RMS coherency measure, then the error in determining t_{cc} and assessing whether the system is stable depends on both the difference $V^*_{PE}(t_{cc}) - V^*_{PE}(t_{c_1})$ and the error in predicting $\theta(t_B;t_c)$ for some t_c and t_{c_1}. The elimination of the computation to maximize $V_{PE}^{*}(t_c)$ is justified if this error in determining t_{cc} due to $V_{PE}^{*}(t_{cc}) - V_{PE}^{*}(t_{c_1})$ is not large.

Chapter 6 of this thesis defines this RMS coherency measure and outlines the procedure of obtaining the peak angles $\theta(t_B;t_c)$ and identifying the critical generator. Finally, it provides the theoretical justification and verification for the use of the RMS coherency measure as a fault security measure based on analysis on a second order system.

5.2.1. Efficient PEBS Algorithm for Predicting Stability

The procedure for computing the boundary (critical) energy V_{cr} and using it as a stability limit consists of the following steps:

(1) Solve base case load flow equation (5.6) to obtain generator angles at prefault (initial) operating point θ^{s1}.

$$M_i\dot{\omega}_i = P_i - \sum_{\substack{j=1 \\ j\neq i}}^{n} [C_{ij} \sin \theta_{ij} - D_{ij} \cos \theta_{ij}] = 0 \tag{5.6}$$

where

$$\theta_{ij} = \theta_i - \theta_j$$

$$\theta_i = \delta_i - \delta_0$$

$$\delta_0 \triangleq \frac{1}{M_T}\sum_{i=1}^{n} M_i\delta_i$$

$$M_T \triangleq \sum_{i=1}^{n} M_i$$

$\delta_0 \triangleq$ center of inertial angle

(2) For an arbitrary large clearing time ($t_{c_1} >> t_{cc}$) use the linear or nonlinear RMS coherency measure for the particular fault to obtain the peak angles θ^{max} as well as the critical group or critical generator.

(3) Having determined the critical generator i which is necessary to determine the proper generator to write the individual machine energy function, the prefault operating point θ^{s1} and the peak angles $\theta(t_{B_1},t_{c_1}) = \theta^{max}$, calculate the potential energy at time t_{B_1}, $V^{*}_{PE_i}(t_{c_1}) = V_{PE}(t_{B_1};t_{c_1})$

$$V_{cr} = V_{PE_i}\Big|_{\theta^{s1}}^{\theta^{max}} = V_{PE}(t_{B_1},t_{c_1})$$

$$= \frac{1}{M_T}\sum_{\substack{j=1\\ j\neq i}}^{n} (P_iM_j - P_jM_i)(\theta_{ij}^{max} - \theta_{ij}^{s1})$$

$$+ \sum_{\substack{j=1\\ j\neq i}}^{n} C_{ij}(\cos\theta_{ij}^{max} - \cos\theta_{ij}^{s1}) -$$

$$- D_{ij} \frac{\theta_i^{max} + \theta_j^{max} - \theta_i^{sl} - \theta_j^{sl}}{\theta_i^{max} + \theta_j^{max} - \theta_i^{sl} + \theta_j^{sl}} [\sin \theta_{ij}^{max} - \sin \theta_{ij}^{sl}] \qquad (5.7)$$

(4) For a specific clearing time $t_c < t_{c_1}$, where the stability of the system is desired to be tested, repeat steps 2 and 3, and then calculate potential energy of the critical generator $V^*_{PE_i}(t_c)$ and compare it to $V_{cr} = V^*_{PE_i}(t_{c_1})$.

(5) If $V_{PE_i}(t_c) \leqq V_{cr} = V_{PE_i}(t_{c_1})$ the system remains stable, and if $V_{PE_i}(t_c) > V_{cr} = V_{PE_i}(t_{c_1})$ the system would be unstable.

The applications of this algorithm to different fault cases on the Reduced Iowa system are discussed in Chapter 7 and the results obtained from these applications verify the accuracy of the algorithm.

5.3. Fast Equal Area Method

From review of Chapter 3 it is understood that for multi-machine power systems the equal area criterion considers a particular generator (critical generator) against the rest of the generators in the system. The amount of energy produced during the fault period (accelerating energy) $A_1(t_c)$ is added to the energy after the fault is cleared (decelerating energy) $A_3(t)$ and the quantity $\Delta E(t_B, t_c) = A_1(t_c) + A_3(t_B)$ at time t_B, the time at which the system generators peak, determines the stability of the system as shown in Figure 3.2 in Chapter 3 for single machine infinite bus system. In order to determine the stability boundary of the system t_{cc} very accurately, one has to compute the minimum energy difference $\Delta E(t_B,t_c) = \Delta E^*(t_c)$ for different clearing times and search for the smallest value among these minimum energy differences. This search technique, of course, requires more computations and hence it is time consuming and requires significant computation.

An approximation method is proposed that does not require determining the minimum of $\Delta E^*(t_c)$. If $\Delta E^*(t_c)$ is near zero for $t_c \lessapprox t_{cc}$ for any fault case, it may be possible to test for stability of the system by determining whether $\Delta E^*(t_c)$ is less than some small ε. The selection of ε appears to be fault dependent based on the results for the Cooper and Fort Calhoun cases in Tables 4.3 and 4.4, respectively. Furthermore, the assumption that if $\Delta E^*(t_c) < \varepsilon$ stability is assured is not exactly correct since the value of $\Delta E^*(t_c)$ for some interval t_c above t_{cc} is less than ε as shown in Figure 5.2. If this interval is small, and if one could find an ε for all fault cases, the algorithm presented in the next subsection could be used for fast stability assessment.

Determination of the critical generator and the generator angle positions of the system at time t_B (θ^{max}) and clearing time $t_c(\theta^c)$ is the key point in calculating the minimum of energy difference $\Delta E(t_B,t_c) = \Delta E^*(t_c)$. Analogous to the "fast PEBS method," one could apply the same RMS coherency measure (linear/nonlinear) technique referenced in section 5.2 for post-fault network and directly predict the peak angles θ^{max} as well as the critical generator of the system.

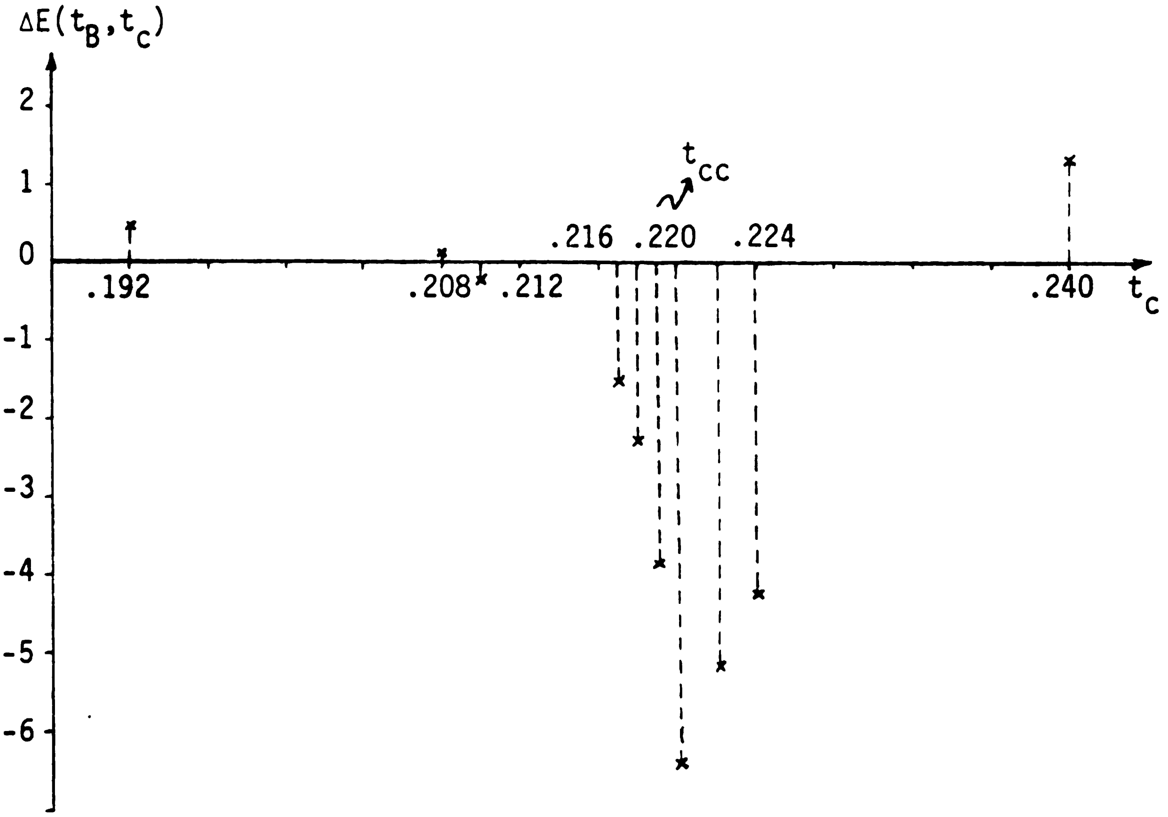

Figure 5.2. Determination of critical boundary for critical generator using minimum energy margin $\Delta E(t_B,t_c)$ method.

The angles at clearing time $t_c(\theta^c)$ can be approximated with enough accuracy by using the Taylor series approximation algorithm as described in subsection 5.1.2 for the faulted network. The following subsection summarizes the algorithm and outlines the procedure in a suitable order.

5.3.1. Efficient Equal-Area Algorithm for Predicting Stability

The procedure for computing the transient energy margin $\Delta E^*(t_c)$ and predicting the stability of the power system involves the following computations:

(1) Solve the base case load flow equation (5.6) to obtain generator angles at prefault (initial) operating point θ^{s1}.

(2) Apply Taylor series approximation algorithm for faulted network to obtain the generator angles at clearing time $t_c, \theta(t_c) = \theta^c$.

(3) Use the linear pulse coherency measure to obtain angles at time $t_B, \theta(t_B) = \theta^{max}$ and the critical generator.

(4) Having determined the critical generator and thus the generator for which the individual machine potential energy is to be evaluated, compute energy $A_1(\theta^{s1}, \theta^c)$ for faulted network using equation (5.1)

$$A_1(\theta^{s1}, \theta^c) = V_{PE_i} \Big|_{\theta^{s1}}^{\theta^c}$$

(5) Compute energy $A_2(\theta^c,\theta^{max})$ for post-fault network using equation (5.1)

$$A_2(\theta^c,\theta^{max}) = V_{PE_i} \Big|_{\theta^c}^{\theta^{max}}$$

(6) Compute the sum of $A_1 + A_2$.

(7) If $A_1 + A_2 \leq \varepsilon$, the system is stable. If $A_1 + A_2 > \varepsilon$, the system is unstable.

This algorithm was tested on the 17-Generator Reduced Iowa System for different fault cases and the results are shown in Chapter 7.

Comparison of the two algorithms, the fast equal-area method and the fast PEBS method, determines that the latter is more efficient and computationally faster because:

(a) it is not necessary to calculate the system parameters for the faulted network, and

(b) there is no need to calculate the generator angles at clearing time $\theta(t_c) = \theta^c$ using the Taylor series approximation which in turn requires a reasonable amount of calculations.

The equal-area method requires both (a) and (b) to compute accelerating energy A_1.

CHAPTER 6

DERIVATION, JUSTIFICATION, AND VERIFICATION OF SECURITY MEASURE, PREDICTION OF PEAK ANGLES

6.1. Introduction

The concepts of this chapter deal with the development of a linearized power system state model, a generalized disturbance model, and the root mean square (RMS) coherency measure. These models and the generalized coherency measure are used to derive algebraic expressions which relate the RMS coherency measure, evaluated over an infinite observation interval for step, impulse, and pulse disturbances in mechanical input power, to the parameters of the power system state model and probabilistic description of the disturbance vector. Finally, the theoretical justification of the fault security measure for a second order system is discussed and the prediction of the peak angles of the power system by RMS pulse coherency measure is verified. The last section derives the computational algorithm of pulse coherency measure for a multimachine power system.

6.2. Linearized Power System Model

A system of linearized state equations is derived for a power system which is composed of classical synchronous machine models, voltage dependent load models, and a transmission network model.

A linear model can be derived from the nonlinear differential equations for the electromechanical motion of the classical synchronous generators plus a set of algebraic equations for the power flows between the generators and the load buses of the system. The electromechanical equations for the motion of each synchronous generator are:

$$\frac{d}{dt}\,\delta_i(t) = \omega_i(t) \tag{6.1a}$$

$$M_i \frac{d}{dt}\,\omega_i(t) = PM_i(t) - PG_i(t) - D_i\omega_i(t) \tag{6.1b}$$

$$i = 1, 2, \ldots, n$$

where

M_i = inertia constant of generator i (in p.u.)
D_i = damping constant of generator i (in p.u.)
δ_i = rotor angle of generator i (in radians)
ω_i = speed of generator i (in rad/sec)
PM_i = mechanical input power of generator i (in p.u.)
PG_i = electrical output power of generator i (in p.u.)
n = total number of generators in the system

In some papers, equation (6.1a) is given as:

$$\frac{d}{dt}\,\delta_i(t) = \omega_0\omega_i(t) = 2\pi f_0\omega_i(t) \tag{6.2}$$

where f_0 is the synchronous frequency of the system in Hertz, and ω_i is in per unit (p.u.) instead of rad/sec. Equations (6.1) are nonlinear because of the nonlinear relationship between PG_i and the bus angles in the interconnected network.

Equations (6.1) can be linearized around the nominal operating conditions δ_i^{sl}, ω_i^{sl}, PG_i^{sl}, and PM_i^{sl} by introducing the following deviations:

$$\Delta\delta_i = \delta_i - \delta_i^{sl}$$

$$\Delta\omega_i = \omega_i - \omega_i^{sl}$$

$$\Delta PG_i = PG_i - PG_i^{sl}$$

$$\Delta PM_i = PM_i - PM_i^{sl}$$

The resulting linear model has the form

$$\frac{d}{dt}\Delta\delta_i(t) = \Delta\omega_i(t) \tag{6.3a}$$

$$M_i\frac{d}{dt}\Delta\omega_i(t) = \Delta PM_i(t) - \Delta PG_i(t) - D_i\Delta\omega_i \tag{6.3b}$$

$$i = 1, 2, \ldots., n$$

where Δ indicates that the variable represents a small deviation from a specified steady state operating point.

The changes in the complex voltages and power injections at the network generator and load buses may be expressed using a Jacobian matrix as [22]

$$\begin{bmatrix} \Delta\underline{PG} \\ \Delta\underline{PL} \\ \Delta\underline{QG} \\ \Delta\underline{QL} \end{bmatrix} = \begin{bmatrix} \partial\underline{PG}/\partial\underline{\delta} & \partial\underline{PG}/\partial\underline{\psi} & \partial\underline{PG}/\partial\underline{E} & \partial\underline{PG}/\partial\underline{V} \\ \partial\underline{PL}/\partial\underline{\delta} & \partial\underline{PL}/\partial\underline{\psi} & \partial\underline{PL}/\partial\underline{E} & \partial\underline{PL}/\partial\underline{V} \\ \partial\underline{QG}/\partial\underline{\delta} & \partial\underline{QG}/\partial\underline{\psi} & \partial\underline{QG}/\partial\underline{E} & \partial\underline{QG}/\partial\underline{V} \\ \partial\underline{QL}/\partial\underline{\delta} & \partial\underline{QL}/\partial\underline{\psi} & \partial\underline{QL}/\partial\underline{E} & \partial\underline{QL}/\partial\underline{V} \end{bmatrix} \begin{bmatrix} \Delta\underline{\delta} \\ \Delta\underline{\psi} \\ \Delta\underline{E} \\ \Delta\underline{V} \end{bmatrix} \tag{6.4}$$

where

$\underline{PG} = [PG_1, PG_2, \ldots., PG_n]^T$	real power injections at internal generator buses (p.u.)
$\underline{QG} = [QG_1, QG_2, \ldots., QG_n]^T$	reactive power injections at internal generator buses (p.u.)
$\underline{PL} = [PL_1, PL_2, \ldots., PL_k]^T$	real power residuals at load buses (p.u.)
$\underline{QL} = [QL_1, QL_2, \ldots., QL_k]^T$	reactive power residuals at load buses (p.u.)
$\underline{E} = [E_1, E_2, \ldots., E_n]^T$	voltages behind transient reactances at generator internal buses (p.u.)
$\underline{\delta} = [\delta_1, \delta_2, \ldots., \delta_n]^T$	angles at internal generator buses (rad)
$\underline{V} = [V_1, V_2, \ldots., V_k]^T$	voltages at load buses (p.u.)
$\underline{\theta} = [\theta_1, \theta_2, \ldots., \theta_k]^T$	angles at load buses (rad)

For low loss systems (resistances in the transmission network are close to zero) equations (6.4) can be simplified by accounting for the decoupling which exists between the real and reactive power flows [23]. The real power flows are largely dependent upon the voltage angles and as a first approximation, the effect of variations in load bus voltage magnitude may be neglected by setting the terms $\partial\underline{PG}/\partial\underline{V}$ and $\partial\underline{PL}/\partial\underline{V}$ in equations (6.4) to zero. The voltages behind the generator transient reactances are constant, thus $\Delta\underline{E} = \underline{0}$. Therefore, in equations (6.4) real power and phase angles are decoupled from reactive power and voltage magnitude. These linearized decoupled equations for real power flows can be written in polar form as:

$$\begin{bmatrix} \Delta\underline{PG} \\ \\ \Delta\underline{PL} \end{bmatrix} = \begin{bmatrix} \partial\underline{PG}/\partial\underline{\delta} & \partial\underline{PG}/\partial\underline{\psi} \\ \\ \partial\underline{PL}/\partial\underline{\delta} & \partial\underline{PL}/\partial\underline{\psi} \end{bmatrix} \begin{bmatrix} \Delta\underline{\delta} \\ \\ \Delta\underline{\psi} \end{bmatrix} \qquad (6.5)$$

The partial derivatives corresponding to the above four terms are most precisely calculated using the voltages and angles at the post-fault steady state operating point δ^{s2}, ψ^{s2}.

The power angle Jacobian matrix in the network equations (6.5) is a sparse, symmetric, and singular matrix. Therefore, a unique solution for $\Delta\underline{\delta}$ and $\Delta\underline{\theta}$, given $\Delta\underline{PG}$ and $\Delta\underline{PL}$, cannot be obtained. This minor problem can be solved by an angle referencing scheme [24].

Equations (6.3) and (6.5) are said to be synchronous frame model since the deviations in generator and bus angles and generator speeds are measured with respect to an external reference rotating at the nominal system speed (f_0 = 60 Hertz). The deviations in generator angles in response to a step disturbance in mechanical input power will appear as ramp function. Therefore, the synchronous frame model has an eigenvalue at the origin (step input, ramp output).

Since a linear state model is desired that has all non-zero eigenvalues, an arbitrary reference is chosen for the angles and speeds of the generators. Selecting generator N of the system as the reference is a common practice in power system analysis, and in a practical power system generator N is usually designated to be one of the generators with a comparatively large inertia. This fact suggests a modified version of the generator N reference known as the "Nth machine reference" frame. The resulting linear model with N-machine reference frame has the form

$$\frac{d}{dt}\,\Delta\theta_i(t) = \Delta\hat{\omega}_i(t) \qquad i = 1, 2, \ldots\ldots, n - 1 \tag{6.6a}$$

$$\begin{aligned}\frac{d}{dt}\,\Delta\hat{\omega}_i(t) = {} & M_i^{-1}[\Delta PM_i(t) - \Delta PG_i(t)] \\ & - M_N^{-1}[\Delta PM_N(t) - \Delta PG_N(t)] - \sigma\Delta\hat{\omega}_i\end{aligned} \tag{6.6b}$$

where

$$\begin{array}{lll} \sigma & = D_i/M_i & i = 1, 2, \ldots\ldots, n - 1 \\ \theta_i(t) & = \delta_i(t) - \delta_N(t) & i = 1, 2, \ldots\ldots, n - 1 \\ \hat{\omega}_i(t) & = \omega_i(t) - \omega_N(t) & i = 1, 2, \ldots\ldots, n - 1 \\ \Psi_j(t) & = \psi_j(t) - \delta_N(t) & j = 1, 2, \ldots\ldots, k - 1 \end{array}$$

The power equations in terms of the new variables can be written as:

$$\begin{bmatrix} \Delta\underline{PG} \\ \\ \Delta\underline{PL} \end{bmatrix} = \begin{bmatrix} \partial\underline{PG}/\partial\underline{\theta} & \partial\underline{PG}/\partial\underline{\Psi} \\ \\ \partial\underline{PL}/\partial\underline{\theta} & \partial\underline{PL}/\partial\underline{\Psi} \end{bmatrix} \begin{bmatrix} \Delta\underline{\theta} \\ \\ \Delta\underline{\Psi} \end{bmatrix} \tag{6.7}$$

where

$$\underline{\theta} = [\theta_1, \theta_2, \ldots, \theta_{n-1}]^T, \; \underline{\Psi} = [\Psi_1, \Psi_2, \ldots, \Psi_{k-1}]^T$$

The network equations can be used to express $\Delta\underline{PG}$ in terms of $\Delta\underline{\theta}$ and $\Delta\underline{PL}$. This can be done by solving the second equation in (6.7) for $\Delta\Psi$ and substituting it in the first equation in (6.7) to obtain

$$\Delta\underline{PG} = \left\{ \frac{\partial\underline{PG}}{\partial\underline{\theta}} - \frac{\partial\underline{PG}}{\partial\underline{\Psi}} \left[\frac{\partial\underline{PL}}{\partial\underline{\Psi}}\right]^{-1} \frac{\partial\underline{PL}}{\partial\underline{\theta}} \right\} \Delta\underline{\theta} + \left\{ \frac{\partial\underline{PG}}{\partial\underline{\Psi}} \left[\frac{\partial\underline{PL}}{\partial\underline{\Psi}}\right]^{-1} \right\} \Delta\underline{PL}$$

or

$$\Delta\underline{PG} = \underline{T}\Delta\underline{\theta} - \underline{L}\Delta\underline{PL} \tag{6.8}$$

where

$$\underline{T} = \frac{\partial\underline{PG}}{\partial\underline{\theta}} - \frac{\partial\underline{PG}}{\partial\underline{\Psi}} \left[\frac{\partial\underline{PL}}{\partial\underline{\Psi}}\right]^{-1} \frac{\partial\underline{PL}}{\partial\underline{\theta}}, \; \underline{L} = - \frac{\partial\underline{PG}}{\partial\underline{\Psi}} \left[\frac{\partial\underline{PL}}{\partial\underline{\Psi}}\right]^{-1} \tag{6.9}$$

$\underline{T}$ is called the synchronizing torque coeffient matrix and $\underline{L}$ is called the load reflection matrix.

Now, a linearized state space model can be derived by substituting $\underline{PG}$ in (6.8) into equation (6.6b) and writing the 2(n - 1) equations in (6.6) in vector form to obtain

$$\dot{\underline{x}}(t) = \underline{\underline{A}}\underline{x}(t) + \underline{\underline{B}}\underline{u}(t) \tag{6.10}$$

where

$$\underline{x} = \begin{bmatrix} \Delta\underline{\theta} \\ \hline \Delta\underline{\hat{\omega}} \end{bmatrix}, \quad \underline{u} = \begin{bmatrix} \Delta\underline{PM} \\ \hline \Delta\underline{PL} \end{bmatrix} \tag{6.10a}$$

$$\underline{A} = \left[\begin{array}{c|c} \underline{0}_{(n-1)\ (n-1)} & \underline{I}_{n-1} \\ \hline -\underline{\underline{MT}} & -\sigma\underline{I}_{n-1} \end{array}\right], \quad \underline{B} = \left[\begin{array}{c|c} \underline{0} & \underline{0} \\ \hline \underline{M} & \underline{ML} \end{array}\right] \tag{6.10b}$$

$$\underline{M} = \left[\begin{array}{cccccccc|c} M_1^{-1} & & & & & & & & -M_N^{-1} \\ & M_2^{-1} & & & & & & & \cdot \\ & & \cdot & & & 0 & & & \cdot \\ & & & \cdot & & & & & \cdot \\ & & & & \cdot & & & & \cdot \\ & & 0 & & & \cdot & & & \cdot \\ & & & & & & \cdot & & -M_N^{-1} \\ & & & & & & & M^{-1}_{n-1} & -M_N^{-1} \end{array}\right] \tag{6.10c}$$

The next task in this chapter is to derive the disturbance model which can be used for deterministic as well as probabilistic system disturbances. The disturbance model has been developed in [21] and the presentation here follows that development.

6.3. Disturbance Model

The input $\underline{u}(t)$, composed of the deviations in the mechanical input power $\Delta \underline{PM}$ on the generators and the deviations in load power $\Delta \underline{PL}$, can be used to model:

(1) loss of generation due to generator dropping

(2) loss of load due to load shedding

(3) changes in load injections due to line switching

(4) electrical faults

These contingencies can be modeled by an input $\underline{u}(t)$ that has the following form

$$\underline{u}(t) = \underline{u}(t) + \underline{u}_2(t) \qquad (6.11)$$

6.3.1. Step Disturbance

The vector function

$$\underline{u}_1(t) = \begin{cases} \underline{u}_1 & t \geq 0 \\ \underline{0} & t < 0 \end{cases} \qquad (6.12)$$

where $\underline{u}_1(t)$ is a vector step function with amplitude $\underline{u}_1$. Thus, the non-zero entries in $\underline{u}_1(t)$ can model the first three types of disturbances.

The uncertainty due to a generator dropping, load shedding, and line switching disturbance could be modelled by

$$E\{\underline{u}_1\} = E\left\{\begin{bmatrix} \Delta\underline{PM} \\ \hline \Delta\underline{PL} \end{bmatrix}\right\} = \begin{bmatrix} \underline{m}_{11} \\ \hline \underline{m}_{12} \end{bmatrix} = \underline{m}_1 \qquad (6.13a)$$

$$E\{[\underline{u}_1 - \underline{m}_1][\underline{u}_1 - \underline{m}_1]^T\} = \left[\begin{array}{c:c} \underline{R}_{11} & \underline{0} \\ \hdashline \underline{0} & \underline{R}_{22} \end{array}\right] = \underline{R}_1 \qquad (6.13b)$$

where

(1) $\underline{m}_{11}$ and $\underline{R}_{11}$ can describe the uncertainty in the location and magnitude of generation changes due to generator dropping when

the particular station, the generator in the station, and the power produced on the generator are unknown.

(2) $\underline{m}_{12}$ and $\underline{R}_{22}$ describe the uncertainty in the location and magnitude of the load being dropped by any manual or automatic load shedding operation.

(3) $\underline{m}_{12}$ and $\underline{R}_{22}$ can describe the uncertainty in the location and the change in injections on buses due to any line switching operation.

The uncertain model of $\underline{u}_1$ can handle the case of a specific deterministic disturbance by setting $\underline{R}_1 = \underline{0}$ and $\underline{m}_1 = \underline{u}_1$ for the particular disturbance.

The function $\underline{u}_1(t)$ can only model disturbances that resemble step changes.

6.3.2. Electrical Faults

To model electrical faults, first define the vector function

$$\underline{u}_2(t) = \begin{cases} \underline{0} & t > T_2 \\ \underline{u}_2 & 0 \leqq t \leqq T_2 \\ \underline{0} & t < 0 \end{cases} \tag{6.14}$$

that represents a pulse of duration T_2 and amplitude $\underline{u}_2$. This vector function can represent the effects of electrical faults where T_2 represents the fault clearing time and

$$\underline{u}_2 = \begin{bmatrix} \Delta\underline{PM} \\ \hline \underline{0} \end{bmatrix}$$

represents the step change in generation output equivalent to the accelerating powers due to a particular fault. This change of mechanical powers, $\Delta\underline{PM}$, which is equal to the accelerating powers on generators due to a particular fault is calculated by an ACCEL program [22], and has been shown to adequately model the effects of that fault when a linearized model based on pre-fault load flow conditions is used.

The above model can be generalized to model the uncertainty of any particular disturbance and yet handle specific deterministic disturbance as a special case. If the size and location of an electrical fault are not known and if the clearing time T_2 for this fault is known, then a probabilistic description of this fault is

$$E\{\underline{u}_2\} = \left[\begin{array}{c} \underline{m}_{21} \\ \hdashline \underline{0} \end{array}\right] = \underline{m}_2 \tag{6.15a}$$

$$E\{[\underline{u}_2 - \underline{m}_2][\underline{u}_2 - \underline{m}_2]^T\} = \left[\begin{array}{c:c} \underline{R}_{21} & \underline{0} \\ \hdashline \underline{0} & \underline{0} \end{array}\right] = \underline{R}_2 \tag{6.15b}$$

where $\underline{m}_{21}$ and $\underline{R}_{21}$ describe the uncertainty in accelerating power on all generators due to this electircal fault. This mean and variance should be determined based on observed historical records or hypothesized based on the present network conditions. If $\underline{R}_2 = \underline{0}$, and $m_{21} = \Delta\underline{PM}$ for a specific fault, this generalized model then reverts to the deterministic model of a specific electrical fault.

It should be noted that $\underline{\Delta PM}$ and $\underline{\Delta PL}$ are assumed to be uncorrelated because this model is to represent only one specific type of contingency at a time. For the same reason $\underline{u}_1$ and $\underline{u}_2$ are assumed uncorrelated with initial conditions, i.e.

$$\begin{aligned} E\{\underline{x}(0)\underline{u}_1^T\} &= \underline{0} \\ E\{\underline{x}(0)\underline{u}_2^T\} &= \underline{0} \end{aligned} \qquad (6.16)$$

where the initial conditions of the linear differential equations (6.10) are assumed random with

$$E\{\underline{x}(0)\} = \underline{0} \qquad (6.17a)$$

$$E\{\underline{x}(0)\underline{x}^T(0)\} = \underline{V}_x(0) \qquad (6.17b)$$

6.4. Linear RMS Coherency Measure

The RMS measure of coherency between generator internal buses k and ℓ based on the uncertain description of disturbances is [25]

$$C_{k\ell}(T_1) = \sqrt{\frac{1}{T_1^p} E\left\{\int_0^{T_1}[(\Delta\delta_k(t) - \Delta\delta_N(t)) - (\Delta\delta_\ell(t) - \Delta\delta_N(t))]^2\right\} dt}$$

$$= \sqrt{\underline{e}_{k\ell}^T \underline{S}_x(T_1)\underline{e}_{k\ell}} \qquad (6.18)$$

where

$$\underline{S}_x(T_1) = \frac{1}{T_1^p}\int_0^{T_1} E\left\{\underline{x}(t)\underline{x}^T(t)\right\} dt \qquad (6.19)$$

is a (2n - 2) × (2n - 2) symmetric matrix which is defined in terms of the state vector $\underline{x}(t)$ of the linear model of the power system.

The integer p is chosen to be one if a load shedding, line switching, or generator dropping contengency occurs and zero if an electrical fault occurs. This integer is chosen as one or zero so that the above integral will be finite and non-zero for an infinite observation interval ($T_1 = \infty$). $\underline{e}_{k\ell}$ is a (2n - 2) × 1 vector defined below for the generator N reference

$$\{\underline{e}_{k\ell}\}_j = \begin{cases} \begin{cases} 1 & j = k \\ -1 & j = k \\ 0 & j \neq k, \ell \end{cases} & \text{for } k \neq N, \ \ell \neq N \\ \begin{cases} 1 & j = k \\ 0 & j \neq k \end{cases} & \text{for } k \neq N, \ \ell = N \\ \begin{cases} 1 & j = \ell \\ 0 & j \neq \ell \end{cases} & \text{for } k = N, \ \ell \neq N \end{cases} \qquad (6.20)$$

since the objective is to compute the n × n coherency matrix $\underline{C}$ where

$$\{C\}_{k\ell} = C_{k\ell}(T_1), \quad k, \ell = 1, 2, \ldots., n$$

The elements of this matrix can be easily computed, provided that the upper-left (n - 1) × (n - 1) submatrix of $\underline{S}_x(T_1)$ is known, because the coherency measure between any pair of generators depends only on the generator angles (6.18). Denoting the upper-left (n - 1) × (n - 1) submatrix of $\underline{S}_x(T_1)$ by $\hat{\underline{S}}_x(T_1)$, the coherency measure $C_{k\ell}(T_1)$ can be found as

$$C_{k\ell}(T_1) = \begin{cases} \sqrt{\{\hat{\underline{S}}_x(T_1)\}_{kk} + \{\hat{\underline{S}}_x(T_1)\}_{\ell\ell} - \{\hat{\underline{S}}_x(T_1)\}_{\ell k} - \{\hat{\underline{S}}_x(T_1)\}_{k\ell}}, & \begin{matrix} k \neq N \\ \ell \neq N \end{matrix} \\ \sqrt{\{\hat{\underline{S}}_x(T_1)\}_{kk}} & k \neq N,\ \ell = N \\ \sqrt{\{\hat{\underline{S}}_x(T_1)\}_{\ell\ell}} & k = N,\ \ell \neq N \end{cases} \qquad (6.21)$$

where

$$\underline{S}_x(T_1) = \frac{1}{T_1^p} \int_0^{T_1} E\{\underline{x}(t)\underline{x}^T(t)\}dt = \left[\begin{array}{c|c} \hat{\underline{S}}_x(T_1) & * \\ \hline * & * \end{array}\right]$$

The matrix $\underline{S}_x(T_1)$ can be easily computed by substituting $\underline{X}(t)$ in equation (6.19). For the input function $\underline{u}(t) = \underline{u}_1(t) + \underline{u}_2(t)$, $\underline{X}(t)$ has the following form

$$\underline{x}(t) = \begin{cases} e^{\underline{A}t}\underline{x}(0) + \int_0^t e^{\underline{A}\tau} d\tau \underline{B}(\underline{u}_1 + \underline{u}_2) & \text{for } t < T_2 \\ e^{\underline{A}t}\underline{x}(0) + \int_0^t e^{\underline{A}\tau} d\tau \underline{B}\underline{u}_1 + e^{\underline{A}(t-T_2)} \int_0^{T_2} e^{\underline{A}\tau} d\tau \underline{B}\underline{u}_2 & \text{for } t > T_2 \end{cases} \qquad (6.22)$$

For a specific step input disturbance (load shedding, loss of generation, or line switching) with the following specification

$p = 1$, $\underline{m}_1 = \underline{u}_1$, $\underline{m}_2 = 0$, $\underline{R}_1 = \underline{R}_2 = \underline{0}$, and $\underline{V}_x(0) = \underline{0}$

the matrix $\underline{S}_x(T_1)$ has the form

$$\underline{S}_x(T_1) = \frac{1}{T_1} \int_0^{T_1} \left\{ [\int_0^{\tau} e^{\underline{A}q} dq\underline{B}]\underline{u}_1\underline{u}_1^T \; [\int_0^{\tau} e^{\underline{A}q} dq\underline{B}]^T \right\} d\tau \qquad (6.23)$$

If the specific deterministic disturbance is an electrical fault since in this case

$$p = 0,\ \underline{m}_1 = \underline{0},\ \underline{m}_2 = \underline{u}_2,\ \underline{R}_1 = \underline{R}_2 = \underline{0},\ \text{and}\ \underline{V}_x(0) = \underline{0}\ ,$$

the matrix $\underline{S}_x(T_1)$ becomes

$$\underline{S}_x(T_1) = \int_0^{T_2} \left\{ \left[\int_0^{\tau} e^{\underline{A}q} dq\underline{B}\right]\underline{u}_2\underline{u}_2^T \left[\int_0^{\tau} e^{\underline{A}q} dq\underline{B}\right]^T \right\} d\tau$$

$$+\int_{T_2}^{T_1} \left\{ \left[e^{\underline{A}(\tau-T_2)} \int_0^{T_2} e^{\underline{A}q} dq\underline{B}\right] \underline{u}_2\underline{u}_2^T \left[e^{\underline{A}(\tau-T_2)} \int_0^{T_2} d^{\underline{A}q} dq\underline{B}\right]^T \right\} d\tau$$

$$(6.24)$$

This RMS coherency measure can handle both deterministic and probabilistic descriptions of power system disturbances. It is shown in [26] that the RMS coherency measure evaluated over an infinite interval ($T_1 = \infty$) can be analytically related to generator inertias, synchronizing power coefficients $t_{k\ell}$ of equivalent lines connecting internal generator buses k, ℓ, and the statistics of the disturbances.

In the following subsections an infinite interval RMS coherency measure will be derived for step, impulse, and pulse disturbances in the mechanical input power of the generators.

6.4.1. RMS Coherency Measure for Impulse Input Disturbance

The RMS coherency measure matrix for the impulse input disturbance can be obtained from the general equation (6.21) provided $\underline{S}_x(\infty)$ for impulse is derived first, using

$$\underline{S}_x(\infty) = \lim_{T_1 \to \infty} \int_0^{T_1} E\{\underline{x}(t)\underline{x}^T(t)\}dt \tag{6.25}$$

where $\underline{x}(t)$ is the solution of

$$\dot{\underline{x}}(t) = \underline{\underline{A}}\underline{x}(t) + \underline{\underline{B}}\underline{u}_I(t) \tag{6.26}$$

for the impulse input $\underline{u}_I(t) = \underline{\alpha} \cdot \delta(t)$. Assuming zero initial conditions, i.e., at $t = 0$, $\underline{X}(0) = 0$, the state of the system at time t can be found as

$$\underline{x}(t) = \int_0^t e^{\underline{A}(t-\tau)} \underline{\underline{B}}\alpha\delta(\tau)d\tau = e^{\underline{A}t}\underline{\underline{B}\alpha} \tag{6.27}$$

Substituting (6.27) into (6.26), $\underline{S}_{x_I}(\infty)$ for impulse becomes

$$\underline{S}_{x_I}(\infty) = \lim_{T_1 \to \infty} \int_0^{T_1} E\{ e^{\underline{A}t} \underline{\underline{B\alpha\alpha}}^T\underline{B}^T e^{\underline{A}^Tt} \} dt$$

$$= \lim_{T_1 \to \infty} \int_0^{T_1} (e^{\underline{A}t} \underline{B}E\{\underline{\alpha\alpha}^T\}B^T e^{\underline{A}^Tt})dt \tag{6.28}$$

where

$$\underline{\alpha} = \left[\begin{array}{c} \underline{\Delta PM} \\ \hline \underline{0} \end{array}\right]$$

represents the step change in generation output equivalent to the accelerating powers due to this impulse. The statistics of this disturbance are defined to be

$$\underline{m}_{\alpha} = E\{\underline{\alpha}\} = \left[\begin{array}{c} \underline{m}_{\alpha 1} \\ \hline \underline{0} \end{array}\right] \qquad (6.29a)$$

$$\underline{R}_{\alpha} = E\{[\underline{\alpha} - \underline{m}_{\alpha}][\underline{\alpha} - \underline{m}_{\alpha}]^{T}\} = \left[\begin{array}{c|c} \underline{R}_{\alpha 1} & \underline{0} \\ \hline \underline{0} & \underline{0} \end{array}\right] \qquad (6.29b)$$

thus

$$E\{\underline{\alpha}\underline{\alpha}^{T}\} = \underline{R}_{\alpha} + \underline{m}_{\alpha}\underline{m}_{\alpha}^{T} = \left[\begin{array}{c|c} \underline{R}_{\alpha 1} + \underline{m}_{\alpha 1}\underline{m}_{\alpha 1}^{T} & \underline{0} \\ \hline \underline{0} & \underline{0} \end{array}\right] \qquad (6.30)$$

where $\underline{R}_{\alpha 1}$ is the variance matrix and $\underline{m}_{\alpha 1}$ is the mean vector of the uncertainty in accelerating power on all generators due to this impulse (electrical fault).

Defining $\underline{V}_{\alpha} = \underline{B}(\underline{R}_{\alpha} + \underline{m}_{\alpha}\underline{m}_{\alpha}^{T})\underline{B}^{T}$ equation (6.28) becomes

$$\underline{S}_{\underline{x}_I}(\infty) = \lim_{T_1 \to \infty} \int_0^{T_1} (e^{\underline{A}t} \underline{V}_\alpha e^{\underline{A}^T t})dt \tag{6.31}$$

In order to obtain a closed form solution for $\underline{S}_{\underline{x}_I}(\infty)$ it is appropriate to approximate the impulse as a pulse with very short duration. To clarify this let us start with the pulse and its statistics and try to relate it to the impulse and its statistics approximately.

Define the pulse of duration T_2 as

$$\underline{u}_2(t) = \begin{cases} \underline{0} & t > T_2 \\ \underline{u}_2 & 0 \leqq t \leqq T_2 \\ \underline{0} & t > 0 \end{cases} \tag{6.32}$$

where $\underline{u}_2 = [\Delta \underline{PM} \mid \underline{0}]^T$, and its statistics are

$$\underline{m}_2 = E\{\underline{u}_2\} = \begin{bmatrix} \underline{m}_{21} \\ \hline \underline{0} \end{bmatrix} \tag{6.33a}$$

$$\underline{R}_2 = E\{[\underline{u}_2 - \underline{m}_2][\underline{u}_2 - \underline{m}_2]^T\} = \left[\begin{array}{c:c} \underline{R}_{21} & \underline{0} \\ \hdashline \underline{0} & \underline{0} \end{array}\right] \tag{6.33b}$$

The impulse now can be approximated by the above pulse as follows

$$\underline{u}_I(t) = \underline{\alpha}\delta(t) = \lim_{T_2 \to 0} \underline{u}_2(t) \cong \begin{cases} \underline{0} & t > T_2 \\ 1/T_2 \ \alpha & 0 \leqq t \leqq T_2 \\ \underline{0} & t < 0 \end{cases}$$

and the statistics of pulse and impulse may be related as

$$\underline{m}_2 = \frac{1}{T_2}\,\underline{m}_\alpha \tag{6.34a}$$

$$\underline{R}_2 = \frac{1}{T_2^2}\,\underline{R}_\alpha \tag{6.34b}$$

It has been shown in [26] that for a pulse of very short duration (impulse), $\underline{S}_{x_I}(\infty)$ can be determined from the following equation

$$\underline{S}_{x_I}(\infty) = T_2^2 \cdot \underline{W} \tag{6.35}$$

where $\underline{W}$ is the solution of the following Lyapunov equation

$$\underline{A}\underline{W} + \underline{W}\underline{A}^T = -\,\underline{V}_2 \tag{6.36a}$$

and

$$\underline{V}_2 = \underline{B}[\underline{R}_2 + \underline{m}_2\underline{m}_2^T]\underline{B}^T \tag{6.36b}$$

$$\underline{W} = \lim_{T_1 \to \infty} \int_0^{T_1} (e^{\underline{A}t}\,\underline{V}_2\,e^{\underline{A}^T t})dt$$

$$= \lim_{T_1 \to \infty} \int_0^{T_1 - T_2} (e^{\underline{A}t}\,\underline{V}_2\,e^{\underline{A}^T t})dt \tag{6.36c}$$

Comparing equations (6.31) and (6.36c) and knowing that $\underline{V}_2 = \frac{1}{T_2^2}\underline{V}_\alpha$ it is obvious that $\underline{W} = \frac{1}{T_2^2}\underline{S}_{x_I}(\infty)$. Substituting matrices $\underline{W}$ and $\underline{V}_2$ into equation (6.36a), the following Lyapunov equation is obtained

$$\underline{A}\underline{S}_{\underline{x}_I}(\infty) + \underline{S}_{\underline{x}_I}(\infty)\underline{A}^T = -\underline{V}_\alpha \tag{6.37}$$

This Lyapunov equation (6.37) can be easily solved by considering the symmetric property of the matrix $\underline{S}_{\underline{x}_I}(\infty)$. Thus, partitioning $\underline{S}_{\underline{x}_I}(\infty)$ as

$$\underline{S}_{\underline{x}_I}(\infty) = \left[\begin{array}{c|c} \underline{S}_1 & \underline{S}_2 \\ \hline \underline{S}_2^T & \underline{S}_3 \end{array}\right] \tag{6.38}$$

and calculating

$$\underline{V}_\alpha = \underline{B}(\underline{R}_\alpha + \underline{m}_\alpha\underline{m}_\alpha^T)\underline{B}^T = \left[\begin{array}{c|c} \underline{0} & \underline{0} \\ \hline \underline{0} & \underline{M}(\underline{R}_{\alpha 1} + \underline{m}_{\alpha 1}\underline{m}_{\alpha 1}^T)\underline{M}^T \end{array}\right]$$

along with some algebraic manipulation $\underline{S}_1$ becomes

$$\underline{S}_1 = \hat{\underline{S}}_{\underline{x}_I}(\infty) = \frac{1}{4\sigma}\,[(\underline{MT})^{-1}\underline{M}(\underline{R}_{\alpha 1} + \underline{m}_{\alpha 1}\underline{m}_{\alpha 1}^T)\underline{M}^T$$

$$+ \underline{M}(R_{\alpha 1} + \underline{m}_{\alpha 1}\underline{m}_{\alpha 1}^T)\underline{M}^T(\underline{MT})^{-T}] \tag{6.39}$$

The expression (6.39) shows that for the impulse input disturbance the matrix $\hat{\underline{S}}_{\underline{x}_I}(\infty)$, which defines the infinite interval RMS coherency measure, is related algebraically to the parameters of the linear system model and the disturbance statistics.

6.4.2. RMS Coherency Measure for Pulse Input Disturbances

The RMS coherency measure for a pulse input disturbance $\underline{S}_{x_p}(\infty)$ may be obtained as the limit of $\underline{S}_{x_p}(T_1)$ when T_1 approaches infinity. $\underline{S}_{x_p}(\infty)$ for a pulse disturbance of duration T_2 has been derived in [24] and is shown to be

$$\underline{S}_{x_p}(\infty) = \sum_{n=2}^{\infty} \frac{T_2^n}{n!} [\underline{A}^{n-2} \underline{W} + \underline{W}(\underline{A}^{n-2})^T] \tag{6.40}$$

where $\underline{W}$ is the solution of the Lyapunov equation (6.36a). The solution of this Lyapunov equation is similar to the solution of the Lyapunov equation for the impulse disturbance. The solution of $\underline{W}$ is exactly the same as the solution of $\underline{S}_{x_I}(\infty)$, except that we have to use the statistics of the pulse rather than the impulse statistics. This solution has the form

$$\underline{W} = \begin{bmatrix} \frac{1}{4\sigma} [(\underline{MT})^{-1}\underline{M}\Delta\underline{PM}\cdot\Delta\underline{PM}^T M^T + \underline{M}\Delta\underline{PM}\Delta\underline{PM}^T M^T(\underline{MT})^{-T}] & \underline{0} \\ \underline{0} & \frac{1}{2\sigma} [\underline{M}\Delta\underline{PM}\Delta\underline{PM}^T M^T] \end{bmatrix} . \tag{6.40a}$$

where $\underline{M}$ and $\Delta\underline{PM}$ are the inertia matrix and the accelerating power on all generators due to the pulse input disturbance, respectively (electrical fault). If the pulse duration time T_2 is very short, only the first term in the series (6.40) will be required, and under this assumption $\underline{S}_{x_I}(\infty) = T_2^2 \underline{W}$.

Equation (6.40) shows that for the pulse disturbance, $\underline{S}_{\underline{x}_p}(\infty)$, which defines infinite interval RMS coherency measure, is related algebraically to system structure and disturbance statistics.

6.4.3. Justification of Nonlinear RMS Coherency Measure

The nonlinear RMS coherency measure is now derived based on the linear RMS coherency measure derived in the previous section by showing the term $[\underline{MT}]^{-1}\underline{M}\Delta\underline{PM}$ in $\underline{W}$ is a linearized inertial load-flow.

The inertial load-flow equation is first proven to be defined as a singular point of the global energy function. An expression for a linearized inertial load-flow equation is then obtained. Finally, the angle changes for this inertial load-flow are shown to satisfy

$$\Delta\underline{\theta} = [\underline{MT}]^{-1}\underline{M}\cdot\Delta\underline{PM} \tag{6.41}$$

which appears in $\underline{W}$. This justifies replacing expression (6.41) in $\underline{W}$ by $\underline{\delta}^{u} - \underline{\delta}^{s2}$.

The inertial load-flow equation that defines the singular point of the global energy function is now derived.

Consider the energy function of the system represented by

$$V = \sum_{i=1}^{n-1}\sum_{j=i+1}^{n}\Big[\frac{M_iM_j}{2M_T}(\omega_i - \omega_j)^2 - \Big(\frac{P_iM_j - P_jM_i}{M_T}\Big)(\delta_{ij} - \delta_{ij}^{s2})$$

$$- C_{ij}(\cos\delta_{ij} - \cos\delta_{ij}^{s2})\Big] \tag{6.42}$$

Take partial derivative of V with respect to δ_i and set equal to zero, $\partial V/\partial \delta_i = 0$.

$$-\sum_{\substack{j=1\\ j\neq i}}^{n} \frac{P_i M_j - P_j M_i}{M_T} + \sum_{j=1}^{n} C_{ij} \sin \delta_{ij} = 0 \tag{6.43}$$

$$\frac{P_i \sum_{j=1}^{n} M_j}{M_T} - \frac{M_i}{M_T} \sum_{j=1}^{n} P_j = \sum_{j=1}^{n} C_{ij} \sin \delta_{ij} \tag{6.44}$$

$$P_i - \frac{M_i}{M_T} \sum_{j=1}^{n} P_j = \sum_{j=1}^{n} C_{ij} \sin \delta_{ij} \tag{6.45}$$

Assume that $P_i = PM_i$; therefore

$$PM_i - \frac{M_i}{M_T} \sum_{j=1}^{n} P_j = \sum_{j=1}^{n} C_{ij} \sin \delta_{ij} \triangleq PG_i(I) \tag{6.46}$$

The equation (6.46) is an inertial load-flow equation and is used to solve for an unstable equilibrium point of the system. This equation can be linearized to form the following:

$$\Delta PM_i - \frac{M_i}{M_T} \sum_{j=1}^{n} \Delta PM_i = \sum_{j=1}^{n} T_{ij} \Delta \delta_i \tag{6.47}$$

where

$$T_{ij} = - C_{ij} \cos \delta_{ij}$$

$$T_{ii} = - \sum_{j=1}^{n} T_{ij}$$

$$\Delta\delta_{ij} = \Delta\delta_{i} - \Delta\delta_{j}$$

Expression (6.47) can also be written as

$$\Delta PM_{i} - \frac{M_i}{M_T} \sum_{j=1}^{n-1} \Delta PM_{i} = \sum_{j=1}^{n-1} T_{ij}\Delta\theta_{i} \qquad (6.48)$$

where

$$\Delta\theta_{i} = \Delta\delta_{i} - \Delta\delta_{N}$$

or

$$\underline{T}\Delta\underline{\theta} = \left\{ \underline{I} - \begin{bmatrix} \frac{M_1}{M_T} & \cdot & \cdot & \frac{M_1}{M_T} & \cdot & \cdot & \frac{M_1}{M_T} \\ \frac{M_2}{M_T} & & & \frac{M_2}{M_T} & \cdot & \cdot & \frac{M_2}{M_T} \\ \cdot & & & & & & \\ \cdot & & & & & & \\ \frac{M_n}{M_T} & \cdot & \cdot & \cdot & \cdot & \cdot & \frac{M_n}{M_T} \end{bmatrix} \right\} \Delta\underline{PM} \qquad (6.50)$$

where $\sum_{j=1}^{n} M_j = M_T$. Multiplying both sides of equation (6.50) from the left by $\underline{M}$, where:

$$\underline{M} = \begin{bmatrix} \frac{1}{M_1} & & & & -\frac{1}{M_n} \\ & \cdot & & & \cdot \\ & & \cdot & & \cdot \\ & & & & \cdot \\ & & & \frac{1}{M_{n-1}} & -\frac{1}{M_n} \end{bmatrix}$$

and noting that:

$$\begin{bmatrix} \frac{1}{M_1} & & & & -\frac{1}{M_n} \\ & \cdot & & & \\ & & \cdot & & \cdot \\ & & & \cdot & \cdot \\ & & & \frac{1}{M_{n-1}} & -\frac{1}{M_n} \end{bmatrix} \begin{bmatrix} \frac{M_1}{M_T} & \frac{M_1}{M_T} & \cdot & \cdot & \cdot & \frac{M_1}{M_T} \\ \frac{M_2}{M_T} & \frac{M_2}{M_T} & \cdot & \cdot & \cdot & \frac{M_2}{M_T} \\ \frac{M_n}{M_T} & \frac{M_n}{M_T} & \cdot & \cdot & \cdot & \frac{M_n}{M_T} \end{bmatrix} = \underline{0}$$

then (6.50) may be written as:

$$\underline{M}\underline{\Delta PM} = \underline{MT}\ \underline{\Delta\theta} \qquad (6.51)$$

Thus, the inertial angle changes for step input disturbance (loss of generation i and generator buses are:

$$\underline{\Delta\theta} = [MT]^{-1}\underline{M}\underline{\Delta PM} \qquad (6.52)$$

As a result of this discussion one could use the UEP angles $\theta^u - \theta^{s2} = \underline{\Delta\theta}$, calculated by a special program, instead of $[\underline{MT}]^{-1}\underline{M}\ \underline{PM}$ to calculate the fault coherency measures (non-linear). This leads us to the following equation

$$\hat{S}_{x_I}(\infty) = (\underline{\theta}^u - \underline{\theta}^{s2})\Delta\ddot{\underline{\theta}}^T(0) + \Delta\ddot{\underline{\theta}}(0)(\underline{\theta}^u - \underline{\theta}^{s2})^T \tag{6.53}$$

In the next subsection the method of obtaining the peak angles from matrix $\hat{S}_{x_1}(\infty)$ is described.

6.4.4. Theoretical Justification of Fault Security Measure for Second Order System

Consider a second order system such as single machine infinite bus power system; its behavior can be represented by the following linear second order differential equation

$$M_1\Delta\ddot{\delta}(t) + D\Delta\dot{\delta}(t) + T\Delta\delta(t) = u(t) \tag{6.54}$$

where

M_1 = inertia of the machine
D = damping coefficient

and $u(t)$, $\Delta\delta(t)$ are defined as input and output of the system. The point of concern here is to study the response of this second order system to

(1) step input disturbance
(2) impulse input disturbance

and then show that these responses are related to each other.

System Response to Step Input Disturbance. Defining the step input function as

$$u(t) = \begin{cases} \Delta PM , & t \geq 0 \\ 0 , & t < 0 \end{cases}$$

one could solve the linear differential equation

$$M_1 \Delta\ddot{\delta}_s(t) + D\Delta\dot{\delta}_s(t) + T\Delta\delta_s(t) = \Delta PM \qquad t > 0 \tag{6.55}$$

and obtain the closed form solution $\Delta\delta_s(t)$

$$\Delta\delta_s(t) = \frac{\Delta PM}{T} \Big\{ 1 - e^{-D/2M_1 \, t} \cos \left(\sqrt{4M_1T - D^2}/2M_1 \right) t$$

$$- \frac{D}{\sqrt{4M_1T - D^2}} \, e^{-D/2M_1 \, t} \sin \left(\sqrt{4M_1T - D^2}/2M_1 \right) t \Big\} \tag{6.56}$$

Steady-state response of the system is obtained when $t \to \infty$

$$\Delta\delta_s(\infty) = \frac{\Delta PM}{T} \tag{6.57}$$

To find initial acceleration $\Delta\ddot{\delta}_s(0)$, set $D = 0$ in equation (6.56):

$$\Delta\delta_s(t) = \frac{\Delta PM}{T} \; \{1 - \cos \left(\sqrt{4M_1T}/2M_1 \right) t \tag{6.58}$$

and then take the second derivative of equation (6.58)

$$\Delta\ddot{\delta}_s(t) = \frac{\Delta PM}{M_1} \cos \left(\sqrt{4M_1T}/2M_1\right) t$$

By setting $t = 0$, the initial acceleration will be obtained

$$\Delta\ddot{\delta}_s(0) = \frac{\Delta PM}{M_1} \tag{6.59}$$

Multiplying equation (6.57) by equation (6.59),

$$\Delta\delta_s(\infty) \cdot \Delta\ddot{\delta}_s(0) = \frac{\Delta PM}{T} \cdot \frac{\Delta PM}{M_1} \tag{6.60}$$

Rearrange equation (6.60) and define $M \triangleq \frac{1}{M_1}$ to obtain the result in the compact form

$$\Delta\delta_s(\infty) \cdot \Delta\ddot{\delta}_s(0) = (MT)^{-1} M\Delta PM \cdot \Delta PM \cdot M \tag{6.61}$$

System Response to Impulse Input Disturbance. Consider the same second order model and apply an impulse function $u(t) = \Delta PM \cdot \delta(t)$ where $\delta(t)$ is defined as a delta function.

$$M_1 \Delta\ddot{\delta}(t) + D\Delta\dot{\delta}(t) + T\Delta\delta(t) = \Delta PM \cdot \delta(t) \tag{6.62}$$

The solution of this differential equation can be expressed as

$$\Delta\delta_I(t) = \frac{2\Delta PM}{\sqrt{4M_1T - D^2}}\, e^{\frac{-D}{2M_1} t} \sin\left(\sqrt{4M_1T - D^2}/2M_1\right) t \tag{6.63}$$

The maximum value of $\Delta\delta_I(t)$ can be obtained by taking the first derivative of $\Delta\delta_I(t)$ with respect to t.

$$\Delta\delta_{I_{max}}(t) = \frac{2\Delta PM}{D \cdot \alpha}\, e^{-(\tan^{-1}\alpha)/\alpha} \sin(\tan^{-1}\alpha) \tag{6.64}$$

where

$$\alpha \triangleq \sqrt{4M_1T - D^2/D}$$

For the case where damping is zero (D = 0),

$$\Delta\delta_{I_{max}}(t) = \frac{\Delta PM}{\sqrt{M_1T}} = (M_1T)^{-\frac{1}{2}}\,\Delta PM \tag{6.65}$$

Let $M \triangleq \frac{1}{M_1}$ and rewrite equation (6.65) in desired form

$$\Delta\delta_{I_{max}}(t) = (MT)^{-\frac{1}{2}}\,M \cdot \Delta PM \tag{6.66}$$

By comparing equations (6.66) and (6.61) with each other, the relationship between the response of the system to impulse disturbance and step disturbance is represented by

$$\Delta\delta_{I_{max}}(t) = \sqrt{\Delta\delta_s(\infty)\Delta\ddot{\delta}_s(0)} \tag{6.67}$$

For multimachine power systems, the security measure for impulse input disturbance can be written as

$$\hat{\underline{S}}_{x_I}(\infty) = \frac{T_2^2}{4\sigma}\left[(\underline{MT})^{-1}\underline{M}\Delta\underline{PM}\Delta\underline{PM}^T\underline{M}^T + \underline{M}\Delta\underline{PM}\Delta\underline{PM}^T M^T(\underline{MT})^{-T}\right] \tag{6.68}$$

substitute

$$(\underline{MT})^{-1}\underline{M}\Delta\underline{PM}\Delta\underline{PM}^T\underline{M}^T$$

by

$$\underline{\Delta\theta}_{I_{max}}(t) \cdot \underline{\Delta\theta}^T_{I_{max}}(t)$$

in (6.68) and write the resulted expression in vector form

$$\hat{\underline{S}}_{x_I}(\infty) = k^2[\underline{\Delta\theta}_{I_{max}} \cdot \underline{\Delta\theta}^T_{I_{max}} + \underline{\Delta\theta}^T_{I_{max}} \underline{\Delta\theta}_{I_{max}}] \qquad (6.69)$$

where k^2

$$k^2 = \frac{T_2^2}{4\sigma} \quad .$$

Having calculated the matrix $\hat{\underline{S}}_{x_I}(\infty)$, the diagonal elements of this matrix are proportional to the square of the angle changes of the generators $(\Delta\theta^i_{I_{max}})^2$ for i = 1, 2, ..., n due to impulse disturbance and the post-fault system generator angles at time t_B are

$$\underline{\theta}^i_{I_{max}} = \underline{\theta}^{s2} + k\Delta\theta^i_{I_{max}} \ , \qquad i = 1, 2, ..., n \qquad (6.70)$$

The above development of the expression for the peak angle deviation for the second order system (6.54) is based on the assumption of zero damping. However, the RMS coherency measure depends on the damping to inertia ratio $\sigma = D_i/M_i$ which it should because the peak angle deviation should decrease for increased damping. Thus, σ should be set experimentally to reflect the effect of turbine damping D_i as well as the effective damping caused by the load impedance reflected in the conductances in the transmission network.

Thus, the square root of the diagonal elements of the matrix $\hat{S}_I(\infty)$ can be added to the base case load-flow angles to predict the peak angles for the multimachine system. This prediction (6.70) of the peak angles using the linear or nonlinear RMS coherency measure has not been justified based on analysis of the multimachine model but solely based on the analysis on the special case of the second order system model. The accuracy of the prediction of the peak angles (6.70) using the RMS coherency measure from experimental results in the next chapter justifies the use of this prediction model.

6.5. Computational Algorithm for Infinite Interval Pulse Coherency Measure

From the discussion of subsection (6.4.2) it is understood that the coherency measure for pulse input disturbance, which was derived in [24], has the following expression

$$\underline{S}_{\underline{x}_p}(\infty) = \sum_{n=2}^{\infty} \frac{T_2^n}{n!} [\underline{A}^{n-2}\underline{W} + \underline{W}(\underline{A}^{n-2})^T] \tag{6.71}$$

where $\underline{W}$ is the solution of the Lyapunov equation (6.36a) and has the form shown in (6.40a).

The objective of this section is to derive an algorithm for computing the coefficient matrices $\underline{A}^{n-2}\underline{W}$ in the above series expansion for the pulse coherency measure.

Consider the matrix $\underline{W}$ shown in (6.40a) and define the submatrices $\underline{X}$ and $\underline{Y}$ as

$$\underline{X} = \frac{1}{4\sigma}\,[(\underline{MT})^{-1}\underline{M}\Delta\underline{P}\underline{M}\Delta\underline{P}\underline{M}^T\underline{M}^T + \underline{M}\Delta\underline{P}\underline{M}\Delta\underline{P}\underline{M}^T\underline{M}^T(\underline{MT})^{-T}]$$

$$\underline{Y} = \frac{1}{2\sigma}\,[\underline{M}\Delta\underline{P}\underline{M}\Delta\underline{P}\underline{M}^T\underline{M}^T] \tag{6.72}$$

so that

$$\underline{W} = \begin{bmatrix} \underline{X} & \underline{0} \\ \underline{0} & \underline{Y} \end{bmatrix}$$

For the power system model with zero damping ($\sigma = D/M = 0$), the matrix $\underline{A}$ has the following form

$$\underline{A} = \begin{bmatrix} \underline{0} & \underline{I} \\ \underline{MT} & \underline{0} \end{bmatrix} \tag{6.73}$$

Once $\underline{A}$ and $\underline{W}$ are defined, the matrices $\underline{A}^{n-2}\underline{W}$ have the following form

$$\underline{A}\underline{W} = \begin{bmatrix} \underline{0} & \underline{I} \\ \underline{MT} & \underline{0} \end{bmatrix}\begin{bmatrix} \underline{X} & \underline{0} \\ \underline{0} & \underline{Y} \end{bmatrix} = \begin{bmatrix} \underline{0} & \underline{Y} \\ (\underline{MT})\underline{X} & \underline{0} \end{bmatrix}$$

$$\underline{A}^2\underline{W} = \begin{bmatrix} \underline{0} & \underline{I} \\ \underline{MT} & \underline{0} \end{bmatrix}\begin{bmatrix} \underline{0} & \underline{Y} \\ (\underline{MT})\underline{X} & \underline{0} \end{bmatrix} = \begin{bmatrix} (\underline{MT})\underline{X} & \underline{0} \\ \underline{0} & (\underline{MT})\underline{Y} \end{bmatrix}$$

$$\underline{A}^3\underline{W} = \begin{bmatrix} \underline{0} & \underline{I} \\ \underline{MT} & \underline{0} \end{bmatrix}\begin{bmatrix} (\underline{MT})\underline{X} & \underline{0} \\ \underline{0} & (\underline{MT})\underline{Y} \end{bmatrix} = \begin{bmatrix} \underline{0} & (\underline{MT})\underline{Y} \\ (\underline{MT})^2\underline{X} & 0 \end{bmatrix}$$

$$\vdots \qquad\qquad \vdots \qquad\qquad\qquad\qquad \vdots \tag{6.74}$$

$$\vdots \qquad \vdots \qquad \qquad \qquad \vdots$$

$$\underline{A}^{2n}\underline{W} = \begin{bmatrix} \underline{0} & \underline{I} \\ \underline{MT} & \underline{0} \end{bmatrix} \begin{bmatrix} (\underline{MT})^{n-1}\underline{X} & \underline{0} \\ \underline{0} & (\underline{MT})^{n-1}\underline{Y} \end{bmatrix} = \begin{bmatrix} (\underline{MT})^{n}X & \underline{0} \\ \underline{0} & (\underline{MT})^{n}\underline{Y} \end{bmatrix}$$

Since the pulse coherency measure is computed from upper diagonal submatrix, it is clear that the matrices

$$(\underline{A}^{2k}\underline{W})_{11} = \text{upper diagonal submatrix of } \underline{A}^{2k}\underline{W} = (\underline{MT})^{k}\underline{X} \qquad (6.75a)$$

need to be computed since

$$(\underline{A}^{2k-1}\underline{W})_{11} = \text{upper diagonal submatrix of } \underline{A}^{2k-1}\underline{W} = \underline{0} \qquad (6.75b)$$

for k = 1, 2, ... If we define vectors

$$\begin{aligned} v_0 &\triangleq \frac{1}{2\sqrt{\sigma}} (\underline{MT})^{-1}\underline{M}\Delta\underline{PM} \\ v_1 &\triangleq \frac{1}{2\sqrt{\sigma}} \underline{M}\Delta\underline{PM} \end{aligned} \qquad (6.76)$$

then matrix $\underline{X}$ has the form

$$\underline{X} = v_0 v_1^T + v_1 v_0^T \qquad (6.77)$$

and the series $(\underline{MT})^k\underline{X}$ could be written as a function of these vectors v_o and v_1 as the following

$$(\underline{MT})\underline{X} = (\underline{MT})v_o v_1^T + (\underline{MT})v_1 v_o^T = v_1 v_1^T + v_2 v_o^T$$

$$(\underline{MT})^2\underline{X} = (\underline{MT})v_1 v_1^T + (\underline{MT})v_2 v_o^T = v_2 v_1^T + v_3 v_o^T$$

$$(\underline{MT})^3\underline{X} = (\underline{MT})v_2 v_1^T + (\underline{MT})v_3 v_o^T = v_3 v_1^T + v_4 v_o^T$$

$$\vdots$$

$$(\underline{MT})^k\underline{X} = (\underline{MT})v_{k-1} v_1^T + (\underline{MT})v_k v_o^T = v_k v_1^T + v_{k+1} v_o^T \qquad (6.78) .$$

where

$$v_{k+1} = \underline{MT}\ v_k , \qquad k = 0, 1, 2, \ldots .$$

The series

$$\sum_{k=2}^{\infty} (\underline{A}^{k-2}\underline{W})_{11} \frac{T_2^k}{k!}$$

can then be written as

$$\sum_{k=2}^{\infty} \frac{T_2^k}{k!} (\underline{A}^{k-2}\underline{W})_{11} = \frac{T_2}{2!} (v_1 v_o^T + v_o v_1^T) + \frac{T_2^4}{4!} (v_2 v_o^T + v_1 v_1^T) + \ldots .$$

and

$$\sum_{k=2}^{\infty} \frac{T_2^k}{k!} \left(\underline{W}(\underline{A}^{k-2})^T \right)_{11} = \frac{T_2^2}{2!} (v_1 v_0^T + v_0 v_1^T) + \frac{T_2^4}{4!} (v_0 v_2^T + v_1 v_1^T) + \dots. \tag{6.79}$$

As a result of this analysis, one has to compute the vectors v_i $i = 0, 1, 2, 3$ to compute the pulse coherency measure, which predicts the peak angles of the system for a particular fault.

The computational algorithm of the pulse coherency measure for predicting peak angles of the generators in the system can be summarized in the following order.

(1) Compute generator accelerating power $\underline{\Delta PM}$ using ACCEL program, which requires one linear matrix equation to be solved. Then compute $v_1 = \frac{1}{2\sqrt{\sigma}} \underline{M}\underline{\Delta PM}$ directly.

(2) Compute v_0 from inertial load-flow equation for post-fault network (see Appendix A).

(3) Compute v_{k+1}, $k = 1, 2, \dots$ from iterative equation involving pre-fault network Jacobian network matrix (see Appendix A).

(4) Compute post-fault stable equilibrium points θ^{s2} from DC load-flow equation.

(5) Substitute v_k's in equations (6.79) to obtain the pulse coherency measure matrix $\hat{\underline{S}}_{x_p}(\infty)$. Then take the square root of diagonal elements of this matrix and add them to the post-fault stable equilibrium point angles as was shown in equation (6.70). The results would predict the generator peak angles for this fault disturbance.

This method of finding the peak angles of the system generators is very fast and computationally efficient in comparison with trajectory simulation method. Simulating the system trajectory requires iterative solution of n + m (where n is the number of generator buses and m is the number of load buses) dimensional set of nonlinear equations every integral step size $\Delta t = .01$ seconds during fault and every $\Delta t = .05$ seconds after fault clearing. This approximation algorithm requires solution of only a few sparse linear matrix equations such as:

(1) one linear equation solution for computing $\Delta\underline{PM}$

(2) one solution of a nonlinear load flow for post-fault stable equilibrium point θ^{s2}

(3) one linear equation solution for computing v_o

(4) computational results showed that after four iterations terms $(\underline{MT})^k\underline{X}$, for k = 1, 2, 3, 4, the measure (6.71) converged. Therefore the algorithm requires in total six sparse linear equation solutions and one nonlinear load flow solution.

CHAPTER 7

STABILITY ANALYSIS USING FAST DIRECT METHODS AND COMPUTATIONAL RESULTS

7.1. Introduction

The same power network (Reduced Iowa System) described in Chapter 4 was used to study the stability of the system by fast direct methods for the same three fault cases, Cooper, Fort Calhoun, and Raun, as described in Chapter 4.

The objective of this chapter is to apply the fast direct method stability algorithms (the PEBS and equal-area) and show the results of the direct stability run for each fault case and discuss the accuracy of these results.

7.2. Cooper Case

A three-phase fault is applied to generator 2 (Cooper) and is removed by clearing line 6-439.

The point of interest is to study the behavior of the system due to the fault and directly determine whether the system is stable or unstable without simulating the system trajectory.

Recall the efficient PEBS algorithm described in subsection 5.2.1. To compute the boundary energy $V_{PE_i}(t_B,t_c) = V_{cr}$ from equation (5.1) having the prefault operating state θ^{s1}, it is understood that one needs to determine the peak angles θ^{max} (using linear or nonlinear RMS coherency measure) as well as the critical generator or the critical group. The linear and nonlinear RMS coherency program was run for different clearing times and generator 2 was found to be the generator with the highest peak angle. Therefore, generator 2 is predicted as the critical generator. Tables 7.1 and 7.2 show the peak angles of the generators with respect to generator 13 as a reference generator for two different clearing times $t_c = 0.192$ and 0.210 seconds. Although the predicted peak angles by RMS coherency program (entries of columns 3 and 4) do not match with those obtained from simulation program (entries of column 2) in these tables, the results of computing the maximum potential energy of the critical generator using these approximated peak angles shows that the fast PEBS algorithm works accurately and predicts the stability boundary of the system. For different clearing times, the proposed PEBS method with both linear and nonlinear RMS coherency as peak angle predictors were tested on the Reduced Iowa Test system and the results are summarized in Table 7.3.

In Table 7.3 columns 2 and 3 represent the boundary energies $V^*_{PE}(t_c)$ calculated for different clearing times using the linear RMS coherency measure as predictor, for the energy function (5.1) with conductance term included and excluded, respectively. In both cases the largest peak value of the boundary energies occurs for clearing time within the interval $t_c \in (.210, .224)$ indicating that the critical clearing time is in this interval.

Table 7.1. Generator peak angles ($\theta_i-\theta_{13}$) for Cooper using the RMS coherency measure and simulation programs. Clearing time = .192 seconds.

generator number	simulation peak angles	RMS coherency peak angles	
		linear	nonlinear
1	20.33	50.68	12.91
2	130.20	176.44	119.26
3	28.67	29.94	14.60
4	11.51	22.84	8.43
5	57.28	56.54	25.18
6	58.53	43.11	25.85
7	9.84	49.71	17.29
8	13.27	70.96	20.11
9	19.68	39.28	20.17
10	69.17	101.22	42.58
11	26.98	71.65	21.68
12	64.45	135.99	52.16
13	---	---	---
14	- 0.26	6.49	2.12
15	13.66	16.52	9.40
16	74.12	113.28	46.51
17	92.78	138.14	56.29

Table 7.2. Generator peak angles ($\theta_i - \theta_{13}$) for Cooper using the RMS coherency measure and simulation programs. Clearing time = 0.210 seconds.

generator number	simulation peak angles	RMS coherency peak angles	
		linear	nonlinear
1	20.33	50.68	12.91
2	130.20	176.44	119.26
3	28.67	29.94	14.60
4	11.51	22.84	8.43
5	57.28	56.54	25.18
6	58.53	43.11	25.85
7	9.84	49.71	17.29
8	13.27	70.96	20.11
9	19.68	39.28	20.17
10	69.17	101.22	42.58
11	26.98	71.65	21.68
12	64.45	135.99	52.16
13	---	---	---
14	- 0.26	6.49	2.12
15	13.66	16.52	9.40
16	74.12	113.28	46.51
17	92.78	138.14	56.29

Table 7.3

clearing times
0.192
0.208
0.210
0.216
0.224
0.24

Table 7.3. Determination of maximum potential energy (PEBS) for Cooper using the fast direct method.

	linear		nonlinear	
clearing times	with conductance	without conductance	with conductance	without conductance
0.192	9.907	4.915	9.937	6.886
0.208	9.941	5.156	10.896	7.928
0.210	9.947	5.174	11.009	8.057
0.216	9.949	5.197	11.336	8.187
0.224	9.773	5.112	11.744	8.930
0.24	9.516	5.062	10.917	8.735

Comparison of these results with the actual $t_{cc} \cong .220$ seconds obtained from simulation program (Table 4.2) confirms the accuracy of the algorithm. It should be noted that in this research there was no attempt to determine the stability boundary very accurately. However, one could calculate the boundary energies $V^*_{PE}(t_c)$ for additional clearing times to precisely determine the highest possible value of $V^*_{PE}(t_c)$. The corresponding clearing time for which this maximum energy value occurs was the critical clearing time from the results of Chapter 4. The results in columns 4 and 5 of Table 7.3 show that the boundary energy $V^*_{PE}(t_c)$, where the nonlinear RMS coherency measure was used as the predictor, peaks for clearing time $t_c \in (.216, .240)$, therefore the critical clearing time is within this interval.

Although the critical clearing time t_{cc} for the nonlinear case appears to occur at a later time compared to the critical clearing time of the linear case, the results are still in agreement with actual simulation results.

For the same fault location (Cooper) the fast equal area algorithm was applied to the same test system and stability of the system was tested by computing the energy margin $\Delta E(t_c) = A_1(t_c) + A_2(t_c,t_B)$ for different clearing times. The results of this analysis are summarized in Table 7.4.

From Table 7.4, where the local equal area energy margin for generator 2 is considered, it is observed that when the linear RMS coherency measure is used as the predictor of generator peak angles,

Table 7.4. Determination of minimum energy margin (EAC) for Cooper using the fast direct method.

	linear		nonlinear	
clearing times	with conductance	without conductance	with conductance	without conductance
.192	- .372	1.487	1.548	.791
.208	1.559	2.709	.486	.071
.210	1.832	2.886	.374	.004
.216	2.661	3.021	.018	.0038
.224	3.955	4.287	- .509	-.569
.24	6.244	6.215	1.573	.583

the minimum of $\Delta E_2(t_B)$ increases as the clearing time increases. The critical clearing time based on the second and third columns of this table is not predictable because there is no minimum point for $\Delta E_2(t_B)$ versus clearing time t_c and hence the algorithm based on the linear RMS coherency measure does not work properly. The entries of the fourth and fifth columns with the nonlinear RMS coherency measure show that the energy margin $\Delta E_2(t_B)$ decreases as the clearing time approaches the critical clearing time for $t_c < t_{cc}$ and then $\Delta E_2(t_B)$ starts to increase as clearing time increases for $t_c > t_{cc}$. The critical clearing time based on the fourth and fifth columns of Table 7.4 is again estimated to be in the interval $t_{cc} \in (.216, .240)$. These results confirm that the approximation algorithm based on the nonlinear RMS coherency measure for predicting critical clearing time is very compatible to the results obtained from simulation.

The nonlinear RMS coherency measure requires very significant computation to obtain the unstable equilibrium point. Since the linear RMS coherency measure appears to perform quite well for the PEBS method and since it can be computed at the cost of a decoupled load flow, the nonlinear RMS coherency measure was not applied to either the Fort Calhoun or Raun cases. However, the nonlinear RMS coherency measure performed satisfactorily for both the equal area and the PEBS methods where the linear RMS coherency measure only performed adequately for the PEBS method.

7.3. Fort Calhoun Case

For the critical generator 16 of the Fort Calhoun case, a similar analysis to that of generator 2 of the Cooper case is performed. Generator 16 is correctly selected as critical from the maximum of peak angles predicted by the RMS coherency measure. Tables 7.5a and 7.5b summarize the results obtained by monitoring the individual machine potential energy (PEBS) and energy margin $\Delta E(t_B,t_c)$ for generator 16, respectively. Note that in these analyses only the linear RMS coherency is used to predict the critical generator 16 and the peak angles of the system generators. From Table 7.5a it is clearly observed that as the clearing time increases toward the actual critical clearing time (which is not known at this time), the maximum of the potential energy increases until it reaches its highest value for $t_c \in (.360, .368)$. However, this result is off by .008 seconds from the result obtained from simulation $t_c \in (.352, .356)$ in Table 4.5. From Table 7.5b, where the minimum energy margin for generator 16 is considered, it is observed that again the minimum of $\Delta E_{16}(t_B)$ increases as the clearing time increases. Since there is no minimum point for $\Delta E_{16}(t_B)$ versus clearing time t_c, the critical clearing time once again cannot be predicted using the fast equal-area algorithm and the linear RMS coherency measure.

7.4. Raun Case

For the Raun case, for both the inclusion and exclusion of the transfer conductances the proposed fast PEBS and EAC algorithms for different clearing times were applied. In both cases the linear

Table 7.5a. Determination of maximum potential energy (PEBS) for Fort Calhoun using the fast direct method.

	linear	
clearing times	with conductance	without conductance
.320	11.442	4.232
.336	11.584	4.451
.345	11.678	4.627
.352	11.714	4.721
.360	11.737	4.819
.364	11.748	4.936
.368	11.740	4.907
.384	11.690	4.749

Table 7.5b. Determination of minimum energy margin (EAC) for Fort Calhoun using the fast direct method.

	linear	
clearing times	with conductance	without conductance
.320	-3.647	-1.504
.336	-2.831	-1.125
.345	-2.137	- .844
.352	-1.681	- .601
.360	-1.131	- .294
.364	- .883	- .082
.368	- .549	.046
.384	- .700	.822

RMS coherency measure was used to predict the critical generators and the generator peak angles. This coherency measure indicates generator 6 is the most accelerated generator in the system. Therefore, by definition, generator 6 would determine the stability or instability of the system. Thus, generator 6 is the critical generator in this case. However, in Chapter 4 it was shown that both generators 5 and 6 were accelerated and separated from the rest of the system simultaneously, and it was also shown that more time was needed to drain out the excess clearing energy of generator 5 than that of 6. In other words, although both generators 5 and 6 lose synchronism with respect to the stationary group, generator 6 becomes weakly decoupled where generator 5 is still strongly coupled and becomes weakly decoupled at a later time if the system loses stability. This confirms the fact that the true mechanism of stability is dictated by generator 5 rather than 6. The linear RMS coherency measure therefore did not correctly identify the critical generator in this Raun case.

However, in both algorithms (PEBS and EAC), the energy of generator 6 was used to predict the stability boundary of the system. Tables 7.6a and 7.6b show the results obtained from the direct application of both the PEBS and EAC algorithms on the Reduced Iowa Test System, respectively. From the entries of Table 7.6a, for both the inclusion and exclusion of the transfer conductances, it is clear that the potential energy maximum of generator 6 with respect to the rest of the system has the highest value for clearing time around t_c = .1922 seconds. This phenomenon indicates that the

Table 7.6a. Determination of maximum potential energy (PEBS) for Raun using the fast direct method.

clearing times	linear with conductance	 without conductance
.160	10.384	7.205
.176	10.672	7.711
.1922	10.691	7.858
.208	10.184	7.608
.224	9.420	6.946

Table 7.6b. Determination of minimum energy margin (EAC) for Raun using the fast direct method.

clearing times	linear with conductance	 without conductance
.160	.117	1.251
.176	2.785	3.216
.1922	6.294	5.941
.208	10.623	9.434
.224	15.686	13.640

estimated critical clearing time is approximately equal to t_{cc} = .1922 seconds, which is very compatible to the actual boundary $t_c \varepsilon$ (.1922, .1925) obtained from the simulation results.

Table 7.6b shows the minimum energy margin of generator 6 with respect to the other generators $\Delta E_6(t_c)$ in the system for different clearing times for both the inclusion and exclusion of the transfer conductances. In both cases, the minimum energy margin $\Delta E_6(t_c)$ varies with clearing time, i.e., for increasing clearing time t_c, $\Delta E_6(t_c)$ increases and this relationship holds even for large clearing times. Thus, function $\Delta E_6(t_c)$ does not have a minimum point with respect to clearing time t_c and hence one cannot predict the critical boundary t_{cc} using the fast equal area prediction method with the linear RMS coherency measure.

The PEBS method for the individual machine energy function with the linear RMS coherency measure used to predict the peak angles is quite accurate compared to results obtained:

(1) Using the PEBS method for the individual machine energy function based on the actual simulation [16]. The results in Chapter 4 indicate that the critical clearing time could be determined much more accurately but the accuracy obtained in [16] was deemed adequate to indicate accuracy of the method.

(2) Using the PEBS [17] or critical UEP methods [2] based on the total energy function. These methods have limitations on their accuracy due to use of the total energy function.

The fast PEBS method is quite acceptable in its level of accuracy because:

(1) the results using the PEBS method for the individual energy function with the linear RMS coherency measure are as accurate as these previous results, and

(2) for applications of this fast PEBS method for on line simulation at utility control centers and for screening contingencies for operation planning, and expansion planning it is more than sufficient.

The fast PEBS method with the linear RMS coherency measure does not require the significant computation required for computing the nonlinear RMS coherency measure. Thus, since the linear RMS coherency measure appears to give results with adequate accuracy, the fast PEBS method with the nonlinear RMS coherency measure was not explored in depth.

The linear RMS coherency measure did not perform properly for the equal area criterion method for the individual machine energy function. The nonlinear RMS coherency measure did perform adequately for the equal area method but was not explored in depth due to the significant additional computation required for the nonlinear RMS coherency measure. The equal area method also requires computing the angles at clearing time using a Taylor series which is additional computation.

In conclusion, the fast PEBS method with the linear RMS coherency measure thus appears to provide adequate accuracy at a minimum computational requirement.

CHAPTER 8

REVIEW, CONCLUSION, AND TOPICS FOR FUTURE INQUIRY

8.1. Chapter Review

A fast accurate direct method for assessing whether the power system will or will not lose stability for a particular fault, line clearing action, and fault clearing time has been sought for over thirty-five years. The development of such a direct method should not require simulation of the fault and the clearing action for a particular fault clearing time but should require approximately the computation associated with a fast decoupled AC load flow. If this direct method of assessing stability for faults had the computation requirements of an AC decoupled load flow, it could be applied in the following applications for fault contingencies as the decoupled load flow is presently used for line outage and loss of generation contingencies.

(1) A screening tool for operation planning where all first and second contingencies are evaluated to (a) assess whether the operation plan for any day, week, or season is vulnerable to a loss of stability, (b) determine and rank contingencies for which the system is vulnerable, and (c) select the contingencies to be evaluated on-line at the utility control center. The operation plan would

be modified if the particular operation plan was vulnerable to any credible first or second contingency. The fault contingencies that are found to be most severe can be evaluated using more accurate models to assess the cause and severity of the particular contingency.

(2) As a check for system operators at control centers. The operators could assess the severity and whether the system would lose stability for any fault contingency or set of contingencies that appear of great concern because of loss of generation; line outages or fault contingencies have occurred that were not anticipated in the operation plan. The set of contingencies selected off line as part of the operation plan could also be simulated to determine if any of these contingencies would cause loss of stability or security due to changes in operating conditions. The operator will attempt to modify the operation based on the results of the contingency simulation to eliminate the security or stability problems identified by the contingency simulations.

(3) A screening tool for expansion planning where all first and second contingencies are evaluated for each alternate expansion plan for several operating conditions. The relative security or reliability of the expansion plan will be used to help decide which expansion plan should be implemented. Detailed simulation of fault contingencies found to make the system vulnerable would be undertaken to accurately assess the cause and severity of the security or stability problem.

The proposed contributions of this thesis are:

(1) To further refine the potential energy boundary surface and equal area methods developed previously [16, 19] using an individual machine energy function. The method for identifying the critical generator in [29] is used to select the machine for which the individual machine energy function is written. The potential energy boundary surface method, which determines the maximum potential energy of the individual machine energy function as a function of clearing time, is shown to have a very sharp narrow peak at the critical clearing time. It was thought, based on [16], to be nearly flat for all clearing times greater than critical clearing time. This very sharp narrow peak for the maximum potential energy as a function of clearing time at the critical clearing time (a) makes extremely accurate identification of the critical clearing time quite easy, and (b) indicates that the combination of the method for identifying the critical generator and the method for determining the maximum potential energy produces an energy metric that truly captures the structural conditions that cause the loss of stability for a particular fault. The equal area method measures the accelerating energy and decelerating energy for the individual machine energy function of the critical generator for a particular clearing time. The maximum decelerating energy is determined by noting the maximum of decelerating energy as a function of time. The difference between the accelerating energy as a function of clearing time is shown to be close to zero for small clearing times, have a very sharp negative peak at the critical clearing time, and

have positive values for clearing times greater than the critical clearing time. This result was not known previously and (a) shows that the equal area condition of single machine infinite bus system does apply to the multimachine system if properly applied to the individual machine energy function for the critical generator, (b) makes extremely accurate identification of the critical clearing time quite easy, and (c) shows this difference in accelerating and maximum decelerating energy as a function of time is another energy metric that captures the structural conditions that cause loss of stability for a particular fault, clearing action, operating conditions, and clearing time. The individual machine energy function for the critical generator and the PEBS or equal area method appear to finally have been established experimentally as properly capturing the structural conditions that cause loss of stability in power systems. These methods still require theoretical justification, which is a topic of further research.

(2) The second major contribution of this thesis is the development of a fast accurate method for determining loss of stability without requiring transient stability simulation of the fault, the clearing action, and the fault clearing time as was required in the previous results to date [16, 17, 29]. This method is shown to require computation that is approximately that of an AC decoupled load flow and thus could be utilized in the applications mentioned earlier. The practical contribution of this method cannot be underestimated because the previous literature on direct methods were

principally concerned with showing that the retention or loss of stability obtained from observing angle differences on a transient stability simulation could also be obtained via observing a measure of energy on that same transient stability simulation. The research performed to eliminate the need to perform the transient stability simulation was quite limited, never thoroughly investigated, and either required very extensive computation or was not very accurate. Thus, the development of the fast accurate method is an important contribution because the objective of the research on direct methods of stability assessment for faults is the elimination of the need to simulate the fault contingency.

Such fast algorithms are based on the potential energy of the individual machine with respect to the rest of the generators in the system. Computation of this potential energy requires calculation of the initial operating state, the final operating state (generator peak angles), and the post-fault network conditions. The initial operating state and the network conditions are easily obtained by solving a load flow equation. However, the calculation of the generator peak angles is the key point to implement these algorithms.

A linear RMS coherency measure for pulse input disturbance is a proper fast method to predict the generator peak angles of the system. A nonlinear RMS coherency measure based on the critical unstable equilibrium point is an alternative approach for predicting the peak angles, but it requires significant additional computation compared to that required by the linear RMS coherency measure. As a theoretical basis, the RMS coherency measure is justified for a second order linear single machine infinite bus system model. The theoretical justification of RMS coherency measure, for a multi-machine power system, is a subject for further research.

The algorithms are implemented and tested on the Reduced Iowa System consisting of 17 generators and 163 buses. The results in Chapter 7 indicate the accuracy of the algorithms and their significant promise for further improvement.

8.2. Topics for Future Research

Based on the development of the first seven chapters, it is concluded that for direct stability assessment, the energy behavior of a particular individual machine (critical generator) is the determining factor in accurately estimating the region of stability (critical clearing time). The results obtained from application of the fast direct methods for different fault cases on a test system are extremely promising and could be further investigated as follows:

(1) development of a topological energy function that does not aggregate the network back to internal generator buses, allows arbitrary nonlinear real and reactive load models, and allows arbitrarily complex generator models;

(2) development of an individual machine energy function for this topological energy function;

(3) showing that the PEBS and equal area criterion can easily and accurately identify the critical clearing time for this

topological individual machine energy function based on time simulation of the fault;

(4) development of an RMS coherency measure for the more complex power system model;

(5) development of a fast computational method for predicting the state at which the trajectory most closely approaches or crosses the PEBS using this modified RMS coherency measure;

(6) testing this fast computational method for predicting the state at which the trajectory most closely approaches or crosses the PEBS on several fault cases to show that it is a fast efficient and accurate computational method for direct prediction of stability on this more accurate power system model.

APPENDIX A

APPENDIX A

A.1. Computation of v_{k+1}

In section 6.5 of Chapter 6 it was shown that $v_{k+1} = (\underline{MT})v_k$ for every k = 1, 2, ... Here it will be shown that v_{k+1} can be computed by solving the linear equation

$$\begin{bmatrix} \underline{0} \\ \\ \underline{\Delta PG} \end{bmatrix} = \begin{bmatrix} \underline{J}_{11} & J_{12} \\ \\ \underline{J}_{21} & J_{22} \end{bmatrix} \begin{bmatrix} \underline{\Delta \hat{\theta}} \\ \\ \Delta \hat{\underline{\delta}} \end{bmatrix} \tag{A.1}$$

where

$\Delta\hat{\underline{\theta}} = [\Delta\theta_1, \Delta\theta_2, \ldots., \Delta\theta_m]^T$; angle changes at load buses

$\Delta\hat{\underline{\delta}} = [\Delta\delta_1, \Delta\delta_2, \ldots., \Delta\delta_{n-1}]^T$; angle changes at generator buses

$\underline{\Delta PG} = [\Delta PG_1, \Delta PG_2, \ldots., \Delta PG_{n-1}]^T$; real power changes at internal generator buses

First solve equation (A.1) for $\Delta\hat{\underline{\theta}}$

$$\underline{0} = \underline{J}_{11}\Delta\hat{\underline{\theta}} + \underline{J}_{12}\Delta\hat{\underline{\delta}} \tag{A.2}$$

or

$$\Delta\hat{\underline{\theta}} = - \underline{J}_{11}^{-1} J_{12} \Delta\hat{\underline{\delta}} \tag{A.3}$$

Then substitute this $\Delta\hat{\underline{\theta}}$ value in the second equation of (A.1) to obtain the expression of $\Delta\underline{PG}$

$$\Delta\underline{PG} = - J_{21} J_{11}^{-1} J_{12} \Delta\hat{\underline{\delta}} + J_{22} \Delta\hat{\underline{\delta}} \tag{A.4}$$

$$\Delta\underline{PG} = \underline{T} \cdot \Delta\hat{\underline{\delta}} \tag{A.5}$$

where

$$\underline{T} = \underline{J}_{22} - \underline{J}_{21} \underline{J}_{11}^{-1} \underline{J}_{12} \tag{A.6}$$

Define $v_k \triangleq \Delta\hat{\underline{\delta}}$ and multiply both sides of equation (A.5) by matrix $\underline{M}$

$$\underline{M}\Delta\underline{PG} = \underline{MT}\, v_k \tag{A.7}$$

By comparing $v_{k+1} = \underline{MT}\, v_k$ with equation (A.7) it is obvious that

$$v_{k+1} = \underline{M}\Delta\underline{PG} \tag{A.8}$$

This implies that the v_{k+1} is the solution of linear equation

$$\begin{bmatrix} \underline{0} \\ \\ v_{k+1} \end{bmatrix} = \begin{bmatrix} \underline{J}_{11} & \underline{J}_{12} \\ \\ \underline{M}\underline{J}_{21} & \underline{M}\underline{J}_{22} \end{bmatrix} \begin{bmatrix} \Delta\hat{\underline{\theta}} \\ \\ v_k \end{bmatrix} \tag{A.9}$$

for each k = 1, 2, ...

A.2. Computation of v_0

Recall v_0 and v_1 defined in section 6.5:

$$v_0 = \frac{1}{2\sqrt{\sigma}} (\underline{MT})^{-1}\underline{M}\Delta\underline{PM} \tag{A.10}$$

$$v_1 = \frac{1}{2\sqrt{\sigma}} \underline{M}\Delta\underline{PM} \tag{A.11}$$

$$v_1 = (\underline{MT})v_0 \tag{A.12}$$

Recall equation (A.6) and multiply both sides by matrix $\underline{M}$ and rewrite it in the following form:

$$\underline{M}\Delta\underline{PG} = (\underline{MT})\Delta\hat{\underline{\delta}} \tag{A.13}$$

Again define $v_0 = \Delta\hat{\underline{\delta}}$ and compare equation (A.12) with equation (A.13). As a result $v_1 = \underline{M}\Delta\underline{PG}$. Substitute this value of v_1 in equation (A.11) and write the result as

$$\frac{1}{2\sqrt{\sigma}} \underline{M}\Delta\underline{PM} = M\Delta\underline{PG} \tag{A.14}$$

Based on this analysis, one could obtain v_0 as the solution of linear equation

$$\begin{bmatrix} \underline{0} \\ \frac{1}{2\sqrt{\sigma}} \underline{M}\Delta\underline{PM} \end{bmatrix} = \begin{bmatrix} \underline{J}_{11} & \underline{J}_{12} \\ \underline{M}\underline{J}_{21} & \underline{M}\underline{J}_{22} \end{bmatrix} \begin{bmatrix} \Delta\hat{\theta} \\ v_0 \end{bmatrix} \tag{A.15}$$

Therefore computation of v_o requires one linear equation to be solved.

BIBLIOGRAPHY

BIBLIOGRAPHY

1. P.M. Anderson and A.A. Fouad, "Power System Control and Stability," Iowa State University Press, Ames, Iowa, 1977.

2. A.A. Fouad, "Stability Theory--Criteria for Transient Stability," Conference Paper, presented at "Systems Engineering for Power: Status and Prospects." Heniker, New Hampshire, Aug. 17-22, 1975.

3. N. Kakimoto et al., "Transient Stability Analysis of Electric Power System via Lure type Lyapunov function, Parts I and II," Trans. IEE of Japan, vol. 98, no. 516, May/June 1978. See also their papers in Memoirs of the Faculty of Engineering, Kyoto University, vol. XXXIX, Part 4, October 1977.

4. T. Athay, V.R. Sherket, R. Podmore, S. Virmani, and C. Pnech, "Transient Energy Stability Analysis," Systems Engineering for Power: Engineering Operating State Control. U.S. Department of Energy, Publication no. CONF-790904-PL.

5. M.A. Pai, "Transient Energy Analysis of Large Scale Power Systems, A Tutorial Survey," Presented at University of Illinois, Feb. 1980.

6. J.P. LaSalle, S. Lefschetz, "Stability by Liapunov's Direct Method with Applications," Academic, New York, 1961.

7. J.L. Willems, "Stability Theory of Dynamical Systems," John Wiley and Sons, Inc., New York, 1970.

8. System Control Inc. Final Report, "Transient Energy Stability Analysis," presented at the Engineering Foundation Conference, U.S. Department of Energy, Sept. 30-Oct. 5, 1979, Davos, Switzerland.

9. N. Kakimoto, M. Hayashi, "Transient Stability Analysis of Multimachine Power System by Lyanpunov's Direct Method," Conference on Decision and Control, 1982.

10. C.J. Tavora and O.J.M Smith, "Characterization of Equilibrium and Stability in Power Systems," IEEE Transaction Power App. Sys., vol. PAS-91, 3, pp. 1127-1145.

11. A.H. El-Abiad and Prabhakara, "A Simplified Determination of Transient Stability Regions for Lyapunov Methods," Paper T74-407-3, presented at the IEEE PES Summer Meeting at Anaheim, California, July 1974.

12. M. Ribbens-Pavella, Lj Grujic, J. Sabatel, and A. Buffioux, "Direct methods for stability analysis of large-scale power systems," presented at IFAC Symposium on Computer Applications in Large-Scale Power Systems, New Delhi, India, August 16-18, 1979.

13. A.A. Fouad, "Transient Stability Margin as a Tool for Dynamic Security Assessment," Prepared for EPRI, RP 1355-3.

14. T. Athay, R. Podmore, and S. Virmani, "A practical method for direct analysis of transient stability," IEEE Transaction Power App. Sys., vol. PAS-98, pp. 573-584, 1979.

15. A.A. Fouad, S.E. Stanton, "Transient Stability of a Multimachine Power System, Part II: Critical Transient Energy," IEEE Transaction Power App. Sys., vol. PAS-100, pp. 3408-3424, PES, Winter 1981.

16. A.N. Michel, A.A. Fouad, V. Vittal, "Power System Transient Stability Using Individual Machine Energy Functions," Iowa State University, IEEE Transaction of Circuits and Systems, CAS 30, pp. 266-276, May 1983.

17. T. Athay, R. Podmore, and S. Virmani, "Transient Energy Stability Analysis," Engineering Foundation Conference--System Engineering for Power, Henniker, New Hampshire, August 21-26, 1977.

18. A.A. Fouad and S.E. Stanton, "Transient stability analysis of a multi-machine power system. Part I: Investigation of system trajectory," IEEE Transaction Power App. Sys., vol. PAS-100, pp. 3408-3424, August 1981.

19. M. Ribbens-Pavella, B. Lemal, and W. Pirard, "On-line Operation of Lyapunov Criterion for Transient Stability Studies," IFAC Symp. 1977, Melbourne, Feb. 21-25, pp. 292-296.

20. O.I. Elgerd, "Electric Energy Systems Theory," McGraw-Hill, Inc., New York, 1971.

21. R.A. Schlueter, H. Akhtar, and H. Modir, "An RMS Coherency Measure: A Basis for Unification of Coherency and Modal Aggregation Techniques," IEEE Transaction Power App. Sys., PAS-98, no. 1, pp. 5-6, January 1977 (abstract) and Text of Abstract Papers, 1978 Summer Meeting, IEEE Publication 78 CH1 361-5.

22. R. Podmore and A. Germond, "Development of Dynamic Equivalents for Transient Stability Studies," Final Report on Electric Power Research Institute, Research Project 763, May 1977.

23. B. Stott and O. Alsac, "Fast Decoupled Load Flow," IEEE Transaction Power App. Sys., vol. PAS-93, May/June 1974, pp. 859-869.

24. J.S. Lawler, "Modal-Coherent Equivalents Derived from an RMS Coherency Measure," Ph.D. Thesis, Michigan State University, August 1979.

25. R.A. Schlueter, U. Ahn, and H. Modir, "Modal Analysis Equivalents Derived Based on the RMS Coherency Measure," IEEE Transaction Power App. Sys., vol. PAS-98, no. 4, pp. 1143, July/August 1979 and Text of Abstract Papers--1979 Winter Power Meeting, IEEE Publication 79 CH 1418-3.

26. J. Lawler, R.A. Schlueter, P. Rusche, and D.L. Hackett, "Modal Coherent Equivalents Derived from an RMS Coherency Measure," IEEE Transaction Power App. Sys., vol. PAS-99, no. 4, July/August 1980, pp. 1415-1425.

27. M. Lotfalian, "Simulation and Security Analysis Methods for Transients Due to Loss of Generation Contingencies," Ph.D. Thesis, Michigan State University, August 1982.

28. S.E. Stanton, "Assessment of the Stability of a Multimachine Power System by Transient Energy Margin," Ph.D. Dissertation, Iowa State University, Ames, Iowa, 1982.

29. P. Rastgoufard, "Local Energy Function Methods for Power System Transient Stability," Ph.D. Thesis, Michigan State University, July 1983.

30. P.C. Magnuson, "The Transient-Energy Method of Calculating Stability," IEEE, PES 1947, vol. 66, pp. 747-755.

31. P.D. Aylett, "The Energy-Integral Criterion of Transient Stability Limits of Power Systems," IEEE Transaction Power App. Sys., July 1958, pp. 527-536.

32. A.H. El-Abiad and K. Nagappan, "Transient Stability Regions of Multimachine Power Systems," IEEE on PES, Feb. 1966, pp. 169-179.

33. F.S. Prabhakara and A.H. El-Abiad, "A Simplified Determination of Transient Stability Regions for Lyapunov Methods," IEEE Transaction Power App. Sys., PAS-94, March/April 1975.

34. K. Uyemara et al., "Approximation of an Energy Function in Transient Stability Analysis of Power Systems," Electrical Engineering in Japan, vol. 92, no. 6, pp. 96-100, Nov./Dec. 1972.

35. C.J. Tavora and O.J.M. Smith, "Equilibrium Analysis of Power Systems," IEEE Transaction Power App. Sys., PAS, pp. 1131-1137, May/June 1972.